Insight into Mechanisms of Multiplicity of GPCR-G protein Signaling

by

Rabia U. Malik

A dissertation submitted in partial fulfillment
of the requirements for the degree of
Doctor of Philosophy
(Cell and Developmental Biology)
in the University of Michigan
2017

Doctoral Committee:

Professor Kristen J. Verhey, Chair
Associate Professor Sivaraj Sivaramakrishnan
Professor Roger K. Sunahara, University of California, San Diego
Professor John J. Tesmer
Professor Lois S. Weisman

For Sajjad Ahmed Malik

these past years, as they made sure that I had a glitch-free graduate experience at the University of Michigan.

To my labmates, Shiv, Rizal, Ruth, Tejas, Ashim, Carter, Keehun, Mike, and Ansley one could not ask for better friends. You truly made this journey fun and exciting. In you all, I found a place away from home. I found people to freely converse with and exchange my scientific fancies and personal worries. Thank you for setting the bar high. Thank you for your patience with my *many* eccentricities and personalities quirks. You will be dearly missed.

I now turn to my mother Naghmana Usman Malik, my father Muhammad Usman Malik and my brother Suleman Malik. Coming from a conservative Muslim immigrant family from Pakistan, my parents took a brave step by supporting and encouraging my insatiable desire for learning. This was a new road for all four of us and I thank you for your patience, perseverance, and prayers. Sajjad, my baby brother, will always remain an inspiration to me in my personal and scientific endeavors. It was a joy to have him in my life. Finally, to my mother, I could not have come this far without you.

TABLE OF CONTENTS

LIST OF FIGURES

ABSTRACT

G protein coupled receptors (GPCR) are sensory proteins that transduce a wide range of extracellular stimuli including drugs, neurotransmitters, and hormones into diverse physiological responses by activating intracellular effectors (G proteins or arrestins). Dysfunction in GPCR signaling is implicated in many disease states including cardiomyopathies, neuropathies, and cancer. Multiple factors complicate dissection of GPCR-G protein signaling in live cells. First, there is an imbalance between the number of distinct GPCRs and G proteins. For example, in the human genome, there are over 700 GPCRs but only 16 G proteins. Next, GPCRs are known to adopt multiple structural conformations and differentially activate functionally distinct G proteins through mechanisms that are poorly understood. Additional complexity arises from differences in cellular GPCR and G protein concentrations, localization of GPCR and G protein to micro-domains, and regulation by regulatory elements (RGS's, GRKs, and arrestins). How the cell prevents misfiring and interprets cross talk between different GPCR-G protein interactions remains an ongoing area of research. Studies presented herein aim to understand the mechanisms of specificity and multiplicity of GPCR signaling in live cells.

The first set of studies explores the mechanisms by which GPCRs selectively activate one or more G proteins. Sensors were designed based on the well-established interaction between GPCRs and peptides derived from the Gα C-terminal α5 helix, a known determinant of the specificity of GPCR-G protein interaction. Proof-of-concept studies demonstrate that the Gα C-terminus probes for a G protein-selective conformation of GPCRs in live cells. Following ligand stimulation, G protein-activating GPCR conformations interact specifically with the corresponding Gα C-terminus. Additional collaborative efforts using molecular dynamic simulation (MD), revealed hot spot residues on the Gαs and Gαq C-termini that confer specificity of GPCR-G protein interactions. A second set of MD and functional studies identified the role of conserved Gαi residues, L32 and D333, in G protein activation.

A parallel set of studies examines the influence of GPCR and G protein concentration and interaction strengths on downstream second messenger response. Therein, the well-characterized ER/K linker was leveraged to tether GPCRs to G proteins. The ER/K linker sets the effective concentration of the tethered GPCR-G protein and thus enabled a pairwise comparison across fusions. Linker length systematically modulated association between cognate and non-cognate G proteins; however, it only tuned cognate second messenger response downstream of the Gs, Gi, and Gq coupled receptors. Agonist stimulation provides changes in FRET (ΔFRET) comparable to those previously reported using co-expressed FRET/BRET pairs. Hence, the SPASM sensors serve the dual purpose of probing agonist-stimulated changes in GPCR-G protein interaction while examining the downstream response using the same construct.

These two parallel approaches seek to better understand the mechanism regulating multiplicity in the GPCR-G protein signaling pathway. Findings shed light into the structural basis of GPCR activation and provide a mechanism for ligand-dependent GPCR-G protein selection. Initial studies provide proof of concept for the use of fusions to probe the multiplicity of GPCR-G protein signaling in live cells, however, additional research is needed to explore the functional consequence of these findings in a physiologically relevant context.

Chapter 1

A brief introduction to GPCR-G protein signaling

1.1 Overview of GPCR signaling pathway

G protein coupled receptors (GPCRs/receptors) transmit detection of a wide range of ligands including neurotransmitters, hormones, odorants, photons, chemokines, calcium ions, and drugs from the extracellular milieu to the inside of the cell, by interacting with heterotrimeric G proteins, consisting of α, β and γ subunits (1, 2). GPCR binds and activates G protein by inducing nucleotide exchange from GDP (guanine diphosphate) to GTP (guanine triphosphate). Signal amplification occurs as GTP bound G protein, functionally dissociates in to $G\alpha \bullet GTP$ and $G\beta\gamma$ subunits to activate their respective effectors, resulting in secondary messenger production (1). The G proteins are categorized based on the kind of effectors they activate (see Table 1.1).

Table 1.1: Gα subunit classification and function. Adrenergic receptor (AR), increase ↑, decrease ↓. Table modified from Milligan and Kostenis *BJP* 2006 (2).

Family	Subunit	Expression	Example of GPCRs	Effector	Second Messenger
Gs	Gαs	Ubiquitous	β2-adrenergic receptor (β2-AR), β3-AR, dopamine receptor D1 (D$_1$R)	Adenylyl cyclase (AC)	cAMP ↑
Gi	Gαi	Mostly ubiquitous	α2-AR, A$_1$ adenosine receptor (R), cannabinoid receptor type 1 (CB$_1$)	Adenylyl cyclase (AC)	cAMP ↓
	Gαt	Retina	Rhodopsin	cGMP-phosphodiesterase	cGMP ↓
Gq	Gαq	Ubiquitous	α$_1$-AR, vasopressin 1A receptor (V$_{1A}$R)	Phospholipase C (PLC)	IP$_3$, DAG, Ca^{2+} ↑
Gβγ	β$_{1-5}$ γ$_{1-12}$	Most cell types express multiple βγ subtypes		PLCβ AC I AC II, IV, VII Ca^{2+} channels K$^+$ channels	IP$_3$, DAG, Ca^{2+} ↑ cAMP ↓ cAMP ↑ Ca^{2+} ↓ K$^+$ ↑

Gs and Gi proteins act on adenylyl cyclase to stimulate and inhibit cAMP production respectively (*1*). Gq activates phospholipase C (PLC) to generate inositol 1,4,5 phosphate (IP_3) and diacyl glycerol resulting in a release of Ca^{2+} from the endoplasmic reticulum (*1*). Gβγ subunits can also signal through Gα's effectors and others including potassium channels, calcium channels, and PI3-kinase type C (*2-4*) (Table 1.1). GPCR signaling is attenuated by receptor phosphorylation by G protein receptor kinases (GRKs) and subsequent binding of arrestins, resulting in clathrin dependent endocytosis and desensitization (Fig. 1.1a) (*1, 3*).
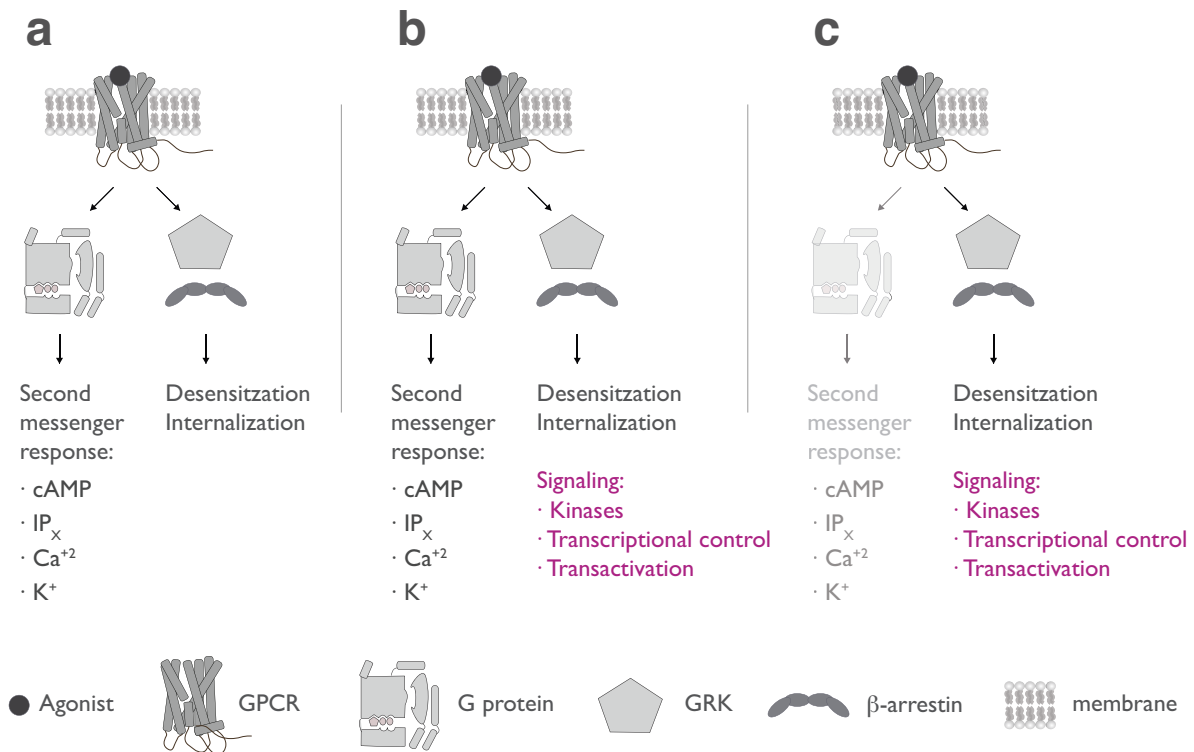
Fig. 1.1: GPCR signaling via G proteins and β-arrestins. a. *Canonical GPCR signaling pathway*. In the canonical pathway, agonist bind to GPCRs and stimulate second messenger response via G proteins, whereas signaling is attenuated by phosphorylation via GRKs and subsequent binding of β-arrestin leading to GPCR internalization and desensitization. **b.** *Current model of GPCR signaling*. Recent studies strongly suggest that agonist binding stimulates GPCR signaling via G proteins and β-arrestin, in addition to internalization and desensitization via β-arrestins. **c.** *Biased agonism*. In the case of biased agonist, (β-arrestin biased agonist is shown as an example), signaling proceeds through one pathway. Figure modified from Rajagopal et al., *Nat Rev Drug Disc*. 2010 (*3*).

1.2 Physiological relevance of GPCR signaling

GPCR signaling is involved in a wide range of physiological processes, including sensory perception (sight, smell, and taste), behavioral and mood regulation, inflammation and immune response, cell growth and cell death, and regulation of cardiac, pulmonary, and digestive

processes (*1, 5*). As such, dysfunction in GPCR signaling machinery has been implicated in a wide range of disease states. Currently, over 30% of prescribed drugs directly or indirectly target a GPCR for treatment of diseases of every major organ system including the nervous, respiratory, metabolic, urogenital, and cardiovascular systems (*6, 7*).

In 2013, Center for Disease Control and Prevention reported heart disease as the leading cause of death in the United States. β-blockers targeting β-adrenergic receptors are the most common type of drugs used to treat cardiovascular diseases including hypertension, angina, myocardial infarctions, and heart failure (*7*). Two β-adrenergic isoforms, β1 and β2 are expressed in the human heart. β-ARs regulate cardiac inotropy (contractility) and chronotropy (heart rate) (*7, 8*). In response to catecholamines (e.g. norepinephrine), which are the endogenous ligands for adrenergic receptors, β-ARs activate Gs to stimulate cAMP production resulting in activation of cAMP dependent protein kinase A (PKA) (*7*). PKA modulates cardiac contractility by phosphorylating myocyte proteins such as the L-type Ca^{2+} channel, resulting in increase in Ca^{2+} release and myofilament contraction (*7*). In contrast, Gi signaling reduces cAMP levels, slows down heart rate, and reduces contractility (*8*). During heart failure, levels of catecholamines increase, as the system attempts to enhance cardiac output by signaling through β-AR-Gs pathway (*9*). Interestingly, β1-AR to β2-AR ratio changes from 80:20 to 60:40 in a failing heart, with a correlative increase in Gi signaling (*10, 11*). Diminished contractile responsiveness to β-AR stimulation and an increase in Gi signaling are together the hallmarks of heart failure (*7, 8*). Additional studies suggest that during heart failure β2-AR switches signaling from Gs to Gi (Fig. 1.2) (*9, 12-14*).
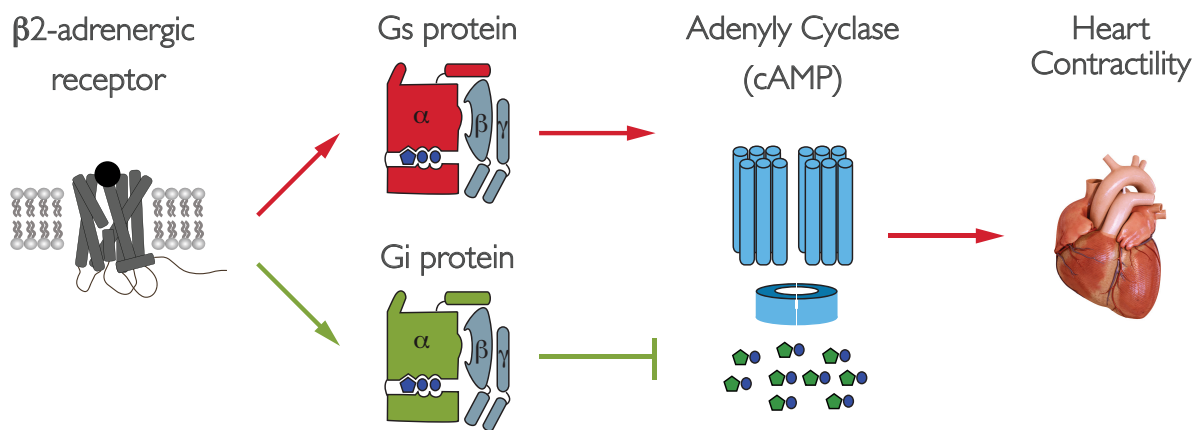
Fig. 1.2: Schematic of β2-AR-G protein signaling in the human heart. Cardiac receptor β2-AR has been suggested to signal through Gs and Gi. However, the molecular basis of β2-AR's signaling via to Gi is poorly understood.

1.3 Multiplicity of GPCR signaling

This multiplicity in GPCR signaling is not unique to adrenergic receptors, and has been demonstrated for a wide range of GPCRs, including a cardiac, Gq coupled, Angiotensin II type 1A receptor ($AT_{1A}R$) (*4, 15*). Differential $AT_{1A}R$ phosphorylation by GRKs result in unique signaling output (*16*). The endogenous angiotensin II (AII) ligand promotes Gαq mediated increase in cytosolic Ca^{+2}, transportation of PKCα to the membrane, and subsequent receptor phosphorylation by GRKs (*17*) (Fig. 1.1a). GRK2 and GRK3 mediate receptor endocytosis, desensitization, and internalization (*16*) (Fig. 1.1a). Whereas, $AT_{1A}R$ phosphorylation by GRK6 results in β-arrestin2 recruitment and signaling via the Extracellular-signal regulated kinase (ERK) pathway (Fig. 1.1b, Fig. 1.3) (*16*).

In comparison, SII peptide 'biases' $AT_{1A}R$ signaling pathway to arrestins (Fig. 1.1c) (*18*). SII, an artificial mutant peptide, has lower binding affinity and poorly activates the Gq pathway (*15, 18*). Instead, SII recruits and induces a conformational change in β-arrestin to activate ERK1/2 (Fig. 1.1c, Fig. 1.3) (*19, 20*). In contrast to AII, SII dependent ERK1/2 phosphorylation relies solely on GRK6 dependent recruitment of β-arrestin (Fig. 1.3) (*20, 21*). In the physiological context, both ligands induce positive ionotropic and lusitropic effects in adult rat cardiomyocytes (*21*). However, only SII response is dependent entirely on GRK6 whereas in the GRK6-/- KO mice, the positive ionotropic response is preserved following AII stimulation (*21*).

Additional studies reveal that spatiotemporal localization and kinetics of ERK1/2 phosphorylation are vastly differently as a result of G protein activation or via β-arrestin recruitment (*22*). G protein dependent activity is rapid, transient, and peaks within 2-5 minutes of activation (*22, 23*). PKC inhibitor Ro-31- 8425 blocks this activity; however, it is insensitive to depletion of endogenous β-arrestins (*22*). In contrast, β-arrestin activation is slower, less robust, and shows little decrement over 30 minutes (*22*). This response is insensitive to G protein inhibitors, but sensitive to levels of β-arrestin, as siRNA knockdown of β-arrestin significantly diminishes this activity (*22*). Subsequent drug screens have lead to discovery of drugs that do not activate G proteins, but selectively enhance β-arrestin recruitment (Fig.1.1c) (*23, 24*).
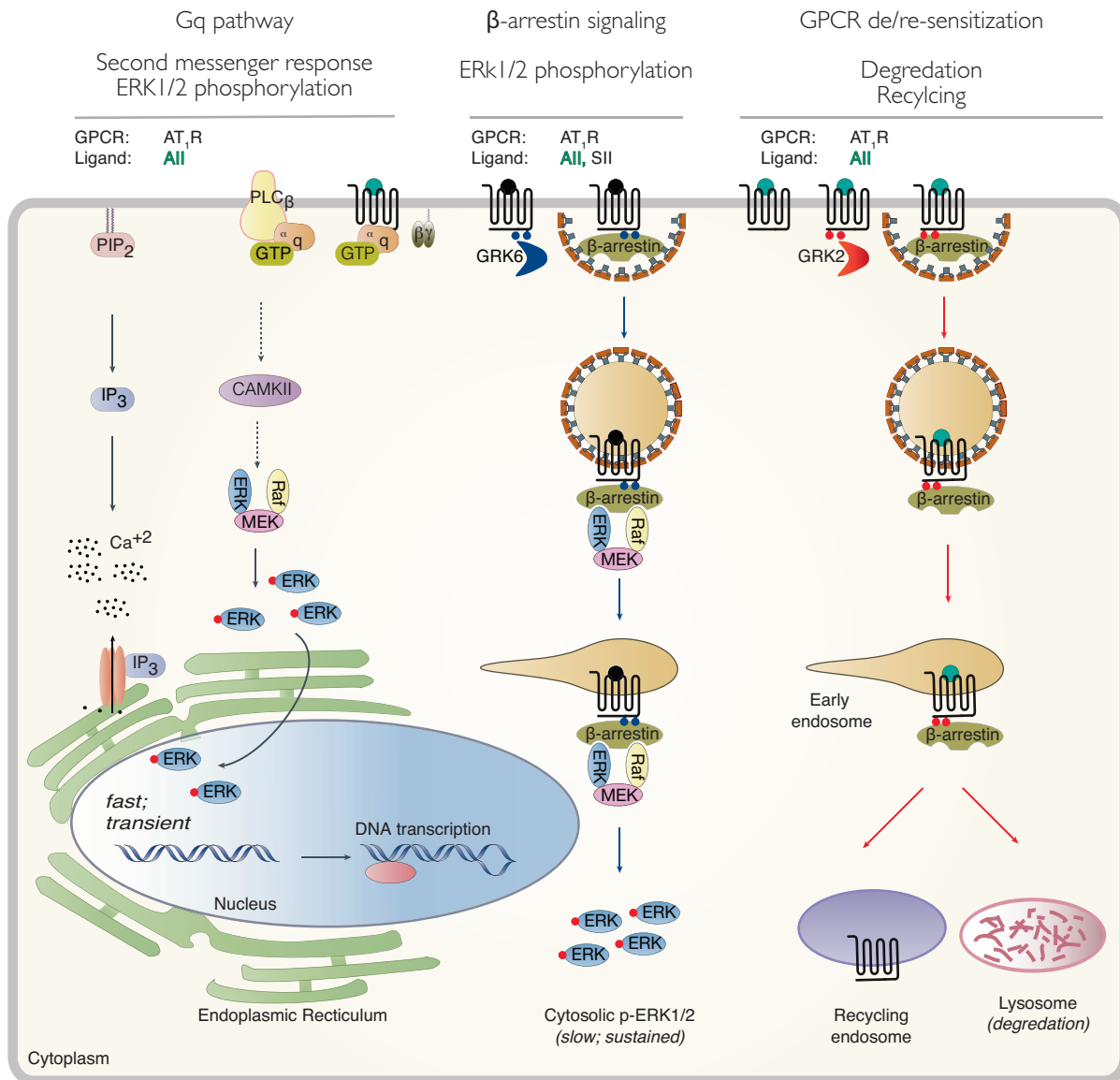
Fig. 1.3: Multiplicity of AT_1R signaling. Cardiac receptor AT_1R has been suggested to signal through Gq and arrestins. *Gq pathway:* The endogenous ligand, AII (aquamarine circle) stimulates Gαq mediated increase in IPx and Ca^{+2} levels and subsequent receptor phosphorylation by GRK 2, 3, and 6. An increase in cellular Ca^{+2} and DAG levels stimulate PLC, resulting in downstream phosphorylation of ERK1/2 via the Raf/Ras pathway. Phosphorylation of ERK1/2 is robust but transient, and the phosphorylated ERK1/2 translocates to the nucleus. AT_1R phosphorylation by GRK6 (shown in blue) results in arrestin mediated ERK1/2 signaling. Phosphorylated ERK1/2 is retained in the cytosol. AT_1R phosphorylation by GRK2 (depicted in red), recruits arrestins to initiate clathirin mediated endocytosis resulting in either lyosomal degradation or recycling of the inactive AT1R to the plasma membrane. SII ligand (black circle), stimulates GRK6 response resulting in ERK1/2 signaling independent of Gq signaling.

1.4 Role of structural diversity in multiplicity of GPCR signaling

Recent studies have emphasized the role of GPCR conformations in the multiplicity of GPCR signaling. An emerging view from spectroscopic, biophysical, molecular dynamics, biochemical, and functional studies support the idea that GPCRs are not simple on or off switches (*15, 25-30*). These studies posit that GPCRs exist in an ensemble of conformations, where ligand binding stabilizes a subset of these conformations that are selective for downstream effectors, and thus result in activation of distinct G proteins and/or arrestin (*25*).

This concept slowly developed over the past few decades. Studies done on the prototypical receptor rhodopsin formed the basis for one of the first models of GPCR signaling (*31*). Rhodospin consists of apoprotein opsin covalently bound to inverse agonist 11-*cis*-retinal, and is required for sensation of low light levels (*32*). *In situ* conversion of the inverse agonist to a full agonist occurs following photon absorption as 11-*cis*-retinal isomerizes to 11-*trans*-retinal (*31*). Site-directed-spin labeling experiments with bovine rhodopsin demonstrated an outward movement of the transmembrane (TM) helix 6 in the active conformation (*33*). As such, rhodopsin goes from an inactive state to a fully activate conformation (*33*). This lead to a bimodal model of GPCR signaling, where receptors were thought to exist in two distinct inactive ('off') or active ('on') conformations with ligand binding promoting structural rearrangements of the 7-transmembrane bundle (*34*).

Multiple active conformations were inferred from the fluorescent studies on purified β2-AR (*35*). Fluorescence Resonance Energy Transfer (FRET) sensor was generated in a minimal cysteine background. FRET reporters were inserted into the cytosolic end of transmembrane helices 3 and 6 by mutating Ile135 and Ala271 to tryptophan (FRET quencher) and cysteine respectively (*35*). Cys271 was subsequently labeled with monobromobimane (*35*). Experiments with full agonists, partial agonist, antagonist, and inverse agonist produced stepwise changes in fluorescence suggesting that agonists stabilize different conformational states of the receptor (*35*). Comparatively, live cell GPCR FRET sensors were generated by genetically inserting YFP (FRET acceptor) into the third intracellular loop of the receptor, and fusing CFP (FRET donor) to the GPCR's C-tail (*36*) (Fig. 1.4a). FRET studies using these sensors in intact cells also demonstrated that agonists and partial agonists induce distinct FRET signals with highly variable kinetics (*36*).
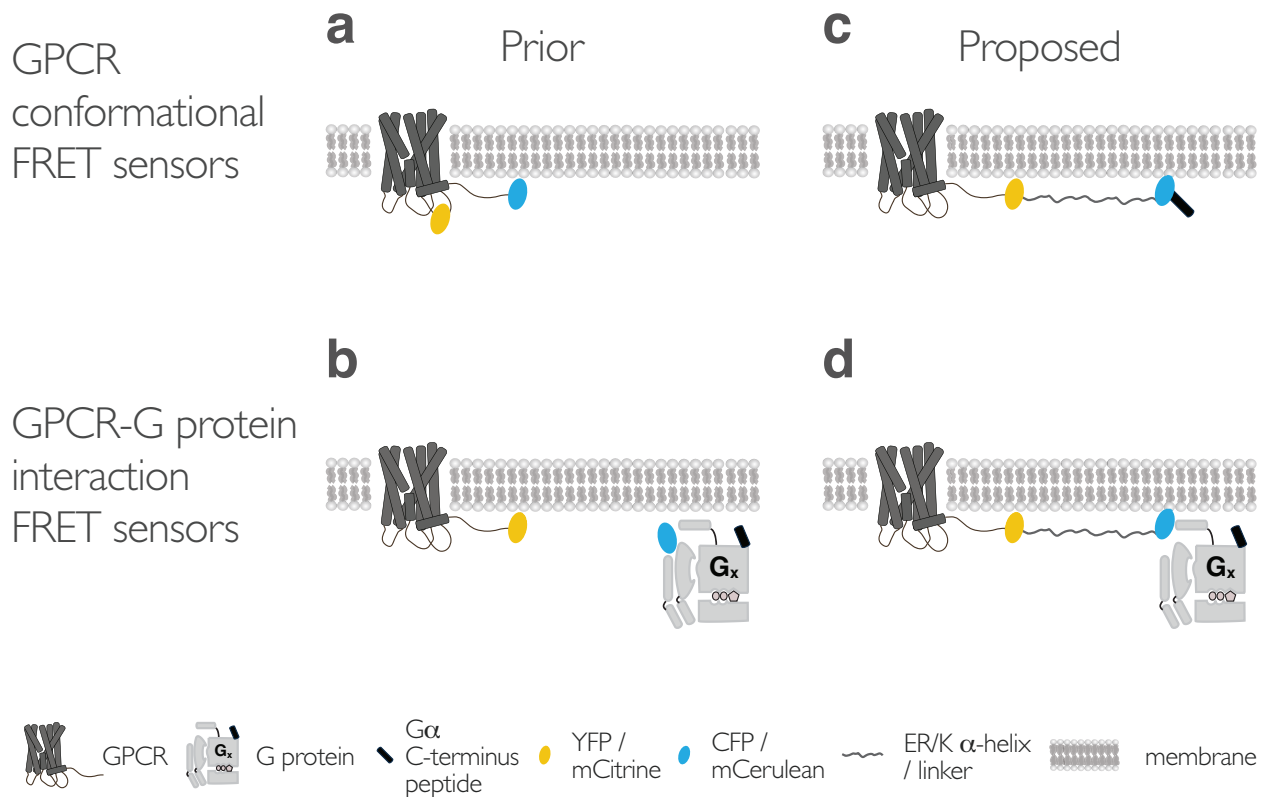
Fig. 1.4: GPCR-G protein fluorescence or bioluminescence sensors. Schematic of the previously described (**a,b**) and proposed (**c,d**) GPCR conformation (**a, c**) and GPCR-G protein interaction sensors (**b,d**). **a.** Previously described GPCR conformation sensors involved labeling the third intracellular loop with FRET or BRET acceptor (YFP) and C-tail with FRET or BRET donor (CFP or luciferase respectively). **b.** Previously reported GPCR-G protein interaction sensors involved co-transfecting individually labeled GPCR and G protein in live cells. Proposed sensors involve generating a single polypeptide by fusing in frame Gα α5 peptide (**c**) or Gα (**d**) to the C-terminus of the GPCR with an ER/K linker flanked by the FRET pair (mCitrine and mCerulean).

1.5 Challenges in exploring mechanism of multiplicity of GPCR signaling in live cells

Despite these initial observations, the molecular basis of how ligands acting on the same GPCR induce signaling via one or more distinct G proteins and/or arrestins remains an open area of research (*37*). Dissecting this phenomenon in live cells poses a significant challenge. In general, functional studies in cells, membranes, or tissue preparations have shown that ligand treatment results in a complex response with changes in multiple secondary messengers including cAMP, IP_x, K^+, and Ca^{2+} as well as signaling via ERK1/2 pathway (*4*). As alluded to above, G protein signaling pathway and arrestin converge on ERK1/2. ERK1/2 activation occurs by multiple mechanisms (*1, 38*). Gs, Gi/o and Gq/11 proteins activate ERK1/2 pathway. Gαs-dependent accumulation in cAMP levels activates protein kinase A (PKA), inducing Raf phosphorylation,

Ligand

α
1
2
3

β
1
2
3

γ
1
2
3

Gq   Gi   Gs

IP$_1$ Ca^{+2} K$^+$ cAMP
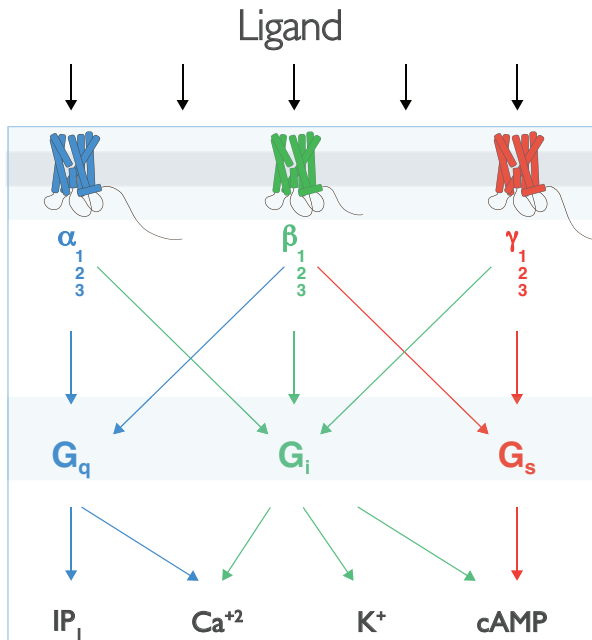
Fig. 1.5: Complexity in GPCR-G protein signaling. Treatment with GPCR ligand can result in a production of a complex second messenger response. Multiplicity of GPCR signaling can arise at three levels: (i) GPCR, (ii) G proteins or (iii) the cellular environment. (i) A GPCR can have multiple isoforms with different subtypes expressed in the same cell. Each subtype can have distinct pharmacological properties, with differences in agonist affinity and preferential activation of one or more unique G proteins. (ii). G proteins can act on the same effector to modulate second messenger response. (iii) Cellular environmental factors such as relative localization and concentration of GPCR and G protein add yet an additional layer of complexity. This pattern of multiplicity can pose a challenge in tracing the pathways that result in second messenger response post ligand stimulation in live cells.

resulting in sequential phosphorylation of ERK1/2. Likewise, Gq mediated increase in cellular Ca^{+2} and DAG levels stimulate PLC, resulting in downstream phosphorylation of ERK1/2 via the Raf/Ras pathway (Fig. 1.3) (*1*). Similarly Gβγ subunits of heterotrimeric Gi protein, can activate the phosphoinositide 3-kinase (PI-3K) resulting in ERK1/2 phosphorylation via recruitment of SOS1 and Raf (*2*). Arrestins are thought to serve as scaffolds of the MAPK pathway, recruit c-Src, Raf/Ras, and thus enhance phosphorylation of MEK1/2 and ERK1/2 (*19*).

To compound the problem further, multiple layers of complexity contribute to the multiplicity of the downstream second messenger response (Fig. 1.5) (*4, 37*). Cellular/environmental factors including differential expression of GPCR and G proteins in different cell types, localization to different membrane compartments such as microdomains, posttranslational modification by kinases, and regulation by scaffolds, RGS proteins, and arrestins, contribute to generation of a complex signaling response (*4*). Multiplicity of signaling can also arise from activation of the same G protein (*4*). The Gα and Gβγ subunits may act on the same or two different effectors (*4*) (Table 1.1). Next, a GPCR can have multiple isoforms expressed within the same cells, each of which can have distinct pharmacological properties as seen by preferential activation of one G protein compared to another (*4*). Thus, stimulation with an agonist can result in activation of distinct G proteins via different GPCR isoforms (*4*). Finally, in response to a ligand, a single GPCR isoform can also activate more than one functionally

distinct G protein (*4*). Together, this complexity poses a challenge in tracing the individual pathways that connect ligand stimulation to second messenger response. <u>The central aim of this thesis is to shed insight onto the molecular mechanisms that influence multiplicity of GPCR signaling in live cells.</u>

1.6 Novel tools to explore the molecular basis of multiplicity of GPCR signaling

<u>Although, spectroscopic studies elegantly demonstrated ligand-specific conformations, prior to this thesis's work, there was no direct link between GPCR conformations and downstream signaling in the absence of pre-documented functional response of ligand in live cells or membrane preparations.</u> This limitation was partly addressed by building a complementary FRET sensor that reports on the relative stabilization of different G protein specific GPCR conformations in live cells.

FRET sensors are based on a technique termed Systematic Protein Affinity Strength Modulation (SPASM) which involves the fusion of a native peptide from the C terminus of a G subunit to the C terminus of the intact GPCR via a flexible ER/K linker flanked by a FRET pair (mCitrine - FRET acceptor; mCerulean – FRET donor) (Fig. 1.4c) (*39, 40*). Multiple studies have established Gα C-terminus as one of the key determinants of specificity of GPCR-G protein interaction and as an important component of the GPCR-G protein-binding interface (*41-44*). Crystal structures of opsin and β2-AR in complex with a Gαt C-terminal peptide (*45*) and nucleotide empty Gs (*46*) respectively demonstrate that the Gα C-terminus binds into the cytosolic core

Fig. 1.6: β2-AR-Gαs interface. Crystal structure of the β2-AR-Gαs complex is shown. Gαs C-terminal α5 helix (red) inserts into the cytosolic core of the active conformation of receptor (blue). (PDB: 3SN6).

of the 7-transmebrane bundle (Figure 1.6). Following studies with amide hydrogen-deuterium exchange mass spectroscopy further demonstrated that the C-terminus of the Gαs α5 helix remains buried within the agonist-bound β2-AR (*47*). Hence, in Chapter 2 we propose that peptides derived from the Gα C terminus could be used as "bait" to detect G protein-selective conformations of a GPCR.

SPASM sensors are distinct from established FRET-based GPCR sensors that rely on the insertion of a FRET probe in the third intracellular loop of the GPCR with its pair (donor/acceptor) at the GPCR C terminus (Fig. 1.4a and c). Previous BRET/FRET sensors report on the conformational diversity of the GPCR post ligand treatment. In comparison, The SPASM sensors use a peptide comprising the α5 helix of a Gα C terminus (see Table 1.2) to probe the stabilization of GPCR conformations that favor interactions with the corresponding G protein.

Table 1.2: Sequence of Gα C termini peptides used to construct GPCR-peptide-FRET sensors. 27 residues were derived from the α5 helix of the indicated Gα C terminus. Negative controls were made by creating a no-pep sensor, which contains repeating GSG sequences, or 'scram' peptide where s-pep residues were scrambled using a sequence randomizer tool.

Gα α5 helix	Peptide name	Sequence
Gαt	t-pep	DTQNVKFVFDAVTDIIIKENLKDCGLF
Gαi	i-pep	DTKNVQFVFDAVTDVIIKNNLKDCGLF
Gαq	q-pep	DTENIRFVFAAVKDTILQLNLKEYNLV
Gαs	s-pep	DTENIRRVFNDCRDIIQRMHLRQYELL
Gαs	s17	DCRDIIQRMHLRQYELL
Gαs	s11	QRMHLRQYELL
Gαs	scram	CLDYNRFIHIDQRLNEMERTDQIRLRV
Control	no-pep	GSGGSGGSGGSG

An important caveat is that Gα C-terminus is one element of the GPCR-G protein interface. The co-crystal structure of active conformation of β2-AR in a complex with a nucleotide empty state of Gs protein at 3.5Å resolution revealed an extensive interface between β2-AR and Gs (Fig. 1.6) (*46*). The interface consists of β2-AR's intracellular loop 2 (ICL2) and transmembrane 5 (TM5) and TM6, with Gαs elements including α5 helix, αN-β1 junction, and α4 helix. In addition, β2-AR's ICL2 and the E/DRY motif make long distance (9-10Å), charged interactions with Gαs N-terminal α5 helix (*46, 48*). Therefore, to understand how GPCR-G protein interaction influence downstream second messenger response, we constructed full-length GPCR-G protein SPASM sensors.

Currently, efforts to monitor and understand the link between GPCR-G protein interactions and downstream second messenger response are also complicated by the range of cellular factors listed and described above (Fig.1.4) (*4*). Current approaches to visualize GPCR-G protein

interaction in cells involve probing the interaction between individually expressed fluorescent or luminescent protein fusions using FRET or bioluminescence resonance energy transfer (BRET) (*49-53*) (Fig.1.4b). Therefore, insights into the GPCR-G protein interaction gained from these studies are limited by their dependence on the relative concentration and co-localization of individually expressed GPCR and G protein. Alternatively, direct GPCR-G protein fusions generated by tethering the N-terminus of the Gα to the GPCR's C-tail with a short or no linker in between have been used to study the influence of tethering different G protein subunits on G protein activation and second messenger signaling (*54, 55*). Such fusions have not been used to monitor the GPCR-G protein interaction using resonance energy transfer approaches (*52*). A limitation of direct fusions is that GPCRs with short C-tails do not efficiently signal to the tethered G protein (*56-59*).

In Chapter 3, we combined the strengths of FRET and fusion proteins by leveraging SPASM, which involves expression of a single polypeptide encoding a GPCR tethered to a G protein via an ER/K α-helix/linker that is flanked by a pair of FRET probes (mCitrine (FRET acceptor) and mCerulean (FRET donor)) (Fig.1.4d). Unstructured (Gly-Ser-Gly)$_4$ linkers are inserted in between each component to provide rotational flexibility. Similar to GPCR fusions, GPCR SPASM sensors enable control over GPCR-G protein stoichiometry and co-localization. Increasing ER/K linker length from 10-30 nm has been shown to systematically modulate the effective concentration of the protein-protein interaction from 100nM to 10μM (*39, 40, 60, 61*). As part of a proof-of-concept study, SPASM sensors are made for four full length GPCRs with varying C-tail lengths: β2-adrenergic receptor (β2-AR), α2-adrenergic receptor (α2-AR), α1-adrenergic receptor (α1-AR), and adenosine type 1 receptor (A$_1$R). Each GPCR was tethered to functionally distinct Gα subunits (Gαs-XL, Gαi$_1$, and Gαq) to bridge the gap between the GPCR-G protein interaction and downstream signaling (*56-59*).

1.7 References

1.   R. T. Dorsam, J. S. Gutkind, G-protein-coupled receptors and cancer. *Nat Rev Cancer* **7**, 79-94 (2007).
2.   G. Milligan, E. Kostenis, Heterotrimeric G-proteins: a short history. *Br J Pharmacol* **147 Suppl 1**, S46-55 (2006).
3.   S. Rajagopal, K. Rajagopal, R. J. Lefkowitz, Teaching old receptors new tricks: biasing seven-transmembrane receptors. *Nat Rev Drug Discov* **9**, 373-386 (2010).
4.   E. Hermans, Biochemical and pharmacological control of the multiplicity of coupling at G-protein-coupled receptors. *Pharmacol Ther* **99**, 25-44 (2003).
5.   M. J. Marinissen, J. S. Gutkind, G-protein-coupled receptors and signaling networks: emerging paradigms. *Trends Pharmacol Sci* **22**, 368-376 (2001).
6.   P. Ma, R. Zemmel, Value of novelty? *Nat Rev Drug Discov* **1**, 571-572 (2002).
7.   J. A. Johnson, S. B. Liggett, Cardiovascular pharmacogenomics of adrenergic receptor signaling: clinical implications and future directions. *Clinical pharmacology and therapeutics* **89**, 366-378 (2011).
8.   N. C. Salazar, J. Chen, H. A. Rockman, Cardiac GPCRs: GPCR signaling in healthy and failing hearts. *Biochimica et biophysica acta* **1768**, 1006-1018 (2007).
9.   W. Zhu, X. Zeng, M. Zheng, R. P. Xiao, The enigma of beta2-adrenergic receptor Gi signaling in the heart: the good, the bad, and the ugly. *Circ Res* **97**, 507-509 (2005).
10.   M. R. Bristow, R. E. Hershberger, J. D. Port, W. Minobe, R. Rasmussen, Beta 1- and beta 2-adrenergic receptor-mediated adenylate cyclase stimulation in nonfailing and failing human ventricular myocardium. *Mol Pharmacol* **35**, 295-303 (1989).
11.   M. Ungerer, M. Bohm, J. S. Elce, E. Erdmann, M. J. Lohse, Altered expression of beta-adrenergic receptor kinase and beta 1-adrenergic receptors in the failing human heart. *Circulation* **87**, 454-463 (1993).
12.   R. P. Xiao *et al.*, Coupling of beta2-adrenoceptor to Gi proteins and its physiological relevance in murine cardiac myocytes. *Circ Res* **84**, 43-52 (1999).
13.   R. P. Xiao, Beta-adrenergic signaling in the heart: dual coupling of the beta2-adrenergic receptor to G(s) and G(i) proteins. *Sci STKE* **2001**, re15 (2001).
14.   W. Zhu *et al.*, Gi-Biased β2AR Signaling Links GRK2 Upregulation to Heart FailureNovelty and Significance. *Circulation research* **110**, 265-274 (2012).
15.   A. Sauliere *et al.*, Deciphering biased-agonism complexity reveals a new active AT1 receptor entity. *Nat Chem Biol* **8**, 622-630 (2012).
16.   J. Kim *et al.*, Functional antagonism of different G protein-coupled receptor kinases for beta-arrestin-mediated angiotensin II receptor signaling. *Proc Natl Acad Sci U S A* **102**, 1442-1447 (2005).
17.   S. K. Shenoy, R. J. Lefkowitz, Angiotensin II-stimulated signaling through G proteins and beta-arrestin. *Sci STKE* **2005**, cm14 (2005).
18.   H. Wei *et al.*, Independent beta-arrestin 2 and G protein-mediated pathways for angiotensin II activation of extracellular signal-regulated kinases 1 and 2. *Proc Natl Acad Sci U S A* **100**, 10782-10787 (2003).
19.   A. K. Shukla *et al.*, Distinct conformational changes in beta-arrestin report biased agonism at seven-transmembrane receptors. *Proc Natl Acad Sci U S A* **105**, 9988-9993 (2008).

20.   B. Zimmerman *et al*., Differential beta-arrestin-dependent conformational signaling and cellular responses revealed by angiotensin analogs. *Sci Signal* **5**, ra33 (2012).

21.   K. Rajagopal *et al*., Beta-arrestin2-mediated inotropic effects of the angiotensin II type 1A receptor in isolated cardiac myocytes. *Proc Natl Acad Sci U S A* **103**, 16284-16289 (2006).

22.   S. Ahn, S. K. Shenoy, H. Wei, R. J. Lefkowitz, Differential kinetic and spatial patterns of beta-arrestin and G protein-mediated ERK activation by the angiotensin II receptor. *J Biol Chem* **279**, 35518-35525 (2004).

23.   M. Azzi *et al*., Beta-arrestin-mediated activation of MAPK by inverse agonists reveals distinct active conformations for G protein-coupled receptors. *Proc Natl Acad Sci U S A* **100**, 11406-11411 (2003).

24.   J. D. Violin, R. J. Lefkowitz, Beta-arrestin-biased ligands at seven-transmembrane receptors. *Trends Pharmacol Sci* **28**, 416-422 (2007).

25.   B. K. Kobilka, X. Deupi, Conformational complexity of G-protein-coupled receptors. *Trends Pharmacol Sci* **28**, 397-406 (2007).

26.   E. Hermans, Multiplicity and regulation of G-protein couplings. *Bull Mem Acad R Med Belg* **164**, 255-262 (2009).

27.   S. Bockenhauer, A. Furstenberg, X. J. Yao, B. K. Kobilka, W. E. Moerner, Conformational dynamics of single G protein-coupled receptors in solution. *J Phys Chem B* **115**, 13328-13338 (2011).

28.   S. Granier, B. Kobilka, A new era of GPCR structural and chemical biology. *Nature chemical biology* **8**, 670-673 (2012).

29.   A. W. Kahsai *et al*., Multiple ligand-specific conformations of the beta2-adrenergic receptor. *Nat Chem Biol* **7**, 692-700 (2011).

30.   J. J. Liu, R. Horst, V. Katritch, R. C. Stevens, K. Wuthrich, Biased signaling pathways in beta2-adrenergic receptor characterized by 19F-NMR. *Science* **335**, 1106-1110 (2012).

31.   K. P. Hofmann *et al*., A G protein-coupled receptor at work: the rhodopsin model. *Trends in Biochemical Sciences* **34**, 540-552 (2009).

32.   J. Lem, G. L. Fain, Constitutive opsin signaling: night blindness or retinal degeneration? *Trends Mol Med* **10**, 150-157 (2004).

33.   D. L. Farrens, C. Altenbach, K. Yang, W. L. Hubbell, H. G. Khorana, Requirement of rigid-body motion of transmembrane helices for light activation of rhodopsin. *Science* **274**, 768-770 (1996).

34.   X. Deupi, B. K. Kobilka, Energy landscapes as a tool to integrate GPCR structure, dynamics, and function. *Physiology (Bethesda)* **25**, 293-303 (2010).

35.   X. Yao *et al*., Coupling ligand structure to specific conformational switches in the beta2-adrenoceptor. *Nat Chem Biol* **2**, 417-422 (2006).

36.   J. P. Vilardaga, R. Steinmeyer, G. S. Harms, M. J. Lohse, Molecular basis of inverse agonism in a G protein-coupled receptor. *Nat Chem Biol* **1**, 25-28 (2005).

37.   P. Samama, S. Cotecchia, T. Costa, R. J. Lefkowitz, A mutation-induced activated state of the beta 2-adrenergic receptor. Extending the ternary complex model. *J Biol Chem* **268**, 4625-4636 (1993).

38.   A. K. Shukla, K. Xiao, R. J. Lefkowitz, Emerging paradigms of beta-arrestin-dependent seven transmembrane receptor signaling. *Trends Biochem Sci* **36**, 457-469 (2011).

39.   S. Sivaramakrishnan, J. A. Spudich, Systematic control of protein interaction using a modular ER/K alpha-helix linker. *Proc Natl Acad Sci U S A* **108**, 20467-20472 (2011).

40. C. J. Swanson, S. Sivaramakrishnan, Harnessing the unique structural properties of isolated alpha-helices. *J Biol Chem* **289**, 25460-25467 (2014).

41. B. R. Conklin, Z. Farfel, K. D. Lustig, D. Julius, H. R. Bourne, Substitution of three amino acids switches receptor specificity of Gq alpha to that of Gi alpha. *Nature* **363**, 274-276 (1993).

42. B. R. Conklin *et al.*, Carboxyl-terminal mutations of Gq alpha and Gs alpha that alter the fidelity of receptor activation. *Mol Pharmacol* **50**, 885-890 (1996).

43. H. E. Hamm *et al.*, Site of G protein binding to rhodopsin mapped with synthetic peptides from the alpha subunit. *Science* **241**, 832-835 (1988).

44. E. L. Martin, S. Rens-Domiano, P. J. Schatz, H. E. Hamm, Potent peptide analogues of a G protein receptor-binding region obtained with a combinatorial library. *J Biol Chem* **271**, 361-366 (1996).

45. P. Scheerer *et al.*, Crystal structure of opsin in its G-protein-interacting conformation. *Nature* **455**, 497-502 (2008).

46. S. G. Rasmussen *et al.*, Crystal structure of the beta2 adrenergic receptor-Gs protein complex. *Nature* **477**, 549-555 (2011).

47. K. Y. Chung *et al.*, Conformational changes in the G protein Gs induced by the beta2 adrenergic receptor. *Nature* **477**, 611-615 (2011).

48. G. H. Westfield *et al.*, Structural flexibility of the G alpha s alpha-helical domain in the beta2-adrenoceptor Gs complex. *Proc Natl Acad Sci U S A* **108**, 16086-16091 (2011).

49. C. Gales *et al.*, Real-time monitoring of receptor and G-protein interactions in living cells. *Nat Methods* **2**, 177-184 (2005).

50. C. Gales *et al.*, Probing the activation-promoted structural rearrangements in preassembled receptor-G protein complexes. *Nat Struct Mol Biol* **13**, 778-786 (2006).

51. P. Hein, M. Frank, C. Hoffmann, M. J. Lohse, M. Bunemann, Dynamics of receptor/G protein coupling in living cells. *EMBO J* **24**, 4106-4114 (2005).

52. M. J. Lohse, S. Nuber, C. Hoffmann, Fluorescence/bioluminescence resonance energy transfer techniques to study G-protein-coupled receptor activation and signaling. *Pharmacol Rev* **64**, 299-336 (2012).

53. K. Qin, C. Dong, G. Wu, N. A. Lambert, Inactive-state preassembly of G(q)-coupled receptors and G(q) heterotrimers. *Nat Chem Biol* **7**, 740-747 (2011).

54. G. Milligan, Insights into ligand pharmacology using receptor-G-protein fusion proteins. *Trends Pharmacol Sci* **21**, 24-28 (2000).

55. R. Seifert, K. Wenzel-Seifert, B. K. Kobilka, GPCR-Galpha fusion proteins: molecular analysis of receptor-G-protein coupling. *Trends Pharmacol Sci* **20**, 383-389 (1999).

56. D. S. Dupuis, S. Tardif, T. Wurch, F. C. Colpaert, P. J. Pauwels, Modulation of 5-HT1A receptor signalling by point-mutation of cysteine351 in the rat Galpha(o) protein. *Neuropharmacology* **38**, 1035-1041 (1999).

57. A. Wise, G. Milligan, Rescue of functional interactions between the alpha2A-adrenoreceptor and acylation-resistant forms of Gi1alpha by expressing the proteins from chimeric open reading frames. *J Biol Chem* **272**, 24673-24678 (1997).

58. T. Wurch, F. C. Colpaert, P. J. Pauwels, Mutation in a protein kinase C phosphorylation site of the 5-HT1A receptor preferentially attenuates Ca2+ responses to partial as opposed to higher-efficacy 5-HT1A agonists. *Neuropharmacology* **44**, 873-881 (2003).

59. T. Wurch, P. J. Pauwels, Analytical pharmacology of G protein-coupled receptors by stoichiometric expression of the receptor and G(alpha) protein subunits. *J Pharmacol Toxicol Methods* **45**, 3-16 (2001).

60. M. Ritt, J. L. Guan, S. Sivaramakrishnan, Visualizing and manipulating focal adhesion kinase regulation in live cells. *J Biol Chem* **288**, 8875-8886 (2013).

61. C. J. Swanson *et al.*, Conserved modular domains team up to latch-open active protein kinase Calpha. *J Biol Chem* **289**, 17812-17829 (2014).

Chapter 2

Detection of G protein selective G protein-Coupled Receptor (GPCR) conformations in live cells*

2.1 Abstract

While several recent studies have reported that GPCRs adopt multiple conformations, it remains unclear how subtle conformational changes are translated into divergent downstream responses. In this study, we report on a novel class of FRET-based sensors that can detect the ligand/mutagenic stabilization of GPCR conformations that promote interactions with G proteins in live cells. These sensors rely on the well-characterized interaction between a GPCR and the c-terminus of a Gα subunit. We use these sensors to elucidate the influence of the highly conserved E/DRY motif on GPCR conformation. Specifically, E/D but not R mutants of the E/DRY motif are known to enhance basal GPCR signaling. Hence, it is unclear whether ionic interactions formed by the E/DRY motif (ionic-lock) are necessary to stabilize basal GPCR states. We find that mutagenesis of the β2-AR E/DRY ionic-lock enhances interaction with Gs. However, only E/D but not R mutants increase G protein activation. In contrast, mutagenesis of the opsin E/DRY ionic-lock does not alter its interaction with transducin. Instead, opsin-specific ionic interactions centered on residue K296 are both necessary and sufficient to promote interactions with transducin. Effective suppression of β2-AR basal activity by inverse agonist ICI 118,551 requires ionic interactions formed by the E/DRY motif. In contrast, the inverse agonist metoprolol suppresses interactions with Gs and promotes Gi binding, with concomitant pertussis-toxin sensitive inhibition of adenylyl cyclase activity. Taken together, these studies

validate the use of the new FRET sensors while revealing distinct structural mechanisms for ligand-dependent GPCR function.

2.2 Introduction

A fundamental unanswered question in GPCR signaling is the role of GPCR structural conformations in G protein selection. An emerging view from several studies is that GPCRs are not simple 'on-off' switches, but adopt a continuum of conformations (1). Structural studies show that ligands stabilize different subsets of structural conformations (2-5). In turn, these ligands are observed to elicit diverse functional responses through the activation of specific G protein heterotrimers or G protein independent effectors such as arrestins (6). This model would explain the phenomenon of functional selectivity, wherein the same GPCR can elicit diverse ligand-dependent responses (7,8). However, currently there is no method to directly link ligand-specific changes in GPCR conformations to differential downstream responses (9). This limitation arises in part due to the wide range of factors that influence GPCR signaling, including differential expression of the GPCR and components of the G protein heterotrimer in different cell types, localization to different membrane surfaces or micro-domains, and the influence of regulatory proteins such as scaffolds, RGS proteins, kinases, arrestins, and the cellular endocytic apparatus. In this study, this limitation is addressed in part with a novel FRET-based sensor that is designed to detect the relative stabilization of G protein specific conformations of the same GPCR.

The FRET sensors used in this study are based on a recently developed technique termed Systematic Protein Affinity Strength Modulation (SPASM) and involve the fusion of a native peptide from the c-terminus of a Gα subunit to the c-terminus of the intact GPCR (10). The Gα c-terminus has been extensively characterized as an important component of the GPCR-G protein binding interface (11-13). Recent structures reveal that the Gα c-terminus inserts itself into a cytosolic groove formed in the active GPCR (14-16). Peptides derived from the Gα c-terminus bind specifically to the activated GPCR (11,17) and can competitively inhibit GPCR-G protein interactions (13). The Gα c-terminus is also a key determinant of G protein selection by a GPCR (18,19). The SPASM sensors use a peptide comprising the α5-helix of a Gα c-terminus to probe the stabilization of GPCR conformations that favor interactions with the corresponding G protein. In this regard, the SPASM sensors are distinct from established FRET-based GPCR

sensors that rely on the insertion of a FRET probe in the third intracellular loop of the GPCR with its pair (donor/acceptor) at the GPCR c-terminus (4).

In this study, SPASM sensors were used to examine the conformational changes accompanying ligand-stimulation or mutagenesis of opsin and β2-AR. Specifically, we address a long-standing paradox in the function of the highly conserved E/DRY motif located at the cytosolic face of the GPCR (20,21). High-resolution structures of GPCRs bound to canonical inverse agonists display electrostatic interactions (termed the ionic-lock) between the positively charged arginine (R) in the E/DRY motif and two negatively charged residues (glutamic acid (E) or aspartic acid (D)) (21,22). In contrast, in high-resolution structures of GPCRs bound to canonical agonists these residues move apart such that the ionic-lock appears to be disrupted (15,21). Therefore, the E/DRY ionic-lock has been proposed to stabilize conformations that suppresses basal signaling (20). Consistent with this model, mutagenesis of the E/D residues that form the ionic-lock typically result in constitutive (ligand-free) signaling from the GPCR (20,23). However, mutagenesis of R (E/D<u>R</u>Y) does not result in constitutive signaling from the GPCR (20). The paradoxical effect of R mutants has muddled the simple model of the E/DRY motif as an ionic-lock. In this study, we use the SPASM sensors to show that mutagenesis of either R or E/D residues in the E/DRY motif of the β2-adrenergic receptor (β2-AR), enhances β2-AR interactions with Gs. However, only E/D but not R mutants increase constitutive GPCR signaling, consistent with our finding that the R mutant does not enhance G protein activation.

Opsin represents a notable exception to the function of the E/DRY motif, since it has a second ionic-lock formed by residue K296 at the ligand-binding site (24). This second ionic-lock is unique to opsin, which covalently binds to its ligand through the formation of a protonated Schiff-base at K296 (25). We find that the K296 ionic-lock dominates the effect of the E/DRY motif, such that E/DRY mutants do not enhance ligand-free interactions with the G protein. In contrast, the intact E/DRY ionic-lock in β2-AR is only observed in high-resolution structures obtained in the presence of inverse agonists that suppress its ligand-free activity (22). Here, we demonstrate that an intact E/DRY ionic-lock is necessary for effective suppression of β2-AR basal signaling by the potent inverse agonist ICI118,551.

Inverse agonist suppression of basal β2-AR signaling can be achieved either by reducing Gs or enhancing Gi activity. Hence, SPASM sensors were used to probe ligand-biased conformations of two beta-adrenergic inverse agonists, ICI118,551 (ICI) and metoprolol (6,26).

We find that metoprolol but not ICI stabilizes conformations that enhance interaction with Gi (Gi conformations). Distinction between Gs suppression and Gi activation is routinely achieved by treatment of cells with pertussis toxin (PTX), which covalently modifies Gi and prevents its coupling to the GPCR (27). PTX treatment has been previously used to uncover a Gi mediated ERK signaling pathway initiated by β2-AR (6). However, PTX has not been used to examine G protein selection by ICI and metoprolol. We find that stabilization of Gi conformations by metoprolol correlates with a PTX-sensitive suppression of cAMP accumulation for this compound. In contrast, cAMP suppression by ICI118,551 is not PTX-sensitive. Taken together, this study validates a new technology to examine G protein-specific GPCR conformations in live cells, while providing new insights into the structure-to-function link for opsin and β2-AR.

2.3. Results

2.3.1. SPASM sensor expression and receptor function - SPASM sensors were developed for two prototypical GPCRs: β2-AR and opsin (Fig. 2.1a). Each SPASM sensor contains - from N-to-C terminus - a GPCR, mCitrine (FRET acceptor), ER/K linker, mCerulean (FRET donor) and a 27 amino acid peptide (*x*-pep; *x* denotes the type of Gα subunit – t, s, i, q; t-mod is a modified peptide that interacts with high affinity to activated rhodopsin (17)) derived from the α5 helix of the Gα c-terminus (see Methods). In addition, we developed sensors containing only the receptor (no-pep), which were used to measure background FRET, cyclic AMP (cAMP) levels, ligand-binding affinities and G protein activation. Intact sensor protein localized primarily at the plasma membrane (Fig. 2.1b,c). β2-AR sensors display a functional response (cAMP) to agonist treatment (isoproterenol - ISO), which can be suppressed by the potent inverse agonist ICI118,551 (ICI) (Fig. 2.1d). Over-expression of β2-AR-no-pep sensors (500±100 fmol/mg) resulted in a substantial increase in basal cAMP relative to untransfected control (Fig. 2.1d). The elevated basal cAMP levels for β2-AR are consistent with previously reported basal activity for this GPCR (31). The specificity of this basal signaling was evident in the reduction in basal cAMP levels following inverse agonist (metoprolol or ICI) treatment (Fig. 2.1d). For the consistent level of sensor expression (see Methods) used throughout the study, sensors are expressed at least 5-fold in excess of endogenous Gαs, Gαi2 and Gαq (Fig 2.2a,b). Over-

expression of Gα subunits (> 5-fold) relative to untransfected levels does reduce the basal FRET in a Gα subtype specific-manner (Fig. 2.2c,d).

2.3.2. Validation of SPASM sensor response – The SPASM sensors are designed for FRET-based detection of ligand/mutagenesis-induced stabilization of GPCR conformations that favor interactions with different G proteins (Fig. 2.3a) (10). Several studies have shown that peptides derived from the Gα c-terminus interact with the GPCR following stimulation with canonical agonists (11-13). Further, the ligand-stimulated GPCR preferentially interacts with the Gα c-terminus that it signals through (18,19). Accordingly, activation of opsin (*9*-cis-retinal + light) results in a greater FRET gain (ΔFRET ratio) for the opsin-t-pep compared to the opsin-s-pep sensor (Fig. 2.3b). The opsin-t-mod sensor uses the previously identified modified t-peptide that binds with a higher affinity than native t-pep, and correspondingly shows a larger ΔFRET ratio compared to the other sensors (Fig. 2.3b). Given that FRET-based detection involves excitation of the sample with light (430 nm) that photoisomerizes *9-cis* retinal (< 600 nm), resulting in the activation of dark rhodopsin, the ΔFRET ratios presented here compare ligand-free opsin with light-activated rhodopsin (metarhodopsin (14)). In contrast, agonist (ISO) stimulation results in enhanced FRET for β2-AR-s-pep but not for the t-pep, i-pep or q-pep sensors (sample spectra Fig. 2.3c,d; compiled data Fig 3e). This is in accordance with the canonical coupling of β2-AR to Gs following activation (Fig. 2.1d). We note that the Gα c-terminus peptides used in this study are 27 amino acids long, essentially encompassing the entire α5 helix of the Gα subunit (12). This length of peptide was selected to potentially preserve their helical structure. Regardless of peptide length, the FRET gain for the β2-AR-s-pep sensor is preserved for three different length native peptides (Fig. 2.3e (inset); s11, s17 and s-pep contain respectively the last 11, 17 and 27 amino acids of the Gα c-terminus; *x*-pep (Fig. 2.3a) contains the last 27 amino acids of the Gα*x* c-terminus). This result is consistent with the involvement of only the last 11 amino acids in the GPCR-G-protein binding interface (11). Specificity in the FRET gain is further evident in the concentration dependence of the ISO response (Fig. 2.3f). The FRET gain at saturating ISO concentrations (100 μM) can be competitively suppressed by the potent inverse agonist ICI (Fig. 2.3f). As an alternative to agonist activation, the FRET levels in sensors expressing constitutively activating mutations, CAM and L272A (see Methods), were also examined (32,33). Introducing

either set of mutations in β2-AR-no-pep resulted in over a 2-fold increase in basal (ligand-free) cAMP accumulation, attesting to the stabilization of Gs conformations of this GPCR (Fig. 2.3g). Correspondingly, mutant versions of the β2-AR-s-pep sensors showed significantly elevated FRET levels compared to their wild-type counterparts (sample spectra Fig. 2.3h; compiled data Fig. 2.3i). None of the β2-AR mutants in this study alter background (β2-AR-no-pep) FRET levels (data not shown). The FRET ratio is an ensemble measurement of ~ 5000 cells in the excitation volume of the fluorometer cuvette (based on measured Optical Density (600 nm) of cell suspension of 0.3 for 3 mm path-length). Hence, unlike fluorescence microscopy based FRET evaluation in individual cells, the FRET ratio represents a bulk measurement that averages over potential heterogeneity across the population of cultured cells. Hence, despite the small changes in FRET, the differences in the measured FRET response are reproducible (Fig. 2.3c,d,h) and statistically significant (Fig. 2.3b,e,i), with a finite spread in the distribution of measurements both within and across experiments (Fig. 2.3j).

2.3.3. Linking E/DRY motif to receptor conformation (β2-AR versus opsin) – High-resolution structures of β2-AR bound to inverse agonist (Fig. 2.4a; top panel) display electrostatic interactions between R131 (E/D<u>R</u>Y) and both D130 (E/<u>D</u>RY) and E268 (22). In contrast, these interactions appear significantly weaker following agonist stimulation (Fig. 2.4a; bottom panel) (15). While there is a correlation between the E/DRY ionic interactions and GPCR conformation, a causative connection between them has not been established. The D130N mutant does show enhanced basal signaling, suggesting the need for these interactions to suppress basal activity (Fig. 2.4b). However, the controversy is evidenced by the absence of enhanced downstream signaling upon mutagenesis of the R131 (R131A; Fig. 2.4b), despite it being essential to form the ionic interactions. The R131A mutant is also deficient in providing an agonist-stimulated functional response (Fig. 2.4c). β2-AR-s-pep sensors provide evidence for stabilization of Gs conformations following mutagenesis of any of the residues (D130N, R131A, E268N) that form the ionic interactions, and the phenotype is compounded by a double-mutant (D130N+E268N – D/E; Fig. 2.4d). The basal stabilization of Gs conformations is also evident in the absence of further FRET gain following stimulation with ISO (Fig. 2.4e). Both D130N and R131A mutants are capable of binding ISO as witnessed by competitive inhibition of [^{3}H]-DHA binding to the

21

receptor in the β2-AR-no-pep sensor (Fig. 2.4f). In fact affinity of ISO binding is substantially enhanced for both D130N and R131A mutants compared to wild-type (K_i = 335 nM for wild-type; K_i = 8 nM for D130N; K_i = 20 nM for R131A). These results are consistent with a conformational change in β2-AR, upon mutagenesis of either D130 or R131, that mimics the effect of G protein binding, leading to ternary complex formation (34). However, only the D130N but not the R131A mutant enhances G protein activation as witnessed by enhanced basal ^{35}S-GTPγS uptake (Fig. 2.4g). Basal ^{35}S-GTPγS uptake is measured as the difference in scintillation counts (counts-per-minute - cpm) between basal and ICI118,551 (10 μM) inhibited conditions for 62 fmol of receptor per condition (wild-type/mutant; see Methods). This measurement facilitates comparison of specific ^{35}S-GTPγS uptake resulting from equal amounts of the wild-type receptor, without the complication of varying levels of non-specific ^{35}S-GTPγS binding caused by differential expression of wild-type and mutant sensors. Importantly, the affinity of ICI118,551 binding is similar between wild-type, D130N, and R131A mutant receptors (K_i ~ 0.1 nM; Fig. 2.4h). Taken together, these complementary approaches dissect the molecular basis for differential signaling from E/D and R mutants. While both E/D and R mutants cause conformational changes in β2-AR that enhances G protein interactions, only E/D but not R mutants increase G protein activation.

In contrast, mutagenesis of either of the residues (E134N (ED/RY), R135A (E/DRY) or E247N; Fig. 2.5a) implicated in similar ionic interactions for opsin (35) does not alter basal (ligand-free) FRET levels (Fig. 2.5b). Activation of opsin (9-cis-retinal + light) provides a substantial FRET gain for E247N and E134N but not R135A (Fig. 2.5c). Thus, the E/DRY motif interactions do not appear to be necessary for stabilization of the basal state in opsin. These results are not surprising, given a second prominent set of opsin-specific ionic interactions that are also important for ligand (retinal) binding (K296, E113; Fig. 2.5d) (24). Mutagenesis of either of these residues (K296A/G/E, E113Q) substantially elevates basal FRET levels (Fig. 2.5e). Presentation of counter-ions to K296 by mutagenesis of G90 (G90D) or A292 (A292E) also enhance basal FRET (24). Thus, the ionic interactions centered on K296 are necessary and sufficient to stabilize opsin in its basal state. Opsin stimulation (9-cis-retinal + light) results in a substantial FRET gain for wild-type, G90D, A292E and E113Q, but not K296A/E/G (Fig. 2.5f). The latter result is consistent with the need for the K296 residue for binding retinal (25).

22

2.3.4. Inverse agonism of β2-AR requires a functional E/DRY motif - High-resolution structures of the receptor bound to inverse agonists display an intact ionic-lock (Fig. 2.6a) (21,22). This suggests that the inverse agonist stabilizes the ionic-lock, however a causative mechanism remains to be established. To test this connection, the effects of the inverse agonist ICI on β2-AR-s-pep sensors were examined in the context of WT and E/DRY motif mutants. Sensors with a single counter-ion (E268N or D130N) mutation showed sensitivity to ICI (suppression of cAMP and decreased FRET; Fig. 2.6b,c) whereas a double mutant that abolishes the ionic-lock (D130N+E268N) showed a reversal of FRET response with minimal suppression of constitutive activity (Fig. 2.6b,c). Together, these results suggest that the function of inverse agonist ICI requires an intact E/DRY motif. In contrast, the inverse agonist metoprolol does not affect the FRET levels for the D130N mutant (Fig. 2.6b). This suggests that inverse agonism of metoprolol is distinct from that of ICI.

2.3.5. Metoprolol stabilizes Gi conformations – Inverse agonist suppression of basal cAMP signaling can be achieved by reducing Gs activity or enhancing Gi. While a previous study has demonstrated that metoprolol suppresses cAMP accumulation, it did not distinguish between effects on Gs and Gi (26). Metoprolol (150 μM) decreases FRET levels for the β2-AR-s-pep sensor, while elevating FRET levels for the β2-AR-i-pep sensor in a dose-dependent manner (Fig. 2.7a,b). Thus metoprolol appears to stabilize Gi conformations at the expense of those that promote interactions with Gs. To test whether the Gi conformations precipitates a Gi-dependent response, we examined the pertussis-toxin (PTX) sensitivity of the forskolin response (10 μM). Metoprolol inhibition of cAMP accumulation was sensitive to PTX treatment, a characteristic of Gi stimulation induced by a receptor-ligand combination (Fig. 2.7c) (36). In contrast, saturating concentrations of ICI (10 μM) did not alter basal FRET levels for either the β2-AR-s-pep or β2-AR-i-pep sensors, nor is its inhibition of cAMP accumulation PTX sensitive (Fig. 2.7a,c). Together, these results suggest that metoprolol stabilizes Gi conformations in β2-AR, which in turn enhance coupling to Gi.

2.4. Discussion

2.4.1. Detecting the stabilization of G protein specific conformations of a GPCR – The phenomenon of functional selectivity, wherein the same GPCR can signal through multiple effectors (G proteins/arrestin) is well established (8). The emerging view in the field suggests that GPCRs exist in a continuum of conformations with certain subsets more or less favorable for interactions with one or more effectors (1). Ligands stabilize non-identical subsets of GPCR conformations leading to their traditional classification as agonists, partial agonists, antagonists, inverse agonists and biased agonists (7). Recent structural studies have detected ligand-specific stabilization of β2-AR conformations (2-5), but do not directly link them to function in the absence of documented functional responses in cell or membrane preparations (6,26,37). Given the wide range of factors that influence the functional response, there is a need for complementary tools that can detect the stabilization of G protein selective conformations (9).

A well-characterized determinant of G protein selection is the c-terminus of the Gα subunit (18,19). The Gα subunit inserts itself into a cytosolic groove formed in the activated GPCR (14,15). Hence, we hypothesized that peptides derived from the Gα c-terminus could be used as 'bait' to detect G protein selective conformations of a GPCR. Sensors developed using the SPASM technique (10) detect ligand/mutagenic stabilization of GPCR conformations that result in changes in interaction with one or more G protein peptides. The enhanced G protein interactions can result in enhanced downstream signaling. However, the conformational states detected by the sensor are not necessarily identical to those that trigger G protein activation. Hence, sensor readout needs to be verified using complementary approaches such as examination of second messenger levels, ligand-binding affinities (evaluates ternary complex formation) and G protein activation.

In this study we show that β2-AR, a GPCR that has been proposed to signal through both Gs (canonical) and Gi (37,38), displays ligand-dependent conformations that promote interactions with Gs and/or Gi (Gs and Gi conformations). While the classic agonist isoproterenol stabilizes Gs conformations, the inverse agonist metoprolol stabilizes Gi conformations (Fig. 2.7). Ligand-free β2-AR is known to stimulate cAMP accumulation and several inverse agonists reduce this basal activity (26,31). Given that cAMP accumulation is regulated by both Gs and Gi, it remains to be established whether inverse agonists suppress Gs and/or activate Gi. Hence, pertussis-toxin (PTX) treatment was used to uncover a new Gi-dependent activity for metoprolol but not ICI.

Accordingly, only metoprolol but not ICI stabilizes Gi conformations. Together, these studies support the presence of Gs and Gi conformations of β2-AR that can be stabilized in a ligand-dependent manner.

2.4.2. What is the role of the E/DRY motif in GPCR conformation? – High-resolution structures of GPCRs stabilized bound to inverse agonists show strong electrostatic interactions centered on residues in the conserved E/DRY motif (22,39). In contrast, these residues move apart in structures of GPCRs activated with agonist (14,15). This has led to the model that the E/DRY ionic interactions (ionic-lock) are required to stabilize GPCRs in an inactive state (20,21). While structural studies support this model, they have not established cause-and-effect between ionic-lock stabilization and GPCR inactivation. This model posits that disrupting the ionic-lock would be sufficient to transition the GPCR to an active conformation, resulting in constitutive (ligand-free) activity (20). However, mutation of the acidic (E/D) but not basic (R) residues enhances basal activity of the GPCR as measured from the downstream functional response (cAMP) (20,40). Therefore, functional studies have not resolved the role of the E/DRY ionic-lock in GPCR conformation. In this study, the SPASM sensors were used to de-couple conformational changes in the GPCR (as detected by Gα c-terminus peptide binding) from the downstream response (cAMP) to show that for β2-AR, mutagenesis of either of the residues that form the ionic-lock is sufficient to enhance interactions with Gs. However, R mutants do not show enhanced cAMP accumulation, in line with our finding that they do not enhance G protein activation. Opsin is a notable exception to the role of the E/DRY motif, in that it has a second, unique, ionic-lock centered residue K296 at the ligand-binding interface (24). We find that mutagenesis of the K296 ionic-lock, but not the one formed by the E/DRY motif is sufficient to transition this GPCR to an active conformation. Thus, while the role of the E/DRY motif continues to be receptor-specific, the use of the SPASM sensors complemented with traditional approaches allows us to directly examine the role of intramolecular interactions on GPCR conformation.

2.4.3. Severity of disease phenotype correlates with stabilization of a GPCR active conformation - Retinitis pigmentosa (RP) affects 1 in 4000 of the general population with symptoms ranging from night blindness to complete loss of eyesight (41). Over 25% of autosomal dominant RP

patients have a single point mutation in opsin, with over 120 mutations documented to date (42). A subset of RP mutations constitutively activates opsin by perturbing the K296-E113 ionic interaction within this receptor (24,43). The effects of these mutations on opsin function have been inferred primarily by examining signaling downstream of transducin (Gαt), such that the molecular mechanisms translating these mutations to differential disease phenotype remain poorly understood (43). Mutation of residue K296 (A/E/G) leads to severe RP, causing blindness (24). Mutations that introduce a destabilizing counter-ion to K296 (G90D or A292E) instead lead to mild RP, resulting in night-blindness (24). We report that most of these mutations (with the exception of G90D) increase the strength of interaction of opsin for a peptide derived from the transducin c-terminus. Our finding is in line with the current model of constitutive activation of opsin in RP (24,43). Importantly, the gain in basal affinity directly correlates with the reported severity of RP phenotype (K296G/A > K296E > A292E > G90D). Hence, our results support a model wherein the K296 mutant enhances its interaction with transducin in a retinal-independent manner (24,44). In contrast, the counter-ion mutants only partially populate an active conformation in the basal state and need a combination of retinal and light for full activity.

2.4.4. Distinct mechanisms for different inverse agonists - The basal activity of β2-AR suggests that it samples both active and inactive states in the absence of ligand (31). Therefore, it is not surprising that high-resolution structures of β2-AR with an intact E/DRY ionic-lock have all been obtained in the presence of ligands that suppress basal signaling (inverse agonists) (22). While these structures suggest a connection between inverse agonists and the E/DRY motif, it remains to be established whether the ionic-lock is necessary for inverse agonist function. Here, we find that efficient suppression of β2-AR basal activity by the potent inverse agonist, ICI118,551, is dependent on the integrity of the E/DRY ionic-lock. Disruption of the ionic interactions formed by the E/DRY motif reduces ICI's ability to suppress β2-AR basal signaling. In contrast, metoprolol suppresses basal activity by enhancing β2-AR interactions with Gi, rather than stabilizing the E/DRY ionic-lock. The distinct mechanisms of inverse agonism for metoprolol and ICI, along with the tools developed here to detect the relative stabilization of G protein selective receptor conformations need to be factored into the identification and selection of inhibitors that target GPCR function.

26

2.4.5. SPASM sensor toolbox - This study uses the recently developed technique termed Systematic Protein Affinity Strength Modulation (SPASM) to directly detect the interaction between a GPCR and native peptides derived from the c-terminus of the Gα subunit. The specificity of the FRET response is validated with two prototypical GPCRs, β2-AR and opsin that show selectively enhanced interaction for the c-terminus of Gαs and Gαt (transducin) respectively, following GPCR activation (opsin – *9-cis*-retinal+light; β2-AR – ISO). Further, as expected, constitutively active mutants of both GPCRs display enhanced interactions relative to their wild-type counterparts. The enhanced FRET with agonist is dose-dependent and can be competitively inhibited with an inverse agonist. The FRET measurements of the sensor can be influenced by competition with endogenous G proteins. However, the consistent levels of sensor expression (± 20%) used throughout the study, along with the tools to measure expression relative to endogenous Gα subtypes factors in the effects of endogenous G proteins.

The functional significance of Gi conformations mediated by metoprolol is verified by a standard pertussis-toxin (PTX) sensitivity assay. The studies with the E/DRY motif and the opsin K296 ionic-lock support existing models for their function, while providing much needed clarity on their influence in stabilizing GPCR conformations. Therefore, taken together, this study is a first defined step towards the use of these sensors to broadly examine G protein selective GPCR conformations.

2.5. Experimental Procedures

2.5.1. Buffer and Reagents - 9-*cis*-retinal, (-)-isoproterenol (+)-bitartrate salt, fenoterol hydrobromide, ICI118,551 hydrochloride, (±)-propranolol hydrochloride, (±)-metoprolol (+)-tartrate salt, forskolin, pertussis toxin (PTX), 3-isobutyl-1-methylxanthine (IBMX), and poly-L-lysine were purchased from Sigma-Aldrich. Bovine retinal cDNA was acquired from Zyagen. Human β2-adrenergic receptor (β2-AR), Gαq, Gαi2, and long splice variant of human Gαs cDNA clones were obtained from Open Biosystems. Gαs (sc-823), Gαq (sc-393), and Gαi2 (sc-13534) antibodies were acquired from Santa Cruz Biotechnology Inc. Buffer A is HEPES buffered saline supplemented with 0.2% dextrose (w/v), 500 μM ascorbic acid and 1.5 μg mL^{-1} aprotinin and 1.5 μg mL^{-1} leupeptin at pH 7.45.

2.5.2. Molecular Cloning - A modular cloning scheme was used to construct the different GPCR sensors. All GPCRs sensors were expressed as single polypeptides. Opsin and β2-AR were derived from PCR of bovine retinal cDNA and human cDNA respectively. Briefly, GPCR (β2-AR or Opsin), mCitrine, 10 nm ER/K α-helix, mCerulean and Gα c-terminus peptide/Gα were sequentially cloned between HindIII, XbaI, EcoRI, AscI, PacI, NotI restriction sites in the PCS2 vector. No-pep sensors did not contain peptide after mCerulean, and instead had a repeating (Gly-Ser-Gly)$_4$ residues. Constructs were then subcloned into the PCDNA5/FRT vector between HindIII and NotI. A (Gly-Ser-Gly)$_4$ linker was inserted between all protein domains as part of the primer sequence to allow for free rotation between domains. An N-terminal HA-tag was inserted in frame to all β2-AR-sensors. All mutant constructs were generated via PCR using oligonucleotide-directed mutagenesis (QuikChange Site-directed Mutagenesis Kit, Stratagene). Peptides encoded the last 27 C-terminal residues of the corresponding Gα. The following amino acid sequences were used:

(1) t-mod: KQRNMLENLKDCGLF

(2) t-pep: DTQNVKFVFDAVTDIIIKENLKDCGLF

(3) s-pep: DTENIRRVFNDCRDIIQRMHLRQYELL

(4) i-pep: DTKNVQFVFDAVTDVIIKNNLKDCGLF

(5) q-pep: DTENIRFVFAAVKDTILQLNLKEYNLV.

All constructs were confirmed by sequencing. The wild-type sensors developed for this study, along with detailed plasmid maps to subclone other GPCRs, are available through the AddGene plasmid depository (http://www.addgene.org/Sivaraj_Sivaramakrishnan).

2.5.3. Sensor Protein Expression and Cell Preparation: HEK293T-Flp-in (Invitrogen) cells were cultured in DMEM supplemented with 10% FBS (v/v), 4.5 g/L D-glucose, 1% Glutamax, 20 mM HEPES, pH 7.5 at 37°C in humidified atmosphere at 5% CO_2. HEK293T-Flp-in cells (Passages 10-30) were plated into tissue-culture treated dishes at ~ 30% confluence. Cells were allowed to adhere for 16-18 hr followed by transient transfection of sensor plasmid DNA (pCDNA/FRT; Invitrogen) with Fugene HD (Promega). Transfection conditions were optimized (2.5 μg DNA + 8 μl reagent) to reproducibly obtain primarily membrane expression of sensors 22-32 h post transfection (evaluated at 40x magnification on a Nikon tissue-culture microscope enabled with

fluorescence detection). For each experiment, expression was quantified to ensure that at least 80% of cells expressed primarily plasma membrane-bound protein, without detectable localization of protein to intracellular compartments. At least 75% transfection efficiency (percentage of visibly fluorescent cells) was consistently achieved using this protocol. The length of transfection (22-32 h) was optimized for each sensor to maintain consistent expression levels (± 20% across experiments and sensors). Sensor expression was evaluated by fluorescence measurement at matched optical density of cell suspension. Cells were re-supsended by gentle pipetting (no trypsin/EDTA treatment) and washed once with Buffer A. Cells were re-suspended at fixed density for all measurements (O.D. of 0.3 (600 nm; 3 mm pathlength)). Sensor expression was evaluated by mCitrine fluorescence (FRET acceptor; Fluoromax-4 – Excitation (Ex) 490 bandpass 8 nm; Emission (Em) 500-600 bandpass 4 nm) and was held within 2.6-3.8×10^6 counts-per-second. For each sensor, both mCitrine fluorescence and percentage of membrane expression were recorded for each experiment to ensure consistency. Cells were maintained at 37 ℃ throughout the experiment (all buffers were pre-warmed to 37° C; fluorometer cuvette-holder was maintained at 37 ℃) and the experiment was completed within 30 min of cell re-suspension in Buffer A (each FRET spectrum required ~ 1 min of acquisition time). For opsin, cells were incubated in the presence or absence of 9-*cis*-retinal for 1 h at 37℃ in the dark in Buffer A. Cells were exposed to ambient light for 1 min before recording FRET spectra. For β2-AR experiments involving ligands, cells were aliquoted (90 μl) and ligand diluted in HBS buffer was added (10 μl). A matched aliquot with Buffer A (10 μl) was used as a control to avoid repeated measurements of the same sample. Measurements of control and ligand-treated conditions were performed either alternately or within 5 min of each other (no measurable difference between procedures). Each agonist (ISO) treated aliquot was incubated for 3-5 min, whereas those treated with inverse agonists were incubated for 5-10 min before acquisition of spectra. Separate micro-cuvettes were used for control and treated samples to avoid cross-contamination.

2.5.4. Fluorescence Resonance Energy Transfer (FRET) Measurements - FRET spectra were generated by exciting cells at 430 nm (spectral bandpass 8 nm), and scanning emission from 450-600 nm (bandpass 4 nm) on a FluoroMax-4 fluorometer (Horiba Scientific). For mCitrine-only measurements, cells were excited at 490 nm (bandpass 8 nm) and emission was recorded from

500-600 nm (bandpass 4 nm). Each experimental condition for β2-AR constructs was collected within 30 min of re-suspension in Buffer A at 37 °C.

2.5.5. Live Cell FRET Ratio Calculations - OD measurements were taken for untransfected and transfected cells in Buffer A; appropriate volumes of media were added to achieve an OD-600nm reading of 0.3 (BioRad SmartSpec Plus Spectophotometer, 3 mm path-length, quartz cuvette). FRET (mCerulean Ex: 430 nm, Em: 450-600 nm) emission spectra were corrected for cell-scattering noise by subtracting spectra for untransfected HEK293 cell suspensions. FRET emission spectra from the FRET emission spectra of transfected cells of matched cell density (OD). The corrected fluorescence emission spectra were then normalized to mCerulean emission (475 nm). FRET ratio was measured by calculating ratio of normalized emission of mCitrine (525 nm) to mCerulean (475 nm).

2.5.6. Quantification of cAMP Production - HEK293T-Flp-in cells were transiently transfected with HD-Fugene (Promega) according to the vendor's instructions and cAMP levels were assessed using the cAMP Glo luminescence based assay (Promega). Where indicated, 12 h after transfection, cells were incubated with 100 ng mL^{-1} PTX for 16 h. Briefly, 24-27 h post transfection, cells were gently resuspended in DMEM containing 10% FBS (v/v), spun down and resuspended in PBS supplemented with 800 μM ascorbic acid and 0.02% glucose, and aliquoted into 96-well flat-bottom opaque microplates. For assessment of basal cAMP levels, cells were incubated with 0.5 mM IBMX/PBS for 20 min at 37°C and exposed to 150 μM metoprolol, 10 μM ICI118,551, or buffer control for an additional 15 min at 37°C. For forskolin treatment, cells were incubated with 10 μM forskolin in the presence or absence of 150 μM metoprolol or 10 μM ICI118,551 for 15 min at 37°C. For isoproterenol treatment, cells were pre-incubated in the presence of absence of 150 μM metoprolol or 10 μM ICI118,551 for 5 min and subsequently treated with 100 μM of isoproterenol for 3 min. After incubation with respective small molecules, cells were lysed and protocol was followed according to manufacturer's recommendations (Promega). Luminescence was measured using a microplate luminometer reader (Synergy 2, BioTek). cAMP production was normalized to the total amount of β2-AR sensor protein expressed as indicated by mCitrine fluorescence levels (Ex: 490 nm, Em: 525 nm).

2.5.7. Live Cell Microscopy and Image Analysis - Cells were imaged at 60x magnification using a Nikon TiE microscope equipped with a mercury arc lamp, 63x and 100x 1.4 Numerical Aperture Plan-Apo oil objectives and on an Evolve 512x512 EM-Charge-Coupled-Device camera (Photometrics). Cells were imaged on 35 mm glass bottom dishes (MatTek Corp) coated with 0.001% poly-L-lysine/PBS. 16 h after plating cells on poly-L-lysine coated MatTek plates, cells were transfected with Mirus-LT or HD-Fugene (Promega). 18-24 h post-transfection cells were washed multiple times with warm Buffer A to remove excess phenol red from the media and were subsequently imaged in warm Buffer A. Z-stack images were taken with 1 μm steps and the resultant stack of images was deconvolved using AutoQuantX software.

2.5.8. Membrane Preparation – Membrane preparation follows a protocol modified from Clark et al. (28). HEK293 cells expressing indicated sensors were washed once with ice-cold PBS buffer. Cells were resuspended in a ice-cold hypotonic buffer (Buffer B - 20 mM HEPES pH = 7.4, 0.5 mM EDTA, aprotinin (1.5 μg mL^{-1}), leupeptin (1.5 μg mL^{-1}), 0.1 mM DTT), incubated for 30 min (4 °C) on a rotator, and lysed with a FisherBrand rotary pestle for 30 s. Lysated were cleared by centrifugation (500g, 5 min), followed by pelleting of membranes (40,000g, 20 min). Membranes were washed once with Buffer B + 3 μM GDP + 5 mM MgCl$_2$ (10s resuspension with rotary pestle) and re-spun at 40,000g for 20 min. Pellets were resuspended in identical buffer to a concentration of 0.5 – 1 mg/ml, aliquoted and frozen at -80 °C. Total protein concentration (mg/ml) was calculated using a DC Protein Assay (BIO-RAD).

2.5.9. Protein Expression Levels - HEK293 cell membranes expressing β2-AR control or β2-AR-s-peptide sensors were collected 24 h post transfection. Samples were treated with PNGase F and Endo H (3 h at room temperature) to remove β2-AR glycosylation sites. Supernatant (S) and pellet (P; containing membranes) were separated on 4-15% gradient polyacrylamide/SDS gel. Concentration (mol/mg) of sensor was assessed by loading mCitrine concentration standards alongside a known concentration (mg/mL) of membranes expressing β2-AR control sensor on a SDS-PAGE. Gels were scanned for fluorescence on a Typhoon Gel Imager (GE Healthcare) by exciting mCit at 488 nm and scanned at 520 nm BP 40.

2.5.10. Western Blotting – Membranes expressing indicated sensor were prepared as described above. Briefly, membranes were separated on 10% polyacrylamide/SDS gels and scanned for fluorescence on a Typhoon Gel Imager (GE Healthcare) before being transferred to PVDF membranes for 3 hours at 300 mA. Blots were blocked with 5% milk/TBST for 1 hour. Primary Gαs antibody (N-terminal; sc-823, Santa Cruz Biotechnology, Inc) or Gαq antibody (N-terminal; sc-393, Santa Cruz Biotechnology, Inc) were used at a concentration of 1:1000 in 2% BSA/TBST and incubated overnight at 4°C. Blots were washed with TBST (3x 10 min) before addition of secondary antibody (goat anti-rabbit (Jackson ImmunoResearch), 1:2000 in 5% milk/TBST) and incubated at room temperature for 1 hour. Blots were washed again with TBST (3x 10 min) and developed using Immobilon Western Chemiluminescent HRP Substrate (Millipore). Blots were either imaged using film or using a ChemiDoc-it Imaging system (UVP) with no discernable difference in quality of signal.

2.5.11. Radio-ligand assays – Radioligand assays follow previously published protocols (29). Bmax values were estimated by incubation of 2.5, 5, and 10 μg of membrane with 5 nM [^{3}H]-dihydroalprenolol ([^{3}H]-DHA; PerkinElmer) for 90 min at room temperature in Tris-Buffered-Saline (TBS) pH 7.4. Samples were transferred to GF/C membranes pre-treated with 0.3% polyethylenimine solution in TBS, washed extensively with TBS, treated with scintillation liquid (Microscint0; PerkinElmer), followed by measurement of radioactivity using a 96-well scintillation counter (TopCount, PerkinElmer). Non-specific binding was estimated with 10 μM propranolol treatment and was < 1% of total binding. Dissociation constant (K_d) of [^{3}H]-DHA binding was determined by incubation of 10 pM (10 fmol/ml) of receptor with increasing concentrations of [^{3}H]-DHA. K_d of [^{3}H]-DHA binding was ~ 0.2 nM for wild-type, D130N and R131A β2-AR-no-pep sensors. Competitive inhibition (K_i) was assessed by incubation of 10 pM of receptor with increasing concentrations of isoproterenol (ISO), ICI118,551 (ICI) or buffer blank with 5 nM [^{3}H]-DHA for 90 min at room temperature. Radioactivity in samples for K_d and K_i experiments was measured as described above. Non-specific binding in all instances was found to be <1%. Each experiment was done at least twice with different membrane preparations, with three separate samples prepared per condition, per experiment.

2.5.12. ³⁵S-GTPγS binding assays – Radio-labeled GTPγS assays follow previously published procedures (28,30). Briefly, 60 fmol of wild-type or mutant (D130N or R131A) β2-AR-no-pep sensor expressing membranes (14–33 µg of membrane; receptor amounts determined by radio-ligand Bmax binding as described above) were incubated in Buffer C (20 mM HEPES pH 7.4, 100 mM NaCl, 5 mM $MgCl_2$, 0.1 mM DTT, 100 µM GDP, 0.02% ascorbic acid) for 10 min at room temperature, followed by incubation with 10 µM ICI118,551 or buffer control for 10 min. Membranes were treated with 1 nM ³⁵S-GTPγS (PerkinElmer) for 60 min at room temperature, followed by assessment of membrane radioactivity levels as described above. GDP concentration and incubation times used were empirically determined to provide the largest specific binding to 14 µg of membrane expressing wild-type sensor (β2-AR-no-pep) relative to equal amount of untransfected membrane protein. Data are presented as difference between radioactivity counts (counts per minute) between untreated and ICI treated membranes. The experiment was repeated three times, with different membrane preparations, and involves three separate samples in each experiment.

2.5.13. Statistical Analysis - Results are expressed as mean values $\pm$ s.e.m of at least three independent experiments with at least six repeats per condition. Statistical analysis was carried out using GraphPad Prism 5.0c (Graphad Software Inc.) Statistical significance was evaluated using Student's paired t-tests performed are indicated in the figure legends with corresponding p-values of *$P \leq 0.05$, **$P \leq 0.01$, ***$P \leq 0.001$. Briefly, statistical significance was calculated using Student's paired t-test comparing samples to respective no-pep sensor (see Methods, Molecular Cloning) for FRET ratio measurements or to matched untreated condition for ΔFRET measurements. Sigmoidal curves from concentration-response experiments were analyzed using non-linear regression curve fitting using log(agonist or inhibitor) vs. response (three parameters). Each condition was repeated at least 6 times, and each experiment was independently conducted at least 3 times (n ≥ 18).

2.6. Notes

2.7. Figures
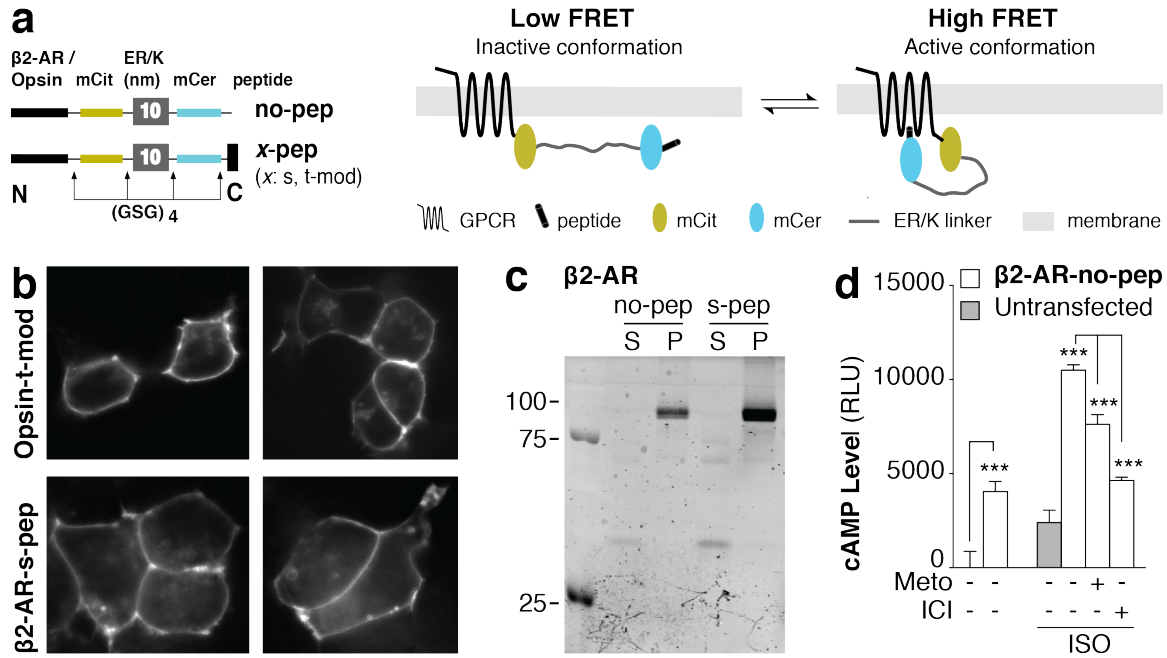
Fig. 2.1: FRET-based SPASM sensors for opsin and β2-AR are intact and functional. SPASM sensor design: **(a)** Schematics of the GPCR-Gα c-terminal peptide sensors (*left*); sensor in the inactive (*middle*) and active (*right*) conformation. Protein domains were separated with Gly-Ser-Gly (GSG)$_4$ linkers to ensure rotational freedom. No-pep sensors do not contain the Gα c-terminus peptide. **(b)** Opsin-t-mod and β2-AR-s-pep sensor localization to the plasma membrane in HEK293 live cells. **(c)** Fluorescence SDS-PAGE gel scans of HEK293 membranes expressing β2-AR no-pep or s-pep sensors. Intact membrane localization is witnessed by distinct 110 kDa bands in fractions containing membrane (P) but not supernatant (S). **(d)** cAMP levels in the presence or absence of agonist (100 μM isoproterenol) for untransfected (grey) or HEK293 cells expressing β2-AR-no-pep sensor (white). Specificity of agonist-stimulated sensor response was verified by suppression with antagonists (150 μM metoprolol or 10 μM ICI118,551). Results are expressed as mean ± s.e.m. ***$P < 0.001$; n > 10.
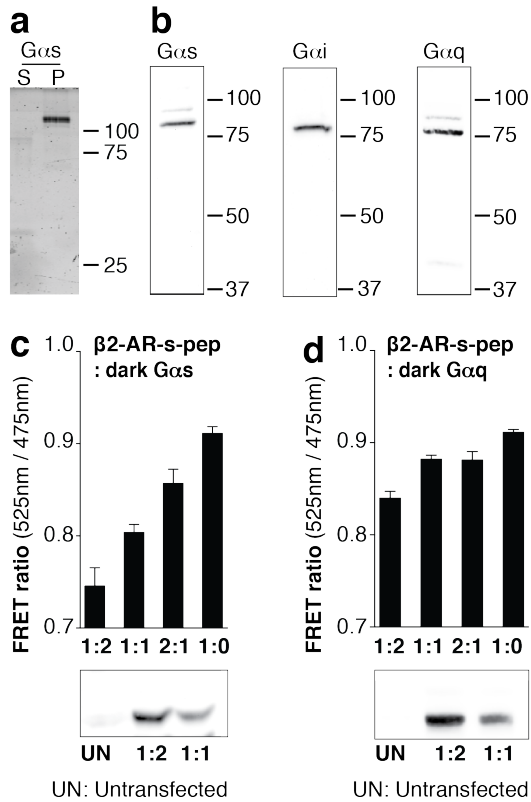
Fig. 2.2: Influence of endogenous Gα levels on sensor FRET measurements. (a-b) β2-AR sensors are expressed at least five-fold in excess of three endogenous Gα subtypes (s/i/q). **(a)** Fluorescence SDS-PAGE gel scans of HEK293 membranes expressing β2-AR-Gαs fusion sensor. **(b)** HEK293 membranes expressing the β2-AR-Gα fusion sensors were digested with TEV-protease to cleave a site between β2-AR-mCit and ER/K-α-helix-mCer-Gα. Membranes were separated by SDS/polyacrylamide gel electrophoresis, transferred onto PVDF membranes, and probed with anti-Gαs (sc-823; 1:1000), anti-Gαq antibody (sc-393; 1:1000) or anti-Gαi2 antibody (sc-13534; 1:200). Intact Gα expression is witnessed by distinct 80, 76 and 75 kDa bands for TEV-digested Gαs, Gαq and Gαi2 fusion sensors respectively. **(c-d)** FRET ratios (mCit/mCer; 525nm/475nm) of the β2-AR-s-pep sensor co-expressed with unlabeled (dark) **(c)** Gαs or **(d)** Gαq. Ratio of plasmid DNA of β2-AR-s-pep:Gα used for the transfections is indicated along abscissa (at least 5-fold over-expression of indicated Gα compared to endogenous Gα by densitometry). (Bottom panels) Immunoblots of membranes transfected with plasmid DNA at indicated ratios probed with **(c)** anti-Gαs or **(d)** anti-Gαq antibodies.
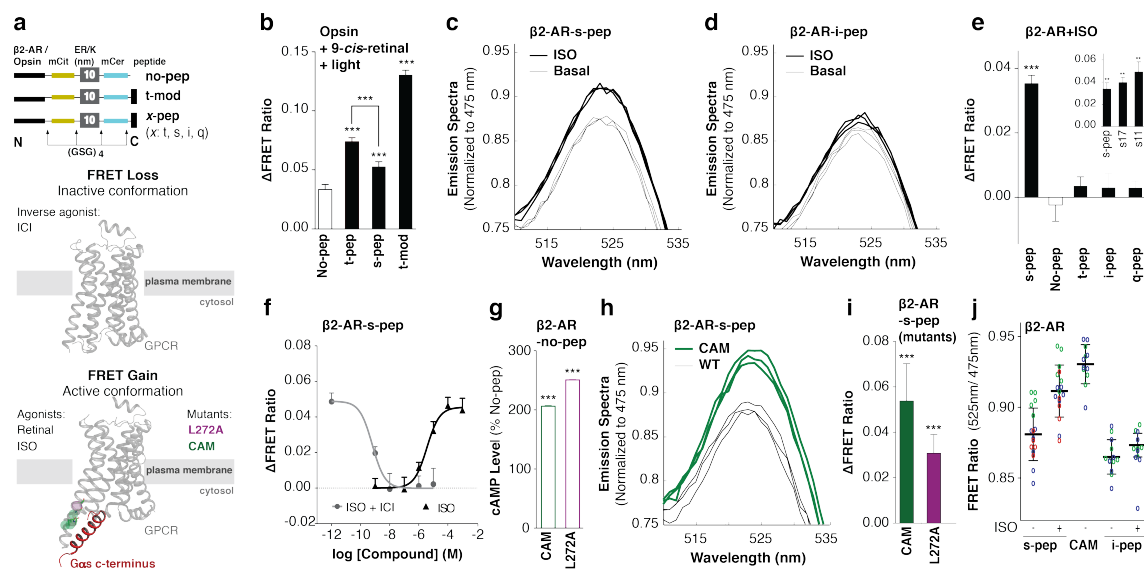
Fig. 2.3: Gα c-terminus peptide specifically binds to the active conformation of GPCRs in live HEK293 cells. (a) Schematics of the GPCR-Gα c-terminal peptide sensors (*top*); crystal structures of β2-AR in the inactive (*middle;* PDB: 3NY8) and active (*bottom;* PDB: 3SN6) conformation. Gαs c-terminus (s-pep; red) binds to the active β2-AR conformation induced via stimulation with agonist. **(b-j)** GPCR/condition specified at top left and sensor abbreviation along abscissa. **(b)** Change in FRET ratio following agonist (*9-cis*-retinal + light) treatment for opsin-pep sensors. FRET spectra (430 nm mCer excitation) normalized to mCer emission (475 nm) for **(c)** β2-AR-s-pep, **(d)** β2-AR-i-pep sensors for samples treated with or without agonist (isoproterenol). **(e-f)** Change in FRET ratio following agonist (isoproterenol) treatment for β2-AR-pep sensors. **(f)** Dose-dependent inhibition of FRET with inverse agonist (ICI118,551; grey line). **(g)** Basal cAMP levels for β2-AR-no-pep sensors expressing the constitutively active β2-AR mutants (CAM, L272A). **(h)** FRET spectra (430 nm mCer excitation) normalized to mCer emission (475 nm) for wild-type (WT; black) and a constitutively active mutant (CAM; green) β2-AR-s-pep sensor **(h)** Gain in FRET following induction of constitutively active mutations (CAM, L272A) for β2-AR-s-pep sensors. **(i)** Scatter-plot of individual FRET ratio measurements (open circles) for indicated β2-AR-pep sensors/conditions derived from three independent experiments (colored red, green and blue), collected on three different days. Results are expressed as mean ± s.e.m. ***$P < 0.001$; n > 18.
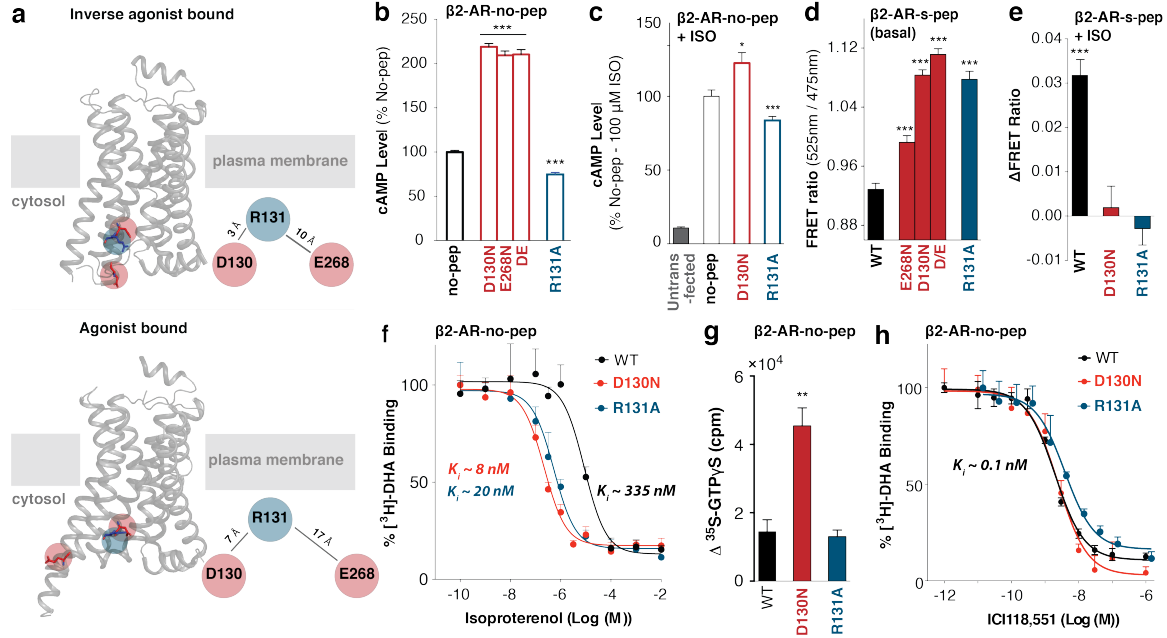
Fig. 2.4: Mutagenesis of E/DRY motif interactions in β2-AR induces an active conformation. (a) Crystal structures of β2-AR in the inactive (*top;* PDB: 3NY8) and active (*bottom*; PDB: 3SN6) conformation. *(Top)* In the inactive state, the DRY motif residues in β2-AR display electrostatic interactions formed between R131 (blue) and D130/E268 residues (red). *(Bottom)* Indicated residues move apart following β2-AR activation. **(b-e)** GPCR/condition specified at top left and sensor abbreviation along abscissa. cAMP levels of HEK293 cells expressing wild-type (no-pep) for the indicated E/DRY mutant β2-AR-no-pep sensor in the **(b)** absence or **(c)** presence of agonist (100 μM isoproterenol). **(d)** FRET ratios (mCit/mCer; 525nm/475nm) of β2-AR E/DRY motif single and double (D/E: D130N+E268N) mutant s-pep sensors. **(e)** Change in FRET following agonist (100 μM isoproterenol) treatment of E/DRY mutant β2-AR-s-pep sensors. **(f)** The affinity for agonist (isoproterenol) was measured for wild-type (WT), D130N, and R131A β2-AR-no-pep sensors by competitive inhibition of [³H]-dihydroalprenolol ([³H]-DHA) binding. Results are expressed as percent of radio-ligand bound in the absence of competitor. **(g)** Change in ³⁵S-GTPγS binding induced by 10 μM of inverse agonist ICI118,551 for wild-type (WT), D130N, and R131A β2-AR-no-pep sensors. **(h)** Competitive displacement of [³H]-dihydroalprenolol binding by ICI118,551 for WT, D130N, and R131A β2-AR-no-pep sensors. Results are expressed as mean ± s.e.m of three independent experiments performed in triplicate. *$P < 0.05$, ***$P < 0.001$; n > 18
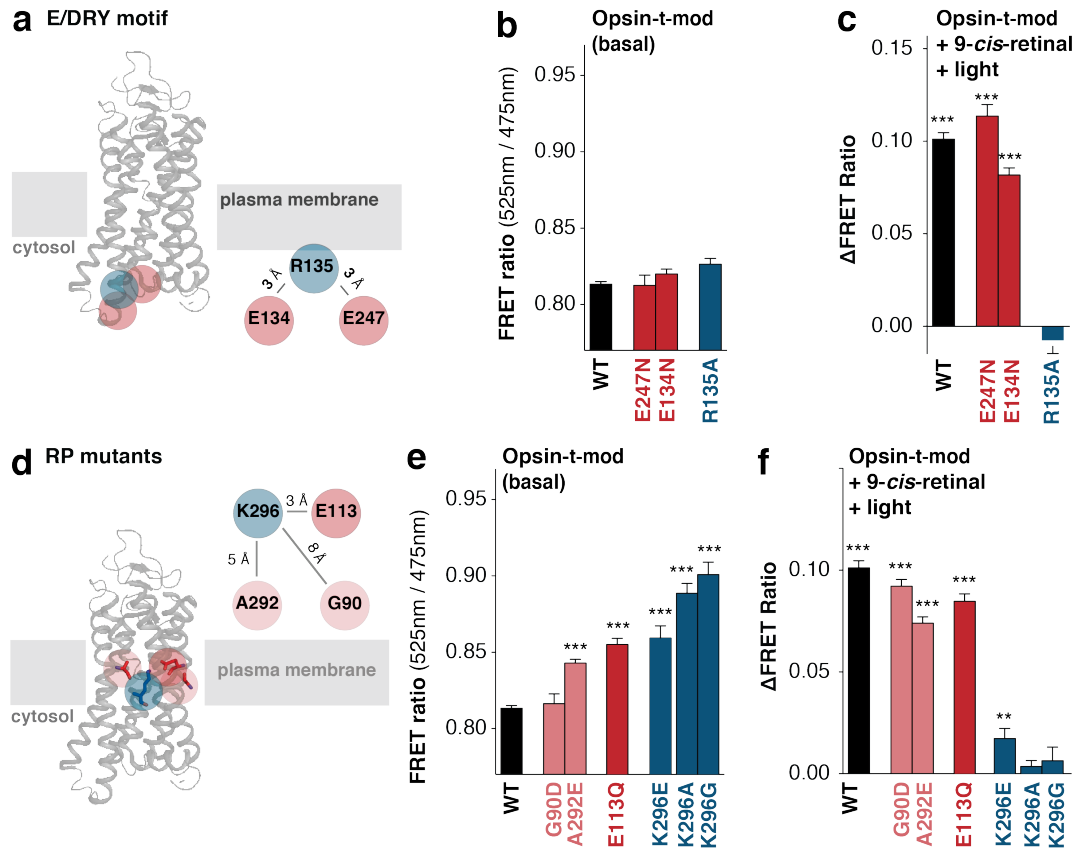
Fig. 2.5: Opsin-specific interactions centered on residue K296 are both necessary and sufficient to stabilize an inactive conformation. (a) Electrostatic interactions formed by the E/DRY motif are indicated on the crystal structure of inactive, dark rhodopsin (opsin + 9-*cis*-retinal; PDB: 1GZM). **(b-f)** GPCR/condition specified at top left and sensor abbreviation along abscissa. **(b-c)** FRET ratios (mCit/mCer; 525nm/475nm) of **(b)** basal (untreated) and **(c)** change in FRET following retinal addition and photo-activation of opsin's E/DRY motif mutant t-mod sensors. **(d)** Retinitis pigmentosa (RP) inducing constitutively active opsin mutations and their interactions are indicated in the inactive dark rhodopsin crystal structure (PDB: 1GZM). **(e-f)** FRET ratios (mCit/mCer; 525nm/475nm) of **(e)** untreated (basal) and **(f)** change in FRET following retinal addition and photo-activation of opsin's RP mutant t-mod sensors. Results are expressed as mean ± s.e.m. **$P < 0.01$, ***$P < 0.001$; n > 18.
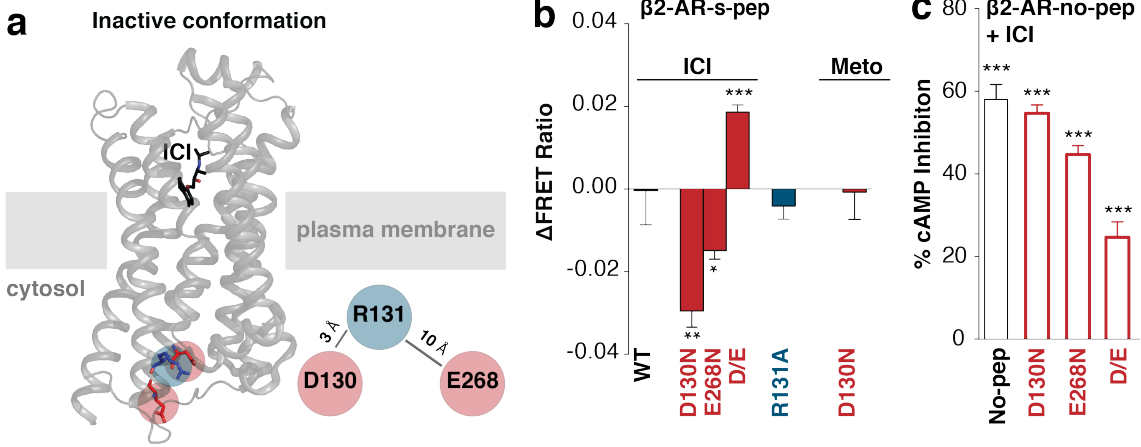
Fig. 2.6: Inverse agonist ICI118,551 requires a functional E/DRY motif to suppress β2-AR basal activity. (a) Electrostatic interactions formed by the E/DRY motif are indicated on the crystal structure of β2-AR bound to inverse agonist (ICI118,551) (PDB: 3NY8). **(b)** Change in FRET following inverse agonists (10 µM ICI118,551 or 150 µM metoprolol) treatment of indicated E/DRY motif mutant β2-AR-s-pep sensors. **(c)** ICI118,551 induced percent cAMP inhibition of HEK293 cells expressing wild-type (no-pep) or the indicated E/DRY motif mutant β2-AR-no-pep sensors. Results are expressed as mean ± s.e.m. *$P < 0.05$, **$P < 0.01$, ***$P < 0.001$; n > 18.
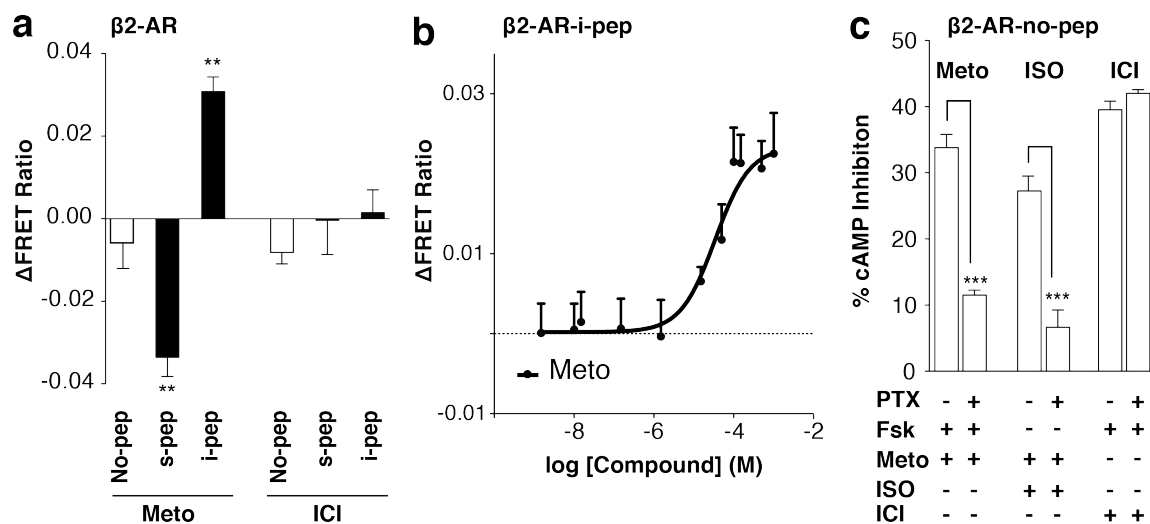
Fig. 2.7: Sensors detect stabilization of Gi conformations in β2-AR stimulated with metoprolol. Change in FRET following treatment of indicated β2-AR-pep sensors with **(a)** inverse agonist (150 μM metoprolol) or **(b)** with varying concentration of metoprolol. **(c)** Percent inhibition of 100 μM isoproterenol or 10 μM forskolin induced cAMP levels with 150 μM metoprolol or 10 μM ICI118,551, in PTX treated or untreated HEK293T cells expressing β2-AR-no-pep sensor. Results are expressed as mean ± s.e.m. *$P < 0.05$, **$P < 0.01$, ***$P < 0.001$; n >18.

β2-AR/peptide

- inactive
- s-state
- s-pep
- i-state
- i-pep

- mCit
- mCer
- ER/K linker

Ligands
- ICI
- ISO
- Meto

(DRY-locked)

(DRY-open)

Gs

Gs

Gi

Adenylyl Cyclase
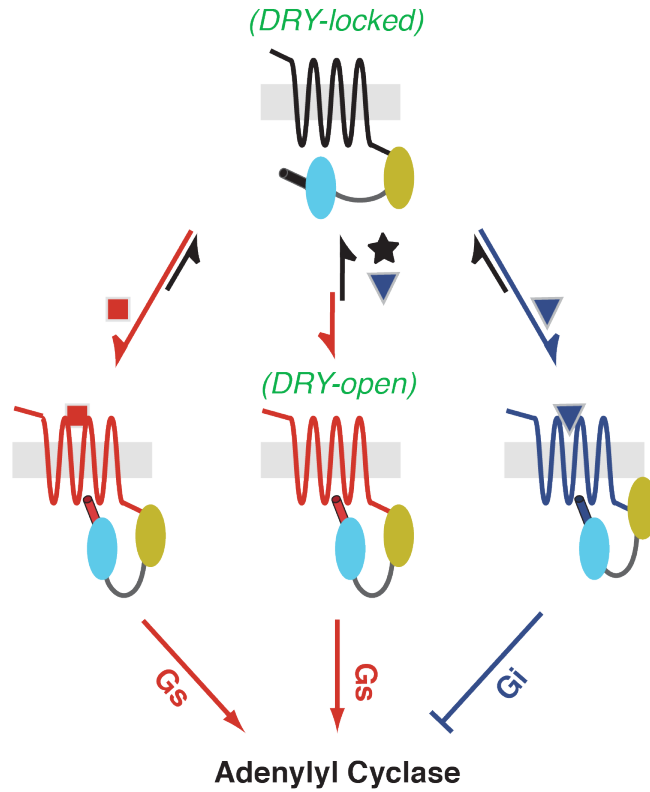
Fig. 2.8: Distinct structural mechanisms of β2-AR agonists and inverse agonists. In the absence of ligand (basal state), only a small proportion of the β2-AR population adopts Gs conformations. Isoproterenol (agonist) treatment destabilizes the DRY ionic-lock and enhances interaction with the Gαs c-terminus, resulting in activation of adenylyl cyclase (AC). Conversely, ICI118,551 (inverse agonist), reinforces the DRY ionic-lock, and shifts the equilibrium toward inactive conformations. Biased agonist (metoprolol) stabilizes Gi conformations, promoting Gi dependent inhibition of AC.

2.8. References

1. Bockenhauer, S., Furstenberg, A., Yao, X. J., Kobilka, B. K., and Moerner, W. E. (2011) *J Phys Chem B* **115**, 13328-13338
2. Liu, J. J., Horst, R., Katritch, V., Stevens, R. C., and Wuthrich, K. (2012) *Science* **335**, 1106-1110
3. Kahsai, A. W., Xiao, K., Rajagopal, S., Ahn, S., Shukla, A. K., Sun, J., Oas, T. G., and Lefkowitz, R. J. (2011) *Nat Chem Biol* **7**, 692-700
4. Vilardaga, J. P., Steinmeyer, R., Harms, G. S., and Lohse, M. J. (2005) *Nat Chem Biol* **1**, 25-28
5. Yao, X. J., Velez Ruiz, G., Whorton, M. R., Rasmussen, S. G., DeVree, B. T., Deupi, X., Sunahara, R. K., and Kobilka, B. (2009) *Proc Natl Acad Sci U S A* **106**, 9501-9506
6. Azzi, M., Charest, P. G., Angers, S., Rousseau, G., Kohout, T., Bouvier, M., and Pineyro, G. (2003) *Proc Natl Acad Sci U S A* **100**, 11406-11411
7. Granier, S., and Kobilka, B. (2012) *Nat Chem Biol* **8**, 670-673
8. Urban, J. D., Clarke, W. P., von Zastrow, M., Nichols, D. E., Kobilka, B., Weinstein, H., Javitch, J. A., Roth, B. L., Christopoulos, A., Sexton, P. M., Miller, K. J., Spedding, M., and Mailman, R. B. (2007) *J Pharmacol Exp Ther* **320**, 1-13
9. Onaran, H. O., and Costa, T. (2012) *Nat Chem Biol* **8**, 674-677
10. Sivaramakrishnan, S., and Spudich, J. A. (2011) *Proc Natl Acad Sci U S A* **108**, 20467-20472
11. Hamm, H. E., Deretic, D., Arendt, A., Hargrave, P. A., Koenig, B., and Hofmann, K. P. (1988) *Science* **241**, 832-835
12. Oldham, W. M., and Hamm, H. E. (2008) *Nat Rev Mol Cell Biol* **9**, 60-71
13. Rasenick, M. M., Watanabe, M., Lazarevic, M. B., Hatta, S., and Hamm, H. E. (1994) *J Biol Chem* **269**, 21519-21525
14. Choe, H. W., Kim, Y. J., Park, J. H., Morizumi, T., Pai, E. F., Krauss, N., Hofmann, K. P., Scheerer, P., and Ernst, O. P. (2011) *Nature* **471**, 651-655
15. Rasmussen, S. G., DeVree, B. T., Zou, Y., Kruse, A. C., Chung, K. Y., Kobilka, T. S., Thian, F. S., Chae, P. S., Pardon, E., Calinski, D., Mathiesen, J. M., Shah, S. T., Lyons, J. A., Caffrey, M., Gellman, S. H., Steyaert, J., Skiniotis, G., Weis, W. I., Sunahara, R. K., and Kobilka, B. K. (2011) *Nature* **477**, 549-555
16. Chung, K. Y., Rasmussen, S. G., Liu, T., Li, S., DeVree, B. T., Chae, P. S., Calinski, D., Kobilka, B. K., Woods, V. L., Jr., and Sunahara, R. K. (2011) *Nature* **477**, 611-615
17. Martin, E. L., Rens-Domiano, S., Schatz, P. J., and Hamm, H. E. (1996) *J Biol Chem* **271**, 361-366
18. Conklin, B. R., Farfel, Z., Lustig, K. D., Julius, D., and Bourne, H. R. (1993) *Nature* **363**, 274-276
19. Conklin, B. R., Herzmark, P., Ishida, S., Voyno-Yasenetskaya, T. A., Sun, Y., Farfel, Z., and Bourne, H. R. (1996) *Mol Pharmacol* **50**, 885-890
20. Rovati, G. E., Capra, V., and Neubig, R. R. (2007) *Mol Pharmacol* **71**, 959-964
21. Hofmann, K. P., Scheerer, P., Hildebrand, P. W., Choe, H.-W., Park, J. H., Heck, M., and Ernst, O. P. (2009) *Trends in Biochemical Sciences* **34**, 540-552
22. Wacker, D., Fenalti, G., Brown, M. A., Katritch, V., Abagyan, R., Cherezov, V., and Stevens, R. C. (2010) *J Am Chem Soc* **132**, 11443-11445
23. Ballesteros, J. A. (2001) *Journal of Biological Chemistry* **276**, 29171-29177
24. Rao, V. R., and Oprian, D. D. (1996) *Annu Rev Biophys Biomol Struct* **25**, 287-314

25. Wald, G. (1968) *Nature* **219**, 800-807
26. Galandrin, S., and Bouvier, M. (2006) *Mol Pharmacol* **70**, 1575-1584
27. Locht, C., Coutte, L., and Mielcarek, N. (2011) *FEBS J* **278**, 4668-4682
28. Clark, M. J., Neubig, R. R., and Traynor, J. R. (2004) *J Pharmacol Exp Ther* **310**, 215-222
29. Fung, J. J., Deupi, X., Pardo, L., Yao, X. J., Velez-Ruiz, G. A., Devree, B. T., Sunahara, R. K., and Kobilka, B. K. (2009) *EMBO J* **28**, 3315-3328
30. Harrison, C., and Traynor, J. R. (2003) *Life Sci* **74**, 489-508
31. Chidiac, P., Hebert, T. E., Valiquette, M., Dennis, M., and Bouvier, M. (1994) *Mol Pharmacol* **45**, 490-499
32. Samama, P., Cotecchia, S., Costa, T., and Lefkowitz, R. J. (1993) *J Biol Chem* **268**, 4625-4636
33. Kjelsberg, M. A., Cotecchia, S., Ostrowski, J., Caron, M. G., and Lefkowitz, R. J. (1992) *J Biol Chem* **267**, 1430-1433
34. De Lean, A., Stadel, J. M., and Lefkowitz, R. J. (1980) *J Biol Chem* **255**, 7108-7117
35. Li, J., Edwards, P. C., Burghammer, M., Villa, C., and Schertler, G. F. (2004) *J Mol Biol* **343**, 1409-1438
36. Rudling, J. E., Richardson, J., and Evans, P. D. (2000) *Br J Pharmacol* **131**, 933-941
37. Daaka, Y., Luttrell, L. M., and Lefkowitz, R. J. (1997) *Nature* **390**, 88-91
38. Xiao, R. P. (2001) *Sci STKE* **2001**, re15
39. Okada, T., Sugihara, M., Bondar, A.-N., Elstner, M., Entel, P., and Buss, V. (2004) *Journal of Molecular Biology* **342**, 571-583
40. Chuang, J. Z., Vega, C., Jun, W., and Sung, C. H. (2004) *J Clin Invest* **114**, 131-140
41. Musarella, M. A., and MacDonald, I. M. (2011) *Journal of Ophthalmology* **2011**, 1-8
42. Daiger, S. P., Bowne, S. J., and Sullivan, L. S. (2007) *Arch Ophthalmol* **125**, 151-158
43. Lem, J., and Fain, G. L. (2004) *Trends in Molecular Medicine* **10**, 150-157
44. Kim, J. M., Altenbach, C., Kono, M., Oprian, D. D., Hubbell, W. L., and Khorana, H. G. (2004) *Proc Natl Acad Sci U S A* **101**, 12508-12513

Chapter 3

ER/K linked GPCR-G protein fusions systematically modulate second messenger response in cells

Rabia U. Malik, Michael Ritt, Roger K. Sunahara, and Sivaraj Sivaramakrishnan

3.1 Abstract

FRET or BRET approaches are well established for detecting ligand induced GPCR-G protein interactions in cells. However, current FRET/BRET assays rely on co-expression of GPCR and G protein, and hence depend on the stoichiometry and expression levels of the donor and acceptor probes. On the other hand, GPCR-G protein fusions have been used extensively to understand the selectivity of GPCR signaling pathways. However, the signaling properties of fusion proteins are not consistent across GPCRs. In this study, we describe novel sensors based on the Systematic Protein Affinity Strength Modulation (SPASM) technique. Sensors consist of a GPCR and G protein tethered by an ER/K linker flanked by FRET probes. SPASM sensors are tested for the $\beta2$-, $\alpha1$-, and $\alpha2$- adrenergic receptors, and adenosine type 1 receptor (A_1R), tethered to Gαs-XL, Gαi_1, or Gαq subunits. Agonist stimulation of $\beta2$-AR and $\alpha2$-AR increases FRET signal comparable to co-expressed FRET/BRET sensors. SPASM sensors retain signaling through the endogenous G protein milieu. Importantly, ER/K linker length systematically tunes the GPCR-G protein interaction, with consequent modulation of second messenger signaling for cognate interactions. SPASM GPCR sensors serve the dual purpose of detecting agonist-induced changes in GPCR-G protein interactions, and linking these changes to downstream signaling.

3.2 Introduction

G protein coupled receptors relay detection of stimuli such as photons, neurotransmitters, hormones, or drugs from the extracellular milieu to the intracellular environment by binding and

activating one or more functionally distinct heterotrimeric G proteins[1]. Coupling between an active GPCR and G proteins stimulates accumulation of second messengers such as cyclic AMP, calcium/potassium ions, and inositol phosphate[1]. Efforts to monitor and understand the link between GPCR-G protein interactions and downstream second messenger response are complicated by the range of cellular factors that influence GPCR signaling including the relative localization and abundance (concentration) of GPCR and G proteins, regulatory proteins such as Regulators of G protein signaling (GRS), G protein kinases (GRKs), and non-G protein effectors such as β-arrestins[2].

Current approaches to visualize GPCR-G protein interaction in cells involve probing the interaction between individually expressed fluorescent or luminescent protein fusions using fluorescence/bioluminescence resonance energy transfer (FRET/BRET)[3-7]. Therefore, insights into the GPCR-G protein interaction gained from these studies are limited by their dependence on the relative concentration and co-localization of individually expressed GPCR and G protein. Alternatively, direct GPCR-G protein fusions generated by tethering the N-terminus of the Gα to the GPCR's C-tail with a short or no linker in between have been used to study the influence of tethering different G protein subunits on G protein activation and second messenger signaling[8,9]. Such fusions have not been used to monitor the GPCR-G protein interaction using resonance energy transfer approaches[6]. A limitation of direct fusions is that GPCRs with short C-tails do not efficiently signal to the tethered G protein[10-13].

In this study, we combine the strengths of FRET and fusion proteins by leveraging the Systematic Protein Affinity Strength Modulation (SPASM) approach[14,15]. SPASM involves expression of a single polypeptide encoding a GPCR tethered to a G protein via an ER/K α-helix/linker that is flanked by a pair of FRET probes (mCitrine (FRET acceptor) and mCerulean (FRET donor) (Fig. 3.1a). Unstructured (Gly-Ser-Gly)$_4$ linkers are inserted in between each component to provide rotational flexibility (Fig. 3.1a). Similar to GPCR fusions, GPCR SPASM sensors enable control over GPCR-G protein stoichiometry and co-localization. ER/K linkers with end-to-end distance of 10-30 nm (measured along the α-helical backbone) are designed to provide adequate separation between the GPCR (~ 3 nm) and the G protein (~ 5 nm)[14,16]. Increasing ER/K linker length from 10-30 nm has been shown to systematically decrease the effective concentration of the protein-protein interaction[14,15,17,18]. We have previously reported on SPASM sensors involving individual fusions of GPCRs with the C-terminal peptide of the Gα

subunit[19-21]. Here, we describe SPASM GPCR sensors with the entire Gα subunit that can bridge the gap between the GPCR-G protein interaction and downstream signaling[10-13].

In this proof-of-concept study, SPASM sensors are made for four GPCRs with varying C-tail lengths (8-87 amino acids). The β2-adrenergic receptor (β2-AR), α2-adrenergic receptor (α2-AR), α1-adrenergic receptor (α1-AR), and adenosine type 1 receptor (A_1R) are each tethered to two functionally distinct Gα subunits (Gαs-XL, $Gαi_1$, and Gαq). Consistent with literature reports of co-expressed GPCR-G protein sensors[3,5], we find SPASM sensors with cognate GPCR-G protein pairs show enhanced interaction following agonist stimulation as indicted by a gain in FRET signal. Varying ER/K linker length from 10 nm to 30 nm systematically tunes the basal interaction between tethered GPCR-G protein pairs. However it only modulates second messenger response from select GPCR-G protein pairs over and above endogenous levels. Together, these features of the SPASM GPCR-G protein sensors facilitate both the detection of GPCR-G protein interactions in cells and establish their link to downstream signaling pathway.

3.3. Results

3.3.1. Integrity of GPCR-G protein fusions – The GPCR and Gα subunit were expressed as a single polypeptide fusion with a SPASM module between them (Fig. 3.1*a*). All individual protein elements are separated by $(Gly-Ser-Gly)_4$ linkers to provide rotational flexibility (Fig. 3.1*a*). The SPASM module provides 1:1 stoichiometry of GPCR-Gα expression and consists of an ER/K α-helical linker flanked by a FRET pair (mCerulean/mCitrine)[14]. FRET probes enable monitoring of cellular expression and sensor integrity. Fusions lacking a G protein (–) served as controls to assess background signaling through endogenous G proteins. Together, these sensor properties facilitate pairwise comparison across fusions at matched cellular expression levels (see Methods). GPCR-G protein fusions were initially generated for the prototypical β2 adrenergic receptor (β2-AR). Fusions are expressed primarily >80% at the plasma membrane of HEK293T cells (Fig. 3.1*b*), are intact as assessed by immuno-blotting membrane preparations (Fig. 3.1*c*), and bind Gβγ subunits to equal extents (Fig. 3.1*d*). Consistent with the known basal activity of this GPCR, over-expression of β2-AR (1-2 pmol/mg total protein) elevates basal cAMP levels relative to the untransfected (UN) cells (Fig. 3.1*e*)[22]. Treatment with the inverse agonist metoprolol (Meto) significantly attenuates the enhanced cAMP levels, attesting to the

role of exogenously expressed β2-AR (Fig. 3.1*e*). The functionality of Gs in the β2-AR-Gs fusion protein is consistent with ~5-fold increase in basal cAMP levels as compared to sensors expressing β2-AR alone (–) (Fig. 3.1*e*).

3.3.2. Agonists modulate fusion interaction and downstream response – In agreement with previous β2-AR-Gs fusions[23,24], tethering β2-AR to Gs with a 10 nm ER/K linker enhances both efficacy (Fig. 3.2*a*) and potency (β2-AR-Gs EC_{50} = 0.09 ± 0.05 nM; β2-AR EC_{50} = 0.44 ± 0.3 nM; Fig. 3.2*b*) of the isoproterenol induced cAMP levels compared to over-expression of β2-AR alone (–). Likewise, epinephrine treatment results in a greater loss in cAMP signaling for ER/K linked α2-AR-Gi compared to α2-AR alone (–) (Fig. 3.2c). To test if agonist stimulation also enhances interaction between the cognate GPCR-G protein pair, changes in FRET ratio were examined. The SPASM module is designed to maintain low FRET levels in the absence of an interaction between the GPCR and G protein (dissociated state; Fig. 3.3*a*) [14]. Interaction between the GPCR and G protein (associated state; Fig. 3.3*a*) should bring the FRET donor and acceptor in closer proximity, leading to higher FRET levels. In accordance with previous studies using co-expressed GPCR and G protein FRET/BRET pair fusions, treatment with agonist (100 μM isoproterenol) results in a gain in FRET for the cognate β2-AR-Gs pairing[3,4], but not for non-cognate Gi, Gq, or fusions lacking a G protein (–) in live cells (Figs. 3*b*, left panel). Likewise, for the Gi coupled receptor, α2-AR, stimulation with 100 μM epinephrine induced a gain in FRET for Gi[4,5], but not Gs or Gq (Fig. 3.3*b,* right panel). ΔFRET for β2-AR-Gs = 0.006 ± 0.001 and α2-A-Gi = 0.01 ± 0.002 are small but statistically significant. These changes are comparable to previously reported measurements using co-expressed sensors of β2-AR-Gs (ΔBRET ~ 0.025) and α2-AR-Gi (ΔFRET ~0.022)[3-5,25].

3.3.3. Fusions interact with endogenous G proteins – One concern with fusions is that the addition of the SPASM module at the C-tail of the GPCR may cause steric hindrance between GPCR interactions with the endogenous signaling machinery. The ER/K linked fusions are designed to spatially separate the GPCR and G protein in the absence of an interaction and should therefore freely permit interactions with non-tethered G proteins[14,26]. To test the ability of the ER/K linked fusions to interact with non-tethered G proteins in the cellular milieu, we focused on β2-AR and α1-AR interactions with Gs and Gq, as they influence distinct second

messengers (cAMP and IP$_1$) and facilitate interpretation of downstream responses. First, an unlabeled (dark) Gα subunit was increasingly co-expressed relative to the ER/K linked fusions, and the FRET ratios were determined for equal levels of expression of the ER/K linked fusion (Fig. 3.4a). Elevated expression of Gs or Gq, relative to β2-AR-Gs or α1-AR-Gq sensors, respectively, systematically decreased FRET ratios attesting to interactions between cellular Gs or Gq and the GPCR in the ER/K linked fusions (Fig. 3.4b and c). Likewise, tethering the cognate G protein (Gs and Gq, respectively, for β2-AR and α1-AR) increases second messenger signaling through the cognate pathway (cAMP and IP$_1$, respectively, for β2-AR and α1-AR), whereas, tethering to the non-cognate G protein (Gq and Gs, respectively, for β2-AR and α1-AR) does not suppress signaling through endogenous G proteins (Fig. 3.4 d and e – no significant difference between sensors without G protein compared to those with non-cognate G protein). Together, these measurements demonstrate that while the ER/K linked G protein does interact with the GPCR, it does not measurably perturb interactions with endogenous components.

3.3.4. ER/K linker length modulates second messenger signaling of cognate GPCR-G protein fusions – Previous studies show that increasing ER/K linker length from 10 to 30 nm decreases the effective concentration of the tethered proteins from 10 µM to 100 nM[14]. FRET ratios are sensitive to the distance between and concentration of acceptor and donor molecules[6]. As expected, FRET ratio measurements for matched sensor expression demonstrate that increasing ER/K linker length from 10 to 30 nm, systematically decreased basal FRET ratios for a range of both cognate and non-cognate GPCR-G protein interactions (Figs. 4 and 5; FRET ratios are depicted by open black circles; GPCR color indicates its cognate G protein). To test whether modulating the GPCR-G protein interaction within the ER/K linked fusion influences downstream signaling, the second messenger corresponding to the tethered G protein was measured under matched protein expression levels (Figs. 5 and 6; Filled circles with colors corresponding to the second messenger; red – cAMP; green – suppression of forskolin-stimulated cAMP; blue – IP$_1$). In correlation with the systematic changes in the relative GPCR-Gx fusions interaction (FRET ratios), significant modulation of second messenger levels was observed only for cognate GPCR-G protein fusions (Figs. 5 and 6). Specifically, tethering β2-AR

(Gs coupled receptor) to Gs modulates cAMP (Fig. 3.5b), whereas tethering α1-AR (Gq coupled receptor) to Gq modulates IPx (Fig. 3.5d). In contrast, tethering β2-AR to Gq or α1-AR to Gs modulates the GPCR-Gx interaction (FRET ratio) but not IP$_1$ or cAMP levels respectively (Figs. 5 c and e). Tethering A$_1$R (Gi coupled receptor) to Gi suppresses forskolin-stimulated cAMP levels, whereas tethering to Gs does not enhance cAMP (Figs. 6 b and c). Interestingly, α2-AR, which has been shown to couple to both Gs and Gi[27], shows both enhanced cAMP upon tethering to Gs and suppression of forskolin-stimulated cAMP upon tethering to Gi (Figs. 6 d and e), unlike previously reported α2-AR fusions[11]. Together, these measurements support the ability of ER/K linked cognate GPCR-G protein fusions to successfully modulate signaling relative to endogenous levels.

3.4. Discussion

In this study, we describe a new approach that relies on ER/K-linked fusions[15] to compare downstream signaling from different GPCR – G protein pairings. In contrast to previous GPCR-G protein fusions that use a short unstructured linker[9-11,13,23,28], in the absence of an interaction, the structured ER/K linker provides a significant spatial separation between the GPCR and the G protein fused to its ends. The ER/K linker has been previously characterized to exist primarily in an extended α-helical conformation, with end-to-end distances of ~ 7 to ~ 22 nm for 10 to 30 nm lengths along the α-helical backbone[26]. We show that SPASM sensors with GPCRs tethered to non-cognate G protein retain signaling through the endogenous pathways (Figs. 3.4 d and e). Likewise, sensors respond to increasing concentration of exogenously expressed unlabeled Gα subunits (Fig. 3.4 b and c). Hence, our data suggest that rather than enforce GPCR-G protein coupling[9,13,23] or sterically hinder interactions with endogenous G proteins[10,11,13] the SPASM sensors can progressively modulate signaling through the tethered G protein relative to endogenous levels.

Unlike current FRET/BRET sensors that rely on the co-expression of labeled GPCR and G protein subunits[3-7,29,30], the SPASM sensors require the expression of a single polypeptide that provides 1:1 stoichiometry between the exogenously expressed GPCR and G protein. Agonist stimulation provides changes in FRET (ΔFRET) comparable to those previously reported using co-expressed FRET/BRET pairs[3-5]. Hence, the SPASM sensors serve the dual purpose of probing

agonist-stimulated changes in GPCR-G protein interaction while examining the downstream response using the same construct.

ER/K linkers are designed to modulate the effective concentration of the intra-molecular interaction[14,15], where the same linker length provides matched effective concentration across different GPCR-G protein pairings. However, given the localization of both GPCRs and G proteins on the plasma membrane, and the potential segregation of GPCRs into membrane micro-domains[31], the measurements from any FRET/BRET based assay in live cells will have contributions from both intra-molecular interactions and those induced by the proximity of sensors on the plasma membrane[32]. Hence, measurements in each figure panel were performed with matched sensor expression, as determined by mCitrine fluorescence per unit cell density (see Methods). Nonetheless, the FRET ratio does decrease systematically with increasing ER/K linker length for all of the GPCR-G protein combinations tested suggesting that the ER/K linker does systematically alter the proximity between GPCR-G protein. In combination with the observed systematic decrease in the second messenger levels for cognate GPCR-G protein pairings our data suggest that the ER/K linker is able to modulate the effective concentration of the GPCR-G protein interaction. Importantly, for non-cognate GPCR-G protein pairings, while the FRET ratio does systematically decrease with ER/K linker length, we do not detect a significant change in non-cognate downstream signaling, attesting to the specificity of the downstream response. Hence, using varying length ER/K linkers is an effective approach to bridge the gap between GPCR-G protein interactions as detected by FRET and consequent downstream signaling as measured by second messenger levels.

3.5. Experimental Procedures

3.5.1. Reagents and buffers – fenoterol hydrobromide, fibronectin, guanosine 5′-diphosphate sodium salt (GDP), 3-isobutyl-1-methylxanthine (IBMX), (-)-isoproterenol (+)- bitartrate salt, and pertussis toxin from *Bordetella pertussis* (PTX) were purchased from Sigma-Aldrich. *n*-dodecyl-β-D-maltopyranoside, Anagrade (DDM) was bought from Anatrace. Purified Gαq (*Mus musculus*) Gαs-long (*Rattus norvegicus*) were obtained from Kerafast. Anti-G α s/olf (SC383) and anti-Gβ antibody (SC378) were purchased from Santa Cruz Biotechnology. Anti-pan Gα antibody (3992) and anti-HA antibody (MMS-101p) were acquired from Cell Signaling Technology and Covance respectively. cDNAs for α1$_A$-AR isoform 3 (*Homo sapiens*), and α2$_A$-

AR (*Sus scrofa*) were kind gifts from Dr. Richard Neubig. cDNAs for human β2-AR, long splice variant of Gαs, Gαi$_2$ isoform 1, and Gαq were purchased from GE (Open Biosystems). Human A$_1$R was acquired from DNASU Plasmid Repository. DNA transfection reagents X-tremeGENE HP and Mirus-LT DNA were acquired from Roche and Mirus respectively. Buffer A is 20 mM HEPES, 5 mM KCl, 145 mM NaCl, 2 mM CaCl$_2$, 1 mM MgCl$_2$, 0.2% dextrose (w/v), 1.5 μg mL^{-1} aprotinin and 1.5 μg mL^{-1} leupeptin at pH 7.45. Buffer B is 20 mM HEPES, 0.5 mM EDTA, 5 mM MgCl$_2$, 0.1 mM DTT, 10 μM GDP, 1.5 μg mL^{-1} aprotinin, 1.5 μg mL^{-1} leupeptin and 50 μg mL^{-1} phenylmethanesulfonyl fluoride at pH 7.4. Buffer C is 20 mM HEPES, 0.5% decaethylene glycol monododecyl ether (C$_{12}$E$_{10}$), 100 mM NaCl, 1 mM MgCl$_2$ 10 mM GDP, 5.5 mM β-mercaptoethanol, 10 mg mL^{-1} phenylmethanesulfonyl fluoride at pH 8.0.

3.5.2. Molecular cloning – PCR products for α1$_A$-AR (isoform 3), β2-AR, A$_1$R, long splice variant of Gαs, Gαi$_2$, and Gαq were obtained from human cDNA. For mammalian HEK293 expression, all GPCR and Gα constructs were cloned into a PCDNA5/FRT vector. A modular scheme was designed for cloning of GPCR sensors. Each GPCR-G protein sensor contained from N- to C-terminus: a full length GPCR, mCitrine (FRET acceptor), ER/K linker, mCerulean (FRET donor), and a Gα subunit. A (Gly-Ser-Gly)$_4$ linker was inserted between all protein domains as part of the primer sequence to allow for free rotation between domains. Control GPCR sensors (–) did not contain a Gα subunit after mCerulean and instead had repeating (Gly-Ser-Gly)$_4$ residues. All β2-AR-sensors also contained either an N-terminal HA-tag or a His-tag. Finally, all constructs were confirmed by sequencing.

3.5.3. Mammalian cell preparation and sensor expression – HEK293T-Flp-In (HEK293T, Invitrogen) cells were cultured in DMEM supplemented with 10% FBS (v/v), 4.5 g L^{-1} D-glucose, 1% Glutamax, 20 mM HEPES, pH 7.5 at 37 °C in a humidified atmosphere at 5% CO$_2$. HEK293T cells were plated into 6-wells tissue culture treated plates at ~30% confluence. Cells were transfected 16-20 h later with X-tremeGENE HP DNA transfection reagent. Transfection conditions including the amount of DNA (1.4 – 4 μg DNA + 4.2 – 6 μl reagent) and the length of transfection (control sensors: 18-24 h; Gα sensors: 22-32 h) were optimized to consistently yield equivalent levels of sensor expression across different conditions. For GPCR-G protein competition assays, 100 ng, 300 ng, or 1 μg of α1-AR-mCherry were co-transfected with 2 or 4

μg of indicated sensors. For all experiments sensor integrity, localization, and sensor expression per optical density (O.D.) were tracked to ensure consistency. Experiments were conducted at 60-80% transfection efficiency evaluated by 20x and 40x magnification on a Nikon tissue-culture microscope enabled with fluorescence detection. Additionally, at the time of the experiment, 60-90% of transfected cells expressed predominately plasma membrane localized sensor with minimal localization to the intracellular compartments. Each experiment was performed at equivalent sensor expression and matched O.D. of the cell suspension using the following steps. First, cells were resuspended by gentle pipetting into their original media. Cells were then spun down (300 g, 3 min) and washed once with Buffer A. Subsequently, cells were resuspended in an appropriate volume of Buffer A to reach a 0.3 O.D (A$_{600\ nm}$, BioMate 3S Spectrophotometer, Thermo Scientific, 3 mm path-length, optical glass cuvette) for all fluorescence-based measurements. Finally, sensor expression was measured by mCitrine fluorescence. mCitrine fluorescence was held within 1.6-2.4x10^6 counts-per-second (c.p.s) for a cell O.D of 0.3. For each experiment, sensor integrity was tracked by measuring the mCitrine (excitation 490 bandpass 8 nm; emission range 500-600 bandpass 4 nm; emission maximum 525 nm) to mCerulean fluorescence ratio (excitation 430 bandpass 8 nm; emission range 450-600 bandpass 4 nm; emission maximum 475 nm). As part of the sensor design, mCitrine and mCerulean label the C-terminus of GPCR and N-terminus of Gα subunit respectively. All experiments were conducted at mCitrine to mCerulean fluorescence ratio of 1.7-2.1. Similarly, mCherry fluorescence was recorded to evaluate α1-AR-mCherry expression for a cell O.D of 0.3.

3.5.4. Live cell microscopy and image analysis – HEK293T cells were plated (~15-20% confluence) on 35 mm glass bottom dishes (MatTek Corp) coated with 10 mg mL^{-1} fibronectin. 14-16 h after plating (30-40% confluence), cells were transfected with Mirus-LT or XtremeGENE HP DNA transfection reagent. 16-22 h post-transfection cells were washed three times with Buffer A (37 °C) to remove excess phenol red from the media. Cells were subsequently imaged for no more than 30 min in Buffer A media. Cell images were collected at 60x magnification using a Nikon TiE microscope equipped with a mercury arc lamp, 60x and 100x 1.4 Numerical Aperture Plan-Apo oil objectives and with an Evolve 512x512 EM-Charge-Coupled-Device camera (Photometrics). Z-stack images were taken with 1 μm steps and the

resultant stack of images was deconvolved using AutoQuantX software. Membrane expression in images was analyzed in ImageJ (NIH) using the threshold and measure tools to select and quantify membrane expression compared to internal localization (Fig. 3.7).

3.5.5. Fluorescence measurements – Using FluoroMax-4 fluorometer (Horiba Scientific), FRET spectra were generated by exciting cells at 430 nm (bandpass 8 nm) in an optical glass cuvette (3-3.30-SOG-3, Starna Cells Inc.). Emission was scanned from 450-600 nm (bandpass 4 nm). For mCitrine-only measurements, cells were exited at 490 nm (band pass 8 nm), and emission was recorded from 500-600 nm (bandpass 4 nm), emission maximum was set at 525 nm. For mCherry expression, cells were excited at 570 nm with an 8 nm bandpass; emission was collected from 600 – 700 nm at 4 nm bandpass. Where indicated, maximum emission value at 610 nm is reported as an estimate of α1-AR-mCherry expression in HEK293T cells. For TR-FRET experiments, eGFP emission maxima at 510 nm was measured by exciting at 480 nm band pass 8 nm, and recording emission from 500-600 nm band pass 4 nm.

3.5.6. Live cell FRET calculations – FRET measurements were conducted at matched O.D. in Buffer A. Untransfected and transfected cells were resuspended in Buffer A at 0.3 O.D. To correct for scattering, FRET emission spectrum of an untransfected cell suspension, at equivalent O.D, was subtracted from FRET spectrum of the transfected cell suspension. The corrected FRET emission spectra were normalized to mCerulean emission (475 nm). FRET ratio was then calculated by dividing mCitrine emission (525 nm) by the mCerulean emission (475 nm).

3.5.7. ΔFRET experiment – Live cell ΔFRET experiments were conducted as previously described [21]. Briefly, cells were prepared and re-suspended into pre-warm Buffer A. 90 μL aliquots of cells were added into eppendorf tubes placed in a 37°C water bath. Samples were treated with buffer control or indicated ligand for 3 or 5 min at 37°C. Separate and clean cuvettes were used to collect FRET spectra for treated and untreated samples to prevent cross-contamination.

3.5.8. Sensor purification from HEK293 cells – For anti-Gβ experiments, purification of His tag-β2-AR-G protein and control (–) sensors from HEK293T cells followed the previously

published protocol [16]. Frozen membranes were thawed quickly to room temperature and briefly re-homogenized with a rotary pestle. 5% cholate buffer (5% sodium cholate in 50 mM HEPES, 3 mM $MgCl_2$, 50 mM NaCl with 1 μg mL^{-1} aprotinin, 1 μg mL^{-1} leupeptin, 10 μg mL^{-1} phenylmethanesulfonyl fluoride, and 5.5 mM β-mercaptoethanol, pH 8.0) was added to a final concentration of 1% cholate. This mixture was incubated on ice for 45 min and separated by ultracentrifugation at ~105,000 g for 40 min at 4 ℃. The supernatant was harvested and diluted drop wise with four volumes of Buffer C to one volume of supernatant, and was pipetted gently to mix. The diluted supernatant was added to nickel-NTA resin (Qiagen) and incubated 30 min at 4 ℃ with rotation. The resin was washed 3x with 500 μL Buffer C + 5 mM imidazole. The final wash was removed and the resin was brought to room temperature and eluted for 3-5 min with 150 μL of elution buffer (Buffer C + 200 mM imidazole). The eluted resin was spun down, the supernatant harvested, and measured for mCerulean and mCitrine fluorescence in a fluorometer (as described above). Samples were stored in SDS laemmli sample buffer at -80 ℃.

3.5.9. Western blot – For anti-HA western blot, 20 μg of membranes containing β2-AR-Gs sensor were boiled in Buffer B supplemented with Glycoprotein Denaturing Buffer (NEB) at 95° C for 5 min. Boiled samples were subsequently treated with 500 units of PNGase F (NEB) for three hours at 37 ℃. For anti-Gβ, equivalent amount of sensors, as measured by mCitrine fluorescence, were loaded on SDS-PAGE Gels (10% polyacrylamide). Gels were imaged for mCitrine fluorescence (excitation 488 nm, emission 520 nm, bandpass 40 nm) using a Typhoon Gel Imager (GE Healthcare). Gels were transferred to PVDF membranes for three hours at 300 mA. Anti-HA and anti-Gβ were blocked with 2% milk/TRIS-buffered saline with 1% Tween (TBST) for either one hour at room temperature or 4 ℃ overnight. Blots were then incubated with indicated primary antibody at a 1:1,000 dilution in 5% milk/TBST. For the anti-Gβ experiment, blots were washed with TBST, and incubated with 1:5,000 or 1:10,000 horseradish peroxidase (HRP) conjugated goat anti-rabbit IgG secondary antibody (0031460, Fisher Scientific) in 5% milk/TBST or 5% BSA/TBST for one hour at room temperature. Similarly for anti-HA experiments, blots were incubated with 1:10,000 Sheep anti-mouse HRP conjugated secondary antibody (GE Healthcare, NA931). All blots were developed with Immobilon Western Chemiluminescent HRP Substrate (Millipore). Blots were imaged using a ChemiDoc-It Imaging system (UVP). Images of gels and blots were prepared using ImageJ (NIH).

3.5.10. cAMP assays – 28-32 h post transfection (XtremeGENE HP) HEK293T cells expressing indicated sensor were harvested to assess cAMP levels using the bioluminescent cAMP Glo assay (Promega). Cells were gently suspended in their original media, were counted using a hemocytometer, and spun down   (300 g, 3 min). Appropriate volume of buffer   (PBS supplemented with 800 μM ascorbic acid and 0.2% dextrose (w/v)) was added to reach 2×10^6 cells mL^{-1} density for basal experiments or 4×10^6 cells mL^{-1} density for ligand based assays. Cell suspensions were aliquoted into 96 wells round-bottom opaque plates. Cells were treated without ligand in the presence of 0.25 mM IBMX for 15 min at 37 ^{o}C or with 100 μM isoproterenol for 3 min at room temperature. For cAMP suppression assays, cells were treated with 1 μM forskolin and with or without ligand for 15 min at 37 ^{o}C. Subsequently, cells were lysed and the protocol was followed according to the manufacturer's recommendation (Promega). Luminescence was measured using a microplate luminometer reader   (SpectraMax M5e, Molecular Devices). cAMP levels (relative luminescence unit, RLU) were evaluated by subtracting the untransfected background from the transfected conditions. Each experiment had four technical repeats per condition and was independently repeated at least three times ($N > 3$).

3.5.11. IP$_1$ assays – 28-32 h post transfection (XtremeGENE HP) HEK293T cells expressing the indicated sensor were harvested to assess IP$_1$ levels using the IP-One HTRF assay kit (Cisbio). Cells were gently suspended in their original media, counted using a hemocytometer, and spun down (300 g, 3 min). An appropriate volume of StimB buffer (CisBio: 10 mM Hepes, 1 mM CaCl$_2$, 0.5 mM MgCl$_2$, 4.2 mM KCl, 146 mM NaCl, 5.5 mM glucose, 50 mM LiCl, pH 7.4) was added to reach 3×10^6 cells mL^{-1} density. Cells were incubated at 37 ^{o}C for 15 min. The manufacturer's protocol was modified in order to achieve a high signal to noise ratio. 150 μL of suspension was incubated for one hour with 30 μL of lysis buffer (Cisbio), 54 μL StimB buffer, 6 μL IP$_1$ conjugated to d2 dye, and 6 μL terbium cryptate-labeled anti-IP$_1$ monoclonal antibody. IP$_1$ FRET spectra were collected by exciting samples at 340 nm (bandpass 15 nm). Emission counts were recorded from 600-700 nm (bandpass 10 nm) using a long pass 475 nm filter (FSQ GG475, Newport). Raw IP$_1$ signal was calculated from the 665 nm to 620 nm ratio. Basal IP$_1$ signal was corrected by subtracting the untransfected IP$_1$ ratio from cells expressing transfected sensor. For ligand experiments, data are presented as a change in raw IP$_1$ ratio following drug

treatment. Each experiment had four repeats per condition and was independently repeated at least three times $(N > 3)$.

3.5.12. Statistical Analysis – Data are expressed as mean values ± S.E.M. Experiments were independently conducted at least three times, with 3-6 technical repeats per condition $(N > 3)$. Statistical analysis was performed using GraphPad Prism 6.0c (Graphpad Software, Inc.) Statistical significance was performed for individual experiments using paired Student's t-test. To assess how the data varied across experimental repeats, data were pooled and paired or unpaired Student's t-tests were conducted to evaluate significance. Where indicated, *p*-values *, $p \leq 0.05; **, p \leq 0.01; ***, p \leq 0.001; ****, p \leq 0.0001$.

3.6. Notes

3.6.2. Conflict of interest – The authors declare they have no conflicts of interest with the contents of this article.

3.6.3. Author contributions – RUM and SS planned and designed experiments; RUM, MR, KK and RFS performed experiments; RUM and SS analyzed the results and wrote the manuscript.

3.7. Figures

a

b

β2-AR - G_s

α2-AR - G_s

c

β2-AR - $G\alpha_s$ anti-HA

25   37   150

d

β2-AR   anti-Gβ

G_s
G_q
G_i
(−)

e

β2-AR

cAMP Levels (% control (−))

600
450
300
150
0

***

**

Meto   − +   − +
        (−) G_s
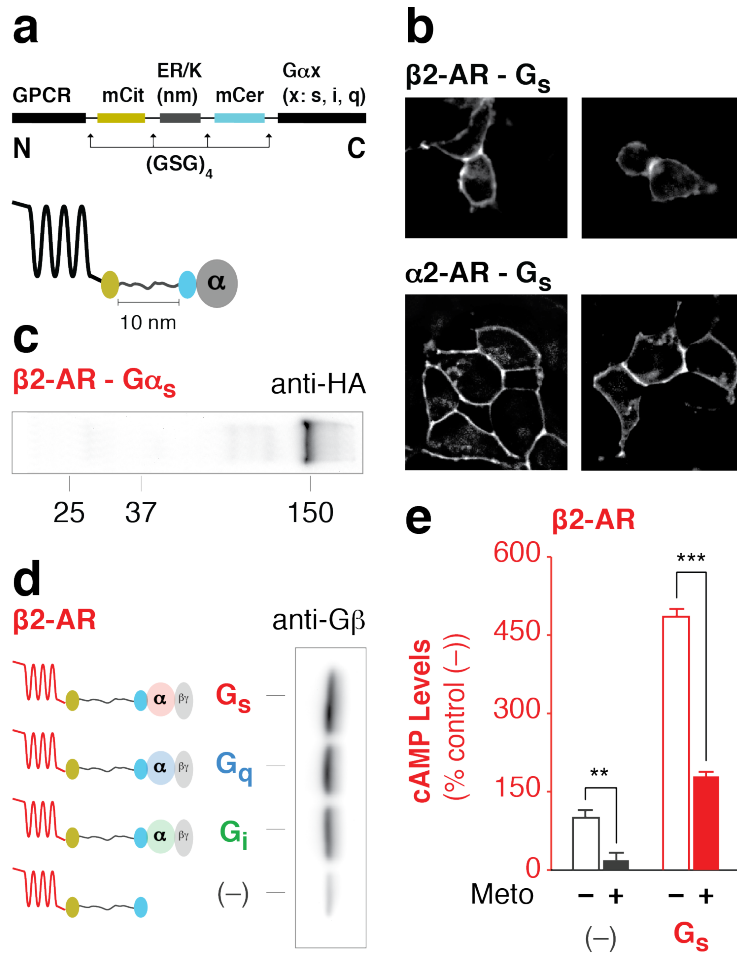
Fig. 3.1: GPCR-G protein fusion sensors are intact and functional. (*a*) Schematic of the GPCR-G protein sensor design. Protein domains are separated by (GSG)$_4$ linkers to ensure rotational freedom. Control (−) sensors do not contain a Gα subunit. (*b*) Sensors localize to the plasma membrane in live HEK293T cells as shown in representative images. (*c*) Western blot of membranes expressing HA-β2-AR-Gαs probed with anti-HA antibody. A distinct 150 kDa band indicates intact sensor expression. (*d*) Membranes expressing HA-β2-AR-Gαx sensors were subjected to HA-affinity purification and probed with anti-Gβ antibody. Equivalent amount of sensor is loaded per lane as assessed by mCitrine fluorescence. Gβ associates with the Gαs, Gαi, or Gαq subunit. (*e*) cAMP production in the presence or absence of inverse agonist (100 μM metoprolol) for β2-AR tethered with or without Gs. Untransfected HEK293T cells (UN) are not transfected with any sensor. Data are derived from at least three independent experiments, with at least three replicates per condition. Data are represented as % no-G protein control (−) (mean ± S.E.M **, *p ≤ 0.01* and ***, *p ≤ 0.001*).
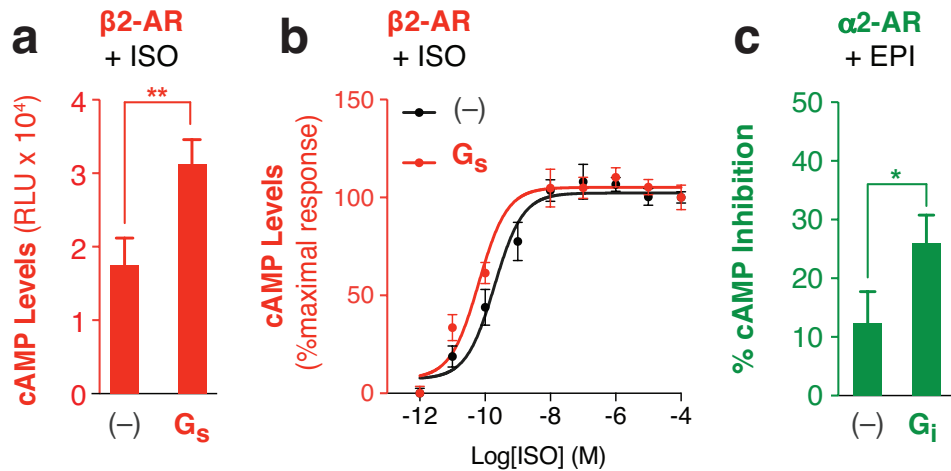
Fig. 3.2: Agonist enhances downstream second messenger response via the fused G protein. (*a*) cAMP production in the presence of (*a*) saturating (100 μM) or (*b*) varying concentration of isoproterenol for β2-AR tethered with or without (-) Gs. (*b*) Data are represented as percent maximum cAMP levels for 100 μM isoproterenol treatment of β2-AR fusions tethered with or without (-) Gs. (c) Percent inhibition of 1 μM forskolin induced cAMP production for α2-AR fusions with or without Gi treated with 100 μM epinephrine. Data are derived from at least three independent experiments, with at least three replicates per condition (mean ± S.E.M. *, $p \leq 0.05$; **, $p \leq 0.01$).
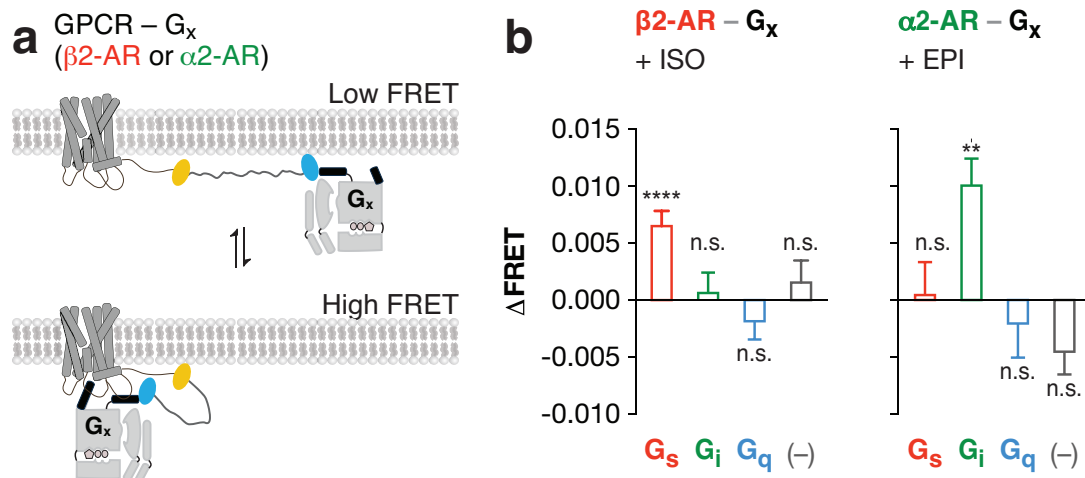
Fig. 3.3: Agonist modulates cognate GPCR-Gx fusion interactions. Schematic of the GPCR-G protein fusions linked with the 10 nm ER/K linker in the associated (high FRET) and dissociated (low FRET) states in live cells. GPCRs are colored by their cognate G proteins; red and green indicate Gs (β2-AR) and Gi (α2-AR) coupled receptors respectively. (*b*) Change in FRET (ΔFRET) for indicated GPCR-Gx fusions following agonist treatment in live cells (100 μM isoproterenol (ISO), 1 mM epinephrine (EPI)). Data are derived from at least three independent experiments, with at least three replicates per condition (mean ± S.E.M. *, $p \leq 0.05$; **, $p \leq 0.01$; ***, $p \leq 0.001$; ****, $p \leq 0.0001$). For additional statistical analysis see Tables 3.1 and 3.2.
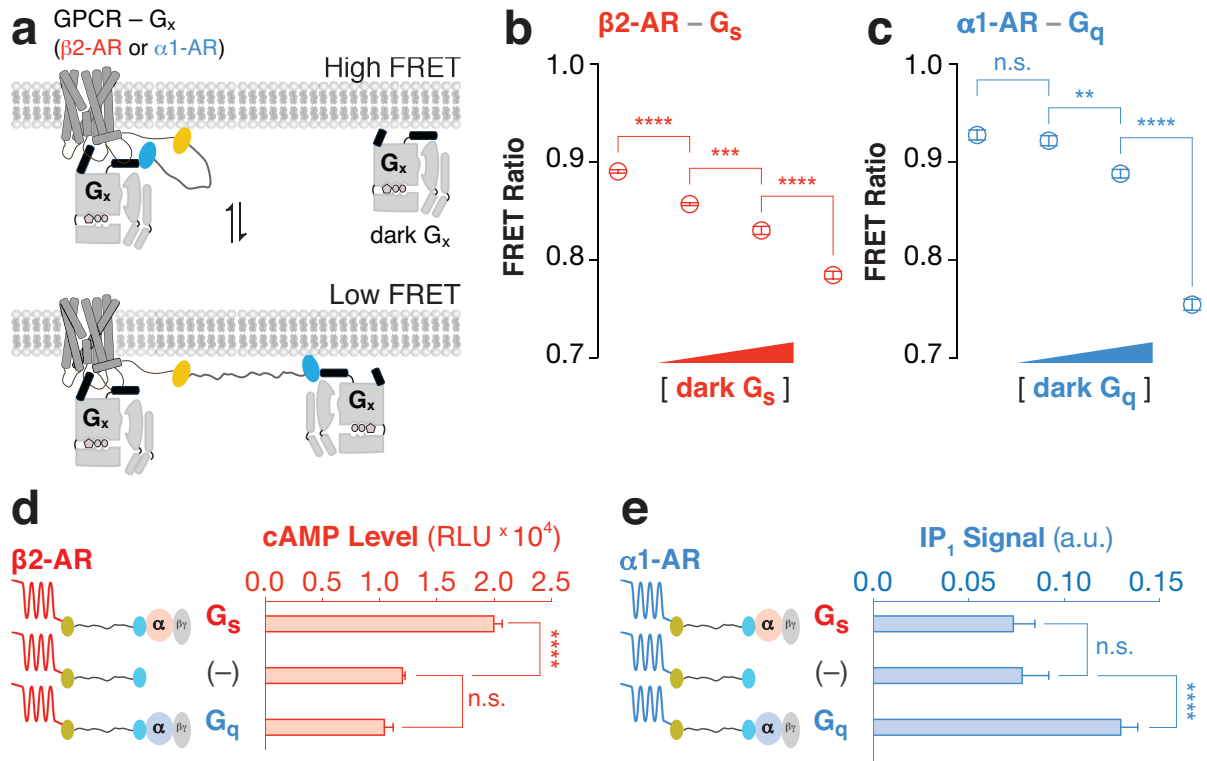
Fig. 3.4: Fusions modulate GPCR-G protein signaling relative to the endogenous cellular environment. (*a*) Schematic of competitive binding of un-tethered Gx ('dark Gx') to GPCR-Gx fusions. (*b* and *c*) FRET Ratios (525 nm/475 nm) for cells expressing GPCR-Gx fusion and cognate Gx after transient co-transfection with different concentrations of dark Gx DNA (0, 2, and 4 µg well^{-1}). GPCR-Gx fusion DNA (2-4 µg well^{-1}) was optimized to maintain equivalent expression across conditions. FRET Ratios for cells co-expressing (*b*) β2-AR-Gs fusions with unlabeled dark Gs (red) or (*c*) α1-AR-Gq fusions with dark Gq (blue). (*d*) Basal cAMP and levels (*e*) IP$_1$ for cells expressing (*d*) β2-AR and (*e*) α1-AR tethered to Gs, Gq, or no G protein (–). (*b-e*) Data are derived from at least three independent experiments, with at least three replicates per condition (mean ± S.E.M. *, $p \leq 0.05$; **, $p \leq 0.01$; ***, $p \leq 0.001$; ****, $p \leq 0.0001$).
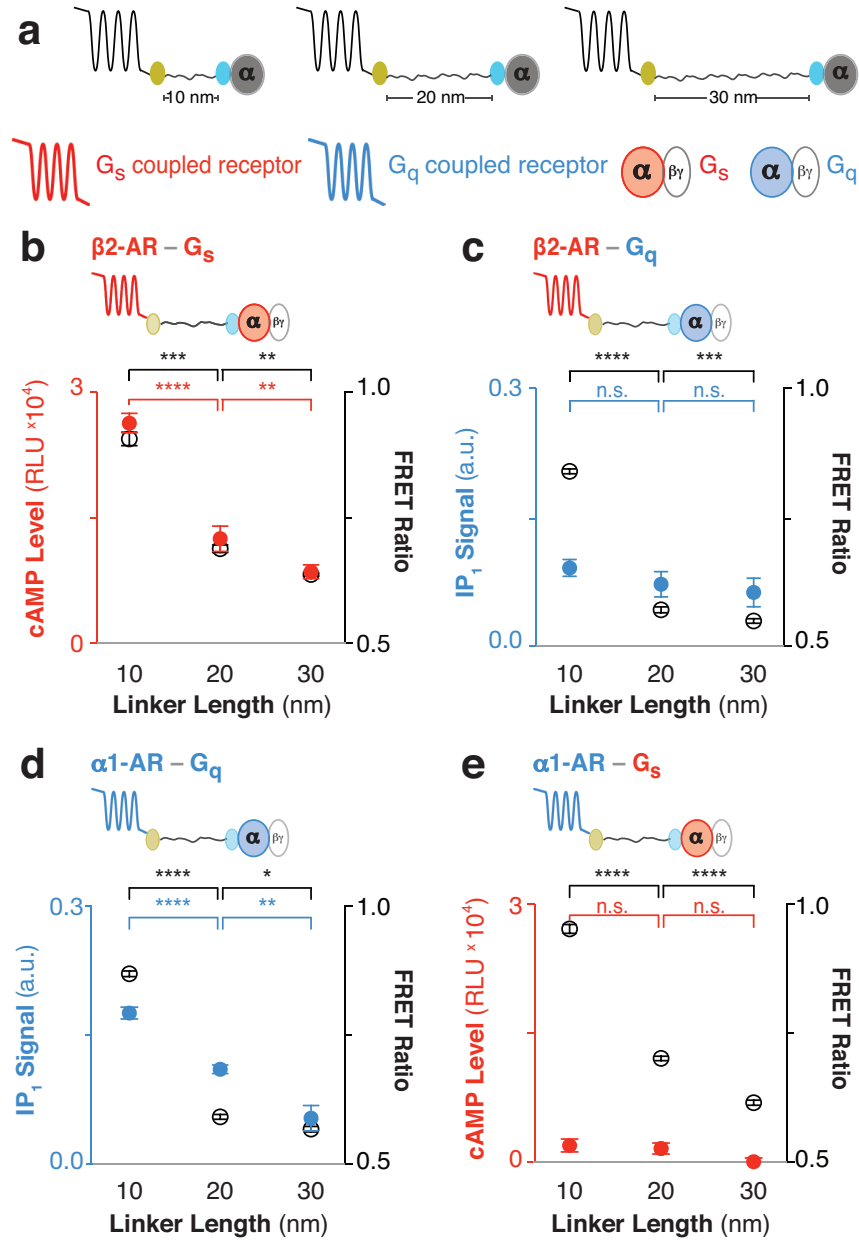
Fig. 3.5: ER/K linker length specifically modulates basal β2-AR-Gs and α1-AR-Gq downstream response in live cells. (*a*) Schematic of the GPCR-G protein fusions. Color represents cognate GPCR-G protein pair and corresponding downstream response (red: β2-AR, Gs, and cAMP levels; blue: α1-AR, Gq, and IP$_1$ signal). (*b-e*) Fusion type is indicated on the top left. FRET Ratios (525 nm/475 nm; open black circles, right y-axis) and basal (ligand-free) downstream response (filled colored circles, left y-axis) are compared to ER/K linker length (nm). (*b*) cAMP levels or (*c*) IP$_1$ signal for β2-AR tethered to cognate Gs or non-cognate Gq respectively. (*d*) IP$_1$ signal for cognate α1-AR-Gq fusions. (*e*) cAMP levels for α1-AR tethered to non-cognate Gs. (*b-e*) Paired Student's t-test was performed for FRET measurements (black) and downstream response (colored). Data are derived from at least three independent experiments, with at least three replicates per condition (mean ± S.E.M. *, $p \leq 0.05$; **, $p \leq 0.01$; ***, $p \leq 0.001$; ****, $p \leq 0.0001$). For additional statistical analysis see Table 3.3.
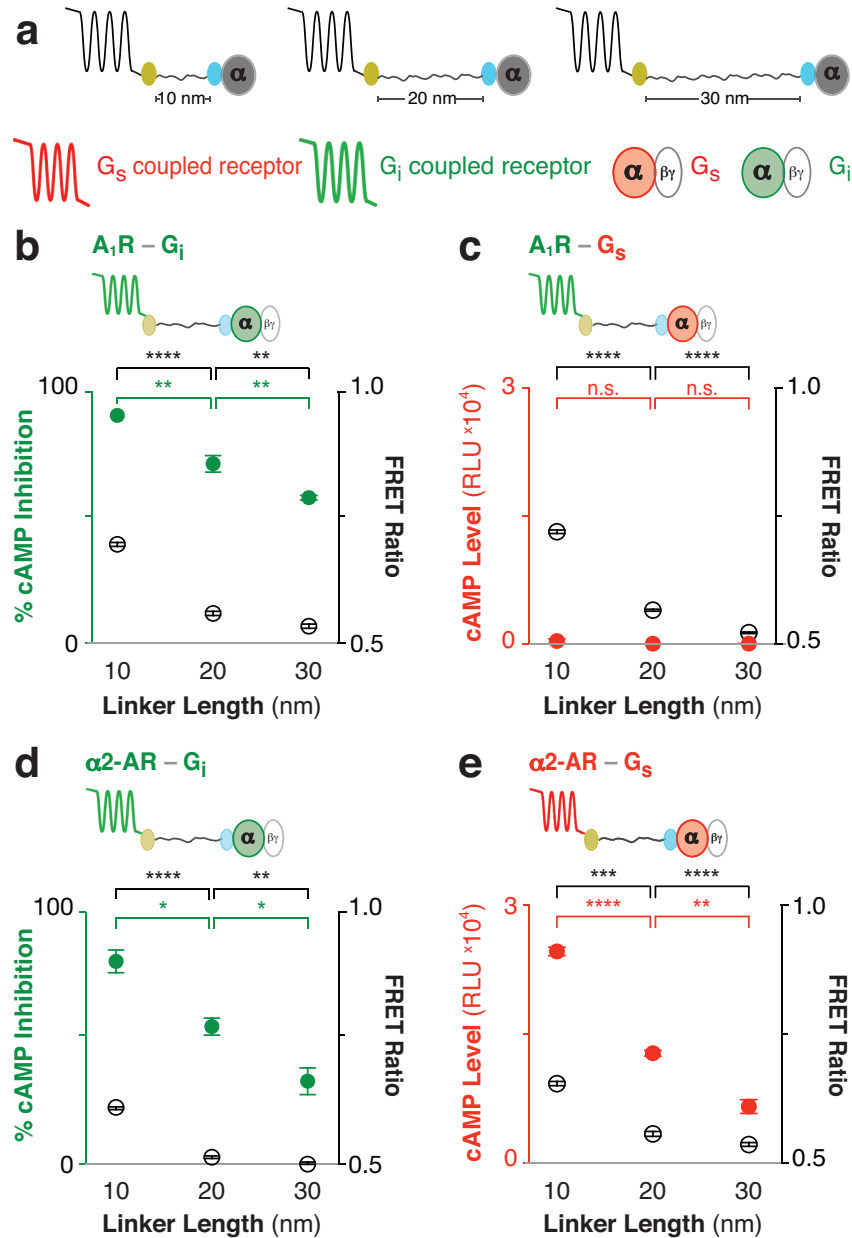
**Fig. 3.6: ER/K linker length tunes basal GPCR-Gi protein downstream response in live cells**. (*a*) Schematic of the GPCR-G protein fusions. Color represents cognate GPCR-G protein pair and corresponding downstream response (red: α2-AR, Gs, and cAMP levels; green: A$_1$R, α2-AR, Gi, and cAMP inhibition). (*b-e*) Fusion type is indicated on the top left. FRET Ratios (525 nm/475 nm; open black circles, right y-axis) and basal (ligand-free) downstream response (filled colored circles, left y-axis) are compared to ER/K linker length (nm). (*b*) Percent inhibition of 1 μM forskolin induced cAMP production for conical Gi coupled adenosine type 1 receptor (A$_1$R). (c) Basal cAMP levels for A$_1$R-Gs fusions. (*d*) % cAMP inhibition for Gi fusions and (*e*) cAMP levels for Gs fusions to α2-AR, a promiscuous Gs/Gi coupled receptor [27]. (*b* and *d*) Representative experiment with at least three replicates per condition. (*c* and *e*) Data are derived from at least three independent experiments, with at least three replicates per condition. (*b-e*) Paired Student's t-test was performed for FRET measurements (black) and downstream response (colored). Data are represented as mean ± S.E.M. *, $p \leq 0.05$; **, $p \leq 0.01$; ***, $p \leq 0.001$; ****, $p \leq 0.0001$). For additional statistical analysis see Table 3.4.

Fig.3.7: GPCR-Gx fusion localize to the plasma membrane. Representative image of live HEK293 cells expressing α2-AR-Gs fusion (see Methods for live cell microscopy). In this image 90% membrane localization was detected. Analysis was performed in ImageJ (NIH) using the threshold tool to select membrane (C; cyan outline) and internal expression (Y; yellow outline). Percent membrane expression was calculated by (C/(C+Y))*100%.

α2-AR - G$_S$
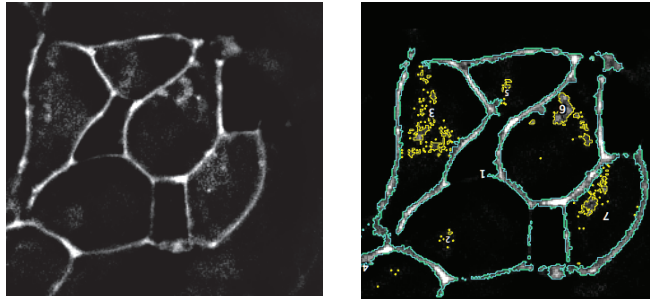
3.8. Tables

Table 3.1: Pairwise student's t-test comparison for β2-AR-Gx fusions. Mean difference is the difference between the means of the indicated β2-AR-Gx (x: s or q) fusions or control sensors (–). A significant difference between the tested fusions are represented with the following legend: *, $p \leq 0.05$; **, $p \leq 0.01$; ***, $p \leq 0.001$; ****, $p \leq 0.0001$, n.s. not significant.

Gx protein comparison	Mean Difference	Significance	Figure
s (minus) vs. s (ISO)	0.006217 ± 0.001242	****	Fig. 3*b* (ΔFRET)
q (minus) vs. q (ISO)	-0.0003354 ± 0.001766	n.s.	
(–) (minus) vs. (–) (ISO)	0.001251 ± 0.001502	n.s.	
s (ΔFRET) vs. q (ΔFRET))	-0.01365 ± 0.003462	**	
s (ΔFRET) vs. (–) (ΔFRET)	-0.01083 ± 0.004473	*	

Table 3.2: Pairwise student's t-test comparison for α2-AR-Gx fusions. Mean difference is the difference between the means of the tested α2-AR-Gx (x: s, i, q) fusions or control sensors (–). Statistical analysis was conducted for FRET ratio for cells treated with (Epi) or without (minus) 1 mM epinephrine. A significant difference between the tested conditions are represented with the following legend: *, $p \leq 0.05$; **, $p \leq 0.01$, n.s. not significant.

Gx protein comparison	Mean Difference	Significance	Figure
s (minus) vs s (Epi)	0.0004172 ± 0.002901	n.s.	
i (minus) vs i (Epi)	0.008794 ± 0.002406	**	
q (minus) vs q (Epi)	-0.002067 ± 0.002647	n.s.	
(–) (minus) vs (–) (Epi)	-0.004545 ± 0.002012	n.s.	Fig.3*b* (ΔFRET)
i (ΔFRET) vs s (ΔFRET)	0.009633 ± 0.003834	*	
i (ΔFRET) vs q (ΔFRET)	0.01212 ± 0.003879	*	
i (ΔFRET) vs (–) (ΔFRET)	0.01459 ± 0.003522	**	

Table 3.3: Pairwise student's t-test comparison for GPCR-Gx fusion. FRET Ratio and downstream response were measured for β2-AR or α1-AR fused to Gs or Gq using three different lengths ER/K linkers (10 nm, 20 nm, or 30 nm) in live cells. Mean difference is the difference between the means of the tested GPCR-Gx fusion FRET ratio or downstream response for Figure 5. A significant difference between the tested conditions are represented with the following legend: *, $p \leq 0.05$; **, $p \leq 0.01$; ***, $p \leq 0.001$; ****, $p \leq 0.0001$, n.s. not significant.

Fusion	Assay	Comparison	Mean Difference ± S.E.M.	Significance	Figure
β2-AR-Gs	cAMP	10 vs 20 nm	-13787 ± 814.6	****	Fig. 3.5b
		20 vs 30 nm	-3937 ± 855.4	**	
		10 vs 30 nm	-17724 ± 498.2	****	
	FRET	10 vs 20 nm	-0.2184 ± 0.01533	***	
		20 vs 30 nm	-0.05144 ± 0.008203	**	
		10 vs 30 nm	-0.2698 ± 0.01372	****	
α1-AR-Gs	cAMP	10 vs 20 nm	-354.3 ± 1129	n.s.	Fig. 3.5d
		20 vs 30 nm	-1915 ± 722.3	n.s.	
		10 vs 30 nm	-2269 ± 1237	n.s.	
	FRET	10 vs 20 nm	-0.2514 ± 0.007691	****	
		20 vs 30 nm	-0.086 ± 0.005317	****	
		10 vs 30 nm	-0.3374 ± 0.007925	****	
β2-AR-Gq	IP$_1$	10 vs 20 nm	-0.0191 ± 0.01366	n.s.	Fig. 3.5c
		20 vs 30 nm	-0.009514 ± 0.01777	n.s.	
		10 vs 30 nm	-0.02861 ± 0.01477	n.s.	
	FRET	10 vs 20 nm	-0.2688 ± 0.006816	****	
		20 vs 30 nm	-0.02158 ± 0.005731	***	
		10 vs 30 nm	-0.2904 ± 0.006323	****	
α1-AR-Gq	IP$_1$	10 vs 20 nm	-0.06594 ± 0.008062	****	Fig. 3.5e
		20 vs 30 nm	-0.05721 ± 0.01508	**	
		10 vs 30 nm	-0.1232 ± 0.01118	****	
	FRET	10 vs 20 nm	-0.2777 ± 0.006475	****	
		20 vs 30 nm	-0.02389 ± 0.005942	*	
		10 vs 30 nm	-0.3016 ± 0.006235	****	

Table 3.4: Pairwise student's t-test comparison for GPCR-Gx fusion. FRET Ratio and downstream response were measured for A_1R or $\alpha 2$-AR fused to Gs or Gi using three different lengths ER/K linkers (10 nm, 20 nm, or 30 nm) in live cells. Mean difference is the difference between the means of the tested GPCR-Gx fusion FRET ratio or downstream response for Figure 6. A significant difference between the tested conditions are represented with the following legend: *, $p \leq 0.05$; **, $p \leq 0.01$; ***, $p \leq 0.001$; ****, $p \leq 0.0001$, n.s. not significant.

Fusion	Assay	Comparison	Mean Difference ± S.E.M.	Significance	Figure
A_1R-Gi	FRET	10 vs 20 nm	-0.1375 ± 0.005836	****	Fig. 3.6.*b*
		20 vs 30 nm	-0.02529 ± 0.005765	**	
		10 vs 30 nm	-0.1628 ± 0.005716	****	
	cAMP inhibition	10 vs 20 nm	-19.25 ± 4.141	**	
		20 vs 30 nm	-13.5 ± 3.41	**	
		10 vs 30 nm	-32.75 ± 2.704	****	
A_1R-Gs	FRET	10 vs 20 nm	-0.1534 ± 0.004006	****	Fig. 3.6*c*
		20 vs 30 nm	-0.04407 ± 0.002722	****	
		10 vs 30 nm	-0.1975 ± 0.004183	****	
	cAMP	10 vs 20 nm	-710.9 ± 363.9	n.s.	
		20 vs 30 nm	228.4 ± 310.1	n.s.	
		10 vs 30 nm	-482.4 ± 349.6	n.s.	
$\alpha 2$-AR-Gi	FRET	10 vs 20 nm	-0.09878 ± 0.003878	****	Fig. 3.6*d*
		20 vs 30 nm	-0.01398 ± 0.00477	**	
		10 vs 30 nm	-0.1128 ± 0.004693	****	
	cAMP inhibition	10 vs 20 nm	-25.83 ± 5.507	*	
		20 vs 30 nm	-21.67 ± 6.28	*	
		10 vs 30 nm	-47.5 ± 7.61	**	
$\alpha 2$-AR-Gs	FRET	10 vs 20 nm	-0.09769 ± 0.006366	****	Fig. 3.6*e*
		20 vs 30 nm	-0.02075 ± 0.005947	**	
		10 vs 30 nm	-0.1184 ± 0.005466	****	
	cAMP	10 vs 20 nm	-11873 ± 692.8	***	
		20 vs 30 nm	-6223 ± 1069	*	
		10 vs 30 nm	-18096 ± 948.2	****	

3.9. References

1   Dorsam, R. T. & Gutkind, J. S. G-protein-coupled receptors and cancer. *Nat Rev Cancer* **7**, 79-94, (2007).

2   Hermans, E. Biochemical and pharmacological control of the multiplicity of coupling at G-protein-coupled receptors. *Pharmacol Ther* **99**, 25-44, (2003).

3   Gales, C. *et al.* Real-time monitoring of receptor and G-protein interactions in living cells. *Nat Methods* **2**, 177-184, (2005).

4   Gales, C. *et al.* Probing the activation-promoted structural rearrangements in preassembled receptor-G protein complexes. *Nat Struct Mol Biol* **13**, 778-786, (2006).

5   Hein, P., Frank, M., Hoffmann, C., Lohse, M. J. & Bunemann, M. Dynamics of receptor/G protein coupling in living cells. *EMBO J* **24**, 4106-4114, (2005).

6   Lohse, M. J., Nuber, S. & Hoffmann, C. Fluorescence/bioluminescence resonance energy transfer techniques to study G-protein-coupled receptor activation and signaling. *Pharmacol Rev* **64**, 299-336, (2012).

7   Qin, K., Dong, C., Wu, G. & Lambert, N. A. Inactive-state preassembly of G(q)-coupled receptors and G(q) heterotrimers. *Nat Chem Biol* **7**, 740-747, (2011).

8   Milligan, G. Insights into ligand pharmacology using receptor-G-protein fusion proteins. *Trends Pharmacol Sci* **21**, 24-28, (2000).

9   Seifert, R., Wenzel-Seifert, K. & Kobilka, B. K. GPCR-Galpha fusion proteins: molecular analysis of receptor-G-protein coupling. *Trends Pharmacol Sci* **20**, 383-389, (1999).

10   Dupuis, D. S., Tardif, S., Wurch, T., Colpaert, F. C. & Pauwels, P. J. Modulation of 5-HT1A receptor signalling by point-mutation of cysteine351 in the rat Galpha(o) protein. *Neuropharmacology* **38**, 1035-1041, (1999).

11   Wise, A. & Milligan, G. Rescue of functional interactions between the alpha2A-adrenoreceptor and acylation-resistant forms of Gi1alpha by expressing the proteins from chimeric open reading frames. *J Biol Chem* **272**, 24673-24678, (1997).

12   Wurch, T., Colpaert, F. C. & Pauwels, P. J. Mutation in a protein kinase C phosphorylation site of the 5-HT1A receptor preferentially attenuates Ca2+ responses to partial as opposed to higher-efficacy 5-HT1A agonists. *Neuropharmacology* **44**, 873-881, (2003).

13   Wurch, T. & Pauwels, P. J. Analytical pharmacology of G protein-coupled receptors by stoichiometric expression of the receptor and G(alpha) protein subunits. *J Pharmacol Toxicol Methods* **45**, 3-16, (2001).

14   Sivaramakrishnan, S. & Spudich, J. A. Systematic control of protein interaction using a modular ER/K alpha-helix linker. *Proc Natl Acad Sci U S A* **108**, 20467-20472, (2011).

15   Swanson, C. J. & Sivaramakrishnan, S. Harnessing the unique structural properties of isolated alpha-helices. *J Biol Chem* **289**, 25460-25467, (2014).

16   Rasmussen, S. G. *et al.* Crystal structure of the beta2 adrenergic receptor-Gs protein complex. *Nature* **477**, 549-555, (2011).

17   Ritt, M., Guan, J. L. & Sivaramakrishnan, S. Visualizing and manipulating focal adhesion kinase regulation in live cells. *J Biol Chem* **288**, 8875-8886, (2013).

18   Swanson, C. J. *et al.* Conserved modular domains team up to latch-open active protein kinase Calpha. *J Biol Chem* **289**, 17812-17829, (2014).

19   Semack, A., Sandhu, M., Malik, R. U., Vaidehi, N. & Sivaramakrishnan, S. Structural Elements in the Galphas and Galphaq C Termini That Mediate Selective G Protein-coupled Receptor (GPCR) Signaling. *J Biol Chem* **291**, 17929-17940, (2016).

20   Semack, A., Malik, R. U. & Sivaramakrishnan, S. G Protein-selective GPCR Conformations Measured Using FRET Sensors in a Live Cell Suspension Fluorometer Assay. *J Vis Exp*, (2016).

21   Malik, R. U. *et al.* Detection of G protein-selective G protein-coupled receptor (GPCR) conformations in live cells. *J Biol Chem* **288**, 17167-17178, (2013).

22   Chidiac, P., Hebert, T. E., Valiquette, M., Dennis, M. & Bouvier, M. Inverse agonist activity of beta-adrenergic antagonists. *Mol Pharmacol* **45**, 490-499, (1994).

23   Seifert, R., Lee, T. W., Lam, V. T. & Kobilka, B. K. Reconstitution of beta2-adrenoceptor-GTP-binding-protein interaction in Sf9 cells--high coupling efficiency in a beta2-adrenoceptor-G(s alpha) fusion protein. *Eur J Biochem* **255**, 369-382, (1998).

24   Seifert, R., Wenzel-Seifert, K., Gether, U., Lam, V. T. & Kobilka, B. K. Examining the efficiency of receptor/G-protein coupling with a cleavable beta2-adrenoceptor-gsalpha fusion protein. *Eur J Biochem* **260**, 661-666, (1999).

25   Vilardaga, J. P., Steinmeyer, R., Harms, G. S. & Lohse, M. J. Molecular basis of inverse agonism in a G protein-coupled receptor. *Nat Chem Biol* **1**, 25-28, (2005).

26   Sivaramakrishnan, S. *et al.* Combining single-molecule optical trapping and small-angle x-ray scattering measurements to compute the persistence length of a protein ER/K alpha-helix. *Biophys J* **97**, 2993-2999, (2009).

27   Eason, M. G., Kurose, H., Holt, B. D., Raymond, J. R. & Liggett, S. B. Simultaneous coupling of alpha 2-adrenergic receptors to two G-proteins with opposing effects. Subtype-selective coupling of alpha 2C10, alpha 2C4, and alpha 2C2 adrenergic receptors to Gi and Gs. *J Biol Chem* **267**, 15795-15801, (1992).

28   Wenzel-Seifert, K. & Seifert, R. Molecular analysis of beta(2)-adrenoceptor coupling to G(s)-, G(i)-, and G(q)-proteins. *Mol Pharmacol* **58**, 954-966, (2000).

29   Hein, P. & Bunemann, M. Coupling mode of receptors and G proteins. *Naunyn Schmiedebergs Arch Pharmacol* **379**, 435-443, (2009).

30   Hein, P. *et al.* Gs activation is time-limiting in initiating receptor-mediated signaling. *J Biol Chem* **281**, 33345-33351, (2006).

31   Neubig, R. R. Membrane organization in G-protein mechanisms. *FASEB J* **8**, 939-946, (1994).

32   Lan, T. H. *et al.* BRET evidence that beta2 adrenergic receptors do not oligomerize in cells. *Sci Rep* **5**, 10166, (2015).

Chapter 4

Perspective: Emerging concepts in multiplicity of GPCR-G protein signaling

4.1 Abstract

Recent studies suggest that GPCRs exist in equilibrium of conformations, where ligand binding stabilizes a subset of these conformations resulting in activation of one or more distinct G proteins and/or arrestins. While these studies support a multiplicity of GPCR conformations they do not directly link the observed conformations to selection of one or more downstream effectors. Utilizing the well-characterized interaction between the GPCR and the C-terminus of the Gα subunit, novel GPCR-peptide sensors probe for ligand-dependent stabilization of GPCR conformations that are selective for one or more G proteins. Extended works by Semack et al. demonstrate "hotspot" residues on the Gα C-terminus that are necessary and sufficient for specificity of β2-AR (Gs/Gi coupled receptor) and V$_1$R's (Gq coupled receptor) interaction with their cognate Gα C-termini. Although, these findings demonstrate the utility of the peptide sensors, Gα C-terminus is only one part of the complex GPCR-G protein interface. As such, complementary GPCR-G protein sensors were build, which serve the dual purpose of probing agonist-stimulated changes in GPCR-G protein interaction while examining the downstream response using the same construct. Collectively, these tools can be used to dissect the complex network of GPCR-G protein interactions in live cells, while exploring questions of specificity of GPCR-G protein interaction and how non-cognate interactions influences GPCR conformational diversity and downstream second messenger signaling.

4.2 Introduction

G protein coupled receptors (GPCRs) can be thought of as information conduits (*1, 2*). They detect perturbations in the external cellular environment by binding to a wide range of ligands,

such as small molecules, neurotransmitters, peptides, and odorants (*3*). GPCRs communicate ligand-binding event to the intracellular environment, by binding to downstream heterotrimeric G proteins and arrestins (*3*). GPCR itself does not perform any catalytic functions (*2*). Instead, active GPCR conformations facilitate internal structural rearrangement of Gα's Ras domain, leading to nucleotide exchange, and subsequent G protein activation (*4*).

Initial studies posited that GPCRs exist in a two-state equilibrium, an inactive (R) and active (R*) conformations (*5*). Site-directed-spin labeling experiments with bovine rhodopsin demonstrated an outward movement of the transmembrane helix 6 (TM6) in the active conformation (*6*). In agreement with earlier works, co-crystal structure of agonist bound β2-AR in complex with Gs, TM6 displayed a 14 Å outward movement with inward movements of TM3 and TM7. These changes create a crevice at the intracellular surface of GPCR to facilitate binding to the C-terminus of the G protein α subunit (*7*). The differences in the inactive conformation (antagonist, or inverse agonist bound β2-AR) (*8*) and the agonist bound β2-AR (*7*) are consistent with the two-state model (*5*). Where the level of downstream activity depends on how ligands effect the R <-> R* equilibrium, with agonists shifting the equilibrium to the right, and inverse agonists shifting the equilibrium to the left (*5*).

However, recent biophysical and functional studies support a multi-state model where ligand binding stabilizes a specific conformation or a subset of conformational states (*5*). Combinatorial approach using chemical labeling and mass spectroscopy was used to elegantly demonstrate ligand-specific β2-AR conformations (*9*). Researchers labeled cysteine and lysine residues with protiated (light chain, NEM-H_5) and deuterated (heavy chain, NEM-D_5) *N*-ethylmalemide (NEM) (*9*). Researchers monitored conformational changes in the presence of different ligands as a function of time. Proteolysis and subsequent mass spectroscopy were used to quantitate labeling efficiency of NEM-H_5 and NEM-D_5 at specific residues (*9*). Quantitative analysis revealed different labeling kinetics in the presence of different ligands, suggesting a broad conformational landscape for β2-AR (*9*).

Subtle changes in GPCR conformation in the presence of ligands were also monitored via ^{19}F-NMR spectroscopy (*10*). Researches monitored changes in NMR signal of two cytosolic cysteines located on transmembrane 6 (Cys265) and transmembrane 7 Cys327) (*10*). To facilitate analysis, singly labeled receptor was used after labeling the appropriate cysteine with 2,2,2 trifluoroethanethiol (*10*). Each of the ten ligands tested altered the NMR signal at the two

residues to unequal extent, demonstrating conformational heterogeneity for β2-AR in response to different ligands (*10*). Temperature dependence of the NMR signal in terms of line width and peak intensity for the agonist isoproterenol suggested a larger degree of conformational plasticity for the active β2-AR state (*10*). These findings were corroborated with a parallel ^{19}F-NMR study, which also demonstrated that ligand free state exhibits distribution of two peaks with a slow transition between states, indicating a two state equilibrium (*11*). Agonist binding induced a redistribution of peak intensity and width, where binding to Gs protein or Gs protein mimetic nanobody further enhanced peak intensity and narrowed the line width suggesting that agonist bound β2-AR maintains significant structural heterogeneity until it binds a G protein (*11*).

4.3 Peptide sensors provide a link between structural and functional studies.

While these studies support a multiplicity of β2-AR conformations they do not directly link the observed conformations to selection of one or more downstream effectors. To bridge this gap, as a first step, sensors were developed in Chapter 2 by leveraging the well-documented interaction between GPCR and Gα C-terminal peptide (*1*). Studies previously established the Gα C-terminus as one of the key determinants of specificity of GPCR-G protein interaction (*12-15*). Crystal structures of light activated metarhodopsin bound to a C-terminal transdusin peptide (Gαt C-terminal peptide) (*16*), and of agonist bound β2-AR in complex with the nucleotide empty Gs (*7*) demonstrated that the C-terminus of the Gα binds into the cytosolic core of the 7-transmebrane bundle. As such, peptides derived from the G C terminus were used as "baits" to detect G protein-selective GPCR conformations (*1*).

As part of sensor design, C-terminal α5 helix from a Gα subunit was tethered to the full length β2-AR with an ER/K α-helical linker flanked by FRET donor and acceptor (mCerulean and mCitrine) (*1*). Sensors are thought to exist in an open, extended conformation in the non-interacting, inactive state (*1*). Studies show that activation of the receptor via mutagenesis or agonist binding, enhance the interaction with the cognate Gα's α5 helical peptide resulting in a gain in FRET ratio (*1*). As part of sensor design 27 residues were derived from the α5 helix of the indicated Gα C terminus (*1*). One concern with the long peptide design is that an increase in FRET can arise from non-specific interaction of the charged or hydrophic residues with the tethered GPCR or the membrane. As such, short peptide sensors with 11 C-terminal residues were tested, which also showed a selective increase in FRET ratio for the cognate peptide (*1*).

As expected, the canonical agonist isoprotenerol enhanced the interaction between β2-AR and the C-terminus of Gαs (*1*). Interestingly, β2-AR's inverse agonist metoprolol decreased the interaction between β2-AR and the C-termini of Gαs but enhanced the interaction with Gαi (*1*). Downstream assays independently verified metoprolol stimulated Gi signaling, as the cAMP suppression was sensitive to pertussis toxin treatment (*1*). As such, FRET sensor facilitates interpretation of the conformational states detected by spectroscopy and also complements established FRET-based sensors that differentially detect agonist and inverse agonist stimuli. Collectively, these spectroscopic studies support the emerging paradigm, which extends the "on/off" switch model to equilibrium of conformations with varying efficacies in activating distinct G proteins and/or arrestin. Ligand binding stabilizes subset of these conformations, resulting in a unique second messenger response (*2, 5, 17*).

4.4 Peptide sensors provide a foothold to explore the molecular basis of specificity of GPCR-G protein interaction

Additional studies arising from this work led by Semack *et al*. sought to explore the molecular basis of G protein selection following agonist stimulation (*18*). Initial studies by Conklin *et al*. in 1993 elegantly demonstrated that the last three amino acids of the Gαi C-terminus were sufficient in determining G protein specificity (*12*). However, this mechanism was not found to be true for additional GPCR-G protein combinations tested in 1996 (*13*). Thus far, only one crystal structure of the GPCR-G protein complex exists (*7*), which greatly hinders pairwise comparison of multiple GPCR-G protein interfaces to dissect the molecular basis of G protein selection. Sensors developed as part of Chapter 2 were apt tools to explore mechanism of G protein selection by comparing a Gs coupled receptor to a Gq coupled receptor.

Semack *et al*. expanded the findings in Chapter 2 to show that six different Class A GPCRs: two Gs coupled receptors (β3-AR and D_1R), two Gi coupled receptors (α2-AR and CB_1), and two Gq coupled receptors (α1-AR and V_1R), exhibit enhanced binding to their cognate Gα C-terminal peptides following stimulation with their respective full agonists in live cells (Fig. 4.1) (*18*). This verification further strengthened the application of this technology to dissect the mechanism of G protein selection.
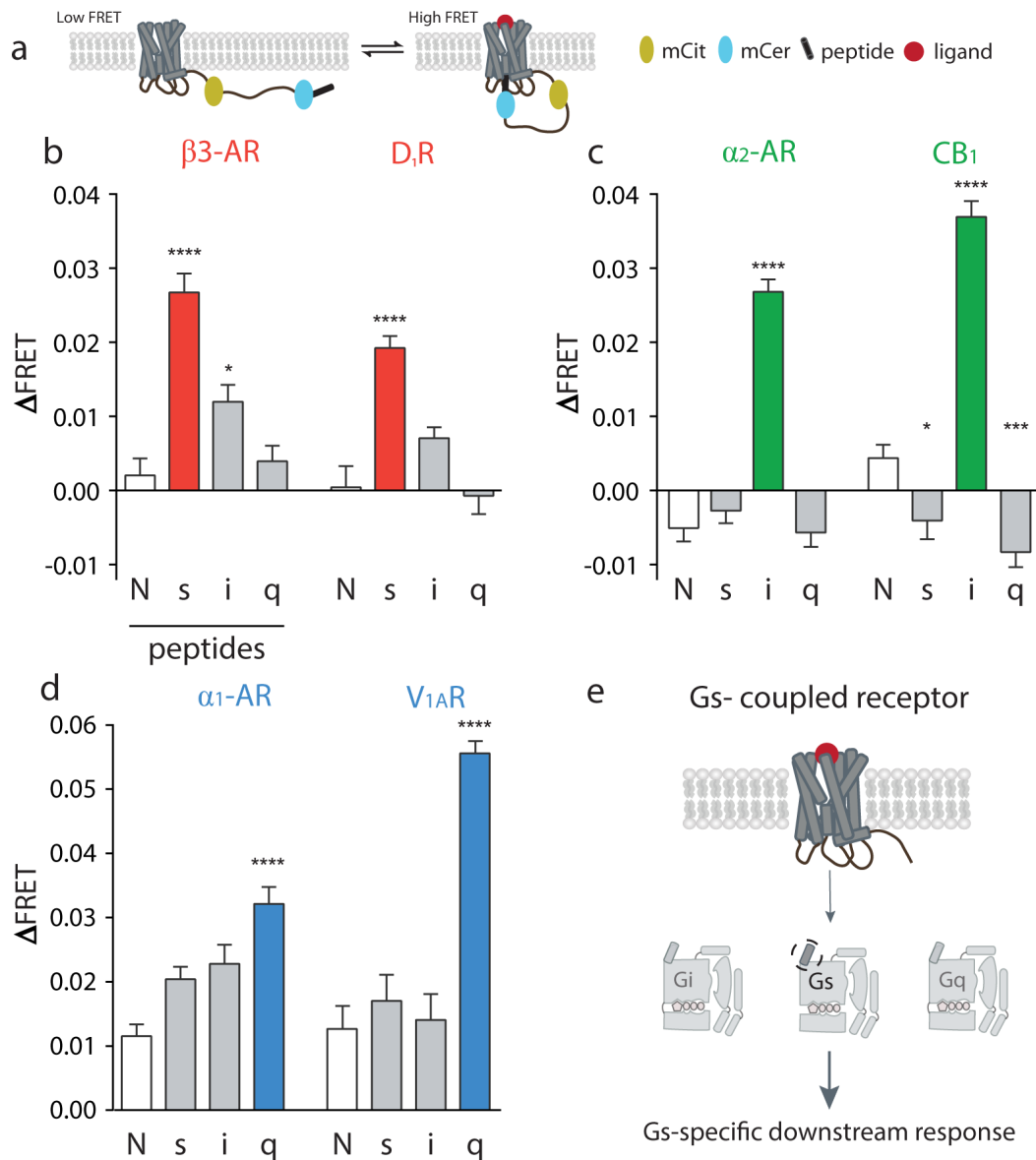
Fig. 4.1 Gα C-terminus minimally sufficient to detect cognate pathway for six Class A GPCRs – (*a*) Schematic of GPCR FRET sensor expressed at plasma membrane in dissociated, low FRET and associated, high FRET state. *(b, c, d)* Gs-coupled GPCRs (β3-adrenergic receptor; dopamine receptor D1), Gi-coupled GPCRs (α₂-adrenergic receptor; cannabinoid receptor type 1) and Gq-coupled GPCR FRET sensors (α₁-adrenergic receptor; vasopressin 1A receptor) tethered to no-peptide (N), s, i, or q peptide and test for change in FRET upon agonist stimulation. *(e)* GPCR selects for G protein via Gα C-terminus. Results are expressed as mean ± S.E. of three independent experiments performed in triplicate ($n \geq 3$). Asterisks represent significant differencs between the indicated peptide compared to no-peptide using Tukey's Multiple comparison's test. *, $p \leq 0.05$; **, $p \leq 0.01$; ***, $p \leq 0.001$; ****, $p \leq 0.0001$.

In agreement with the aforementioned NMR studies (*10, 11*), molecular dynamics simulation

(MD) studies performed with agonist bound β2-AR and V₁R demonstrated that cognate peptide binding decreases β2-AR and V₁R conformational flexibility to stabilize a subset of conformations (*18*). MD simulation confirmed that that cognate GPCR-peptide interactions are energetically favorable compared to non-cognate interactions (Fig. 4.2) (*18*). Structure-based sequence alignment of Gαs and Gαq C-termini identified residues, which could be critical for receptor binding (*18*). Follow-up mutagenesis and chimeric studies identified hotspot residues within the Gα C-termini (Gαs/Gαq – Q384L/L349, Q390/E355, E392/N357) that facilitate selective interaction between β2-AR-Gαs and V₁R-Gαq (Fig. 4.3) (*18*). Overall, this study strongly highlights the collaborative strength of molecular dynamic approach and live cell FRET-based assay to dissect the structural basis of G protein selection.

4.5 GPCR-G protein sensors modulate GPCR-G protein interaction in live cells

An important caveat in the Chapter 2 and Semack et al studies is that Gα C-terminus is one element of the GPCR-G protein interface. The co-crystal structure of active conformation of β2-AR in a complex with a nucleotide empty state of Gs protein at 3.5Å resolution revealed an extensive interface between β2-AR and Gs (Fig. 1.6) (*7*). The interface consists of β2-AR's intracellular loop 2 (ICL2) and transmembrane 5 (TM5) and TM6, with Gαs elements including α5 helix, αN-β1 junction, and α4 helix. In addition, β2-AR's ICL2 and the E/DRY motif make long distance (9-10Å), charged interactions with Gαs N-terminal α5 helix (*7, 19*). Therefore, to understand how GPCR-G protein interaction influence downstream second messenger response, we constructed full-length GPCR-G protein SPASM sensors as described in Chapter 3.

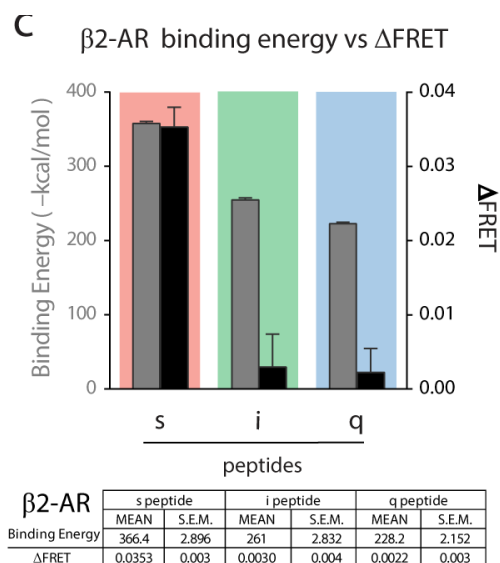| β2-AR	s peptide		i peptide		q peptide	
	MEAN	S.E.M.	MEAN	S.E.M.	MEAN	S.E.M.
Binding Energy	366.4	2.896	261	2.832	228.2	2.152
ΔFRET	0.0353	0.003	0.0030	0.004	0.0022	0.003

Fig. 4.2 Binding energies (-kcal/mol) of β2-AR-peptide complexes with s, i, and q peptides compared to ΔFRET (*1*). Binding energy results are expressed as mean ± S.E of 5 independent replicates of 100 ns simulations. ΔFRET results are expressed as mean ± S.E. of 3 independent experiments of at least 3 repeats per experiments. Table lists the values represented in the graph.
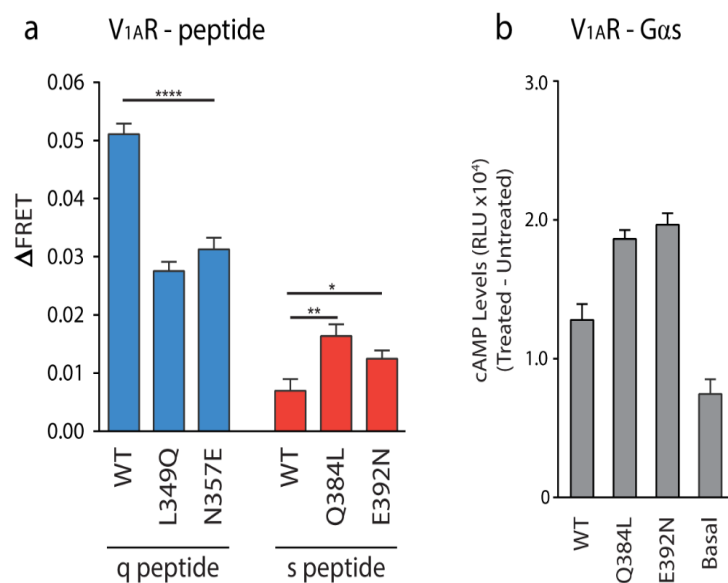
Fig. 4.3. Single point mutations are sufficient to enhance peptide binding in V₁AR *(a)* ΔFRET assay for agonist-stimulated V₁AR testing single point mutations in q peptide (L349Q; N357E) and s peptide (Q384L; E392N) compared to WT q and s peptide, respectively. *(b)* cAMP assay for single point mutations (Q384L; E392N) in Gαs-tethered V₁AR FRET sensor compared to WT or untransfected HEK293 (Basal). Results are expressed as mean ± S.E. of three independent experiments performed in triplicate. Stars represent significance of mutant peptides compared to WT peptide using Student unpaired t test. *, $p \leq 0.05$; **, $p \leq 0.01$; ***, $p \leq 0.001$; ****, $p \leq 0.0001$.

Current approaches to visualize GPCR-G protein interaction in cells involve probing the interaction between individually expressed fluorescent or luminescent protein fusions using FRET or bioluminescence resonance energy transfer (BRET) (*20-24*). Therefore, insights into the GPCR-G protein interaction gained from these studies are limited by their dependence on the relative concentration and co-localization of individually expressed GPCR and G protein. Alternatively, direct GPCR-G protein fusions generated by tethering the N-terminus of the Gα to the GPCR's C-tail with a short or no linker in between have been used to study the influence of tethering different G protein subunits on G protein activation and second messenger signaling (*25, 26*). Such fusions have not been used to monitor the GPCR-G protein interaction using resonance energy transfer approaches (*23*). A limitation of direct fusions is that GPCRs with short C-tails do not efficiently signal to the tethered G protein (*27-30*).

In Chapter 3, we describe a new approach that relies on ER/K-linked fusions (*31*) to compare downstream signaling from different GPCR – G protein pairings. In contrast to previous GPCR-G protein fusions that use a short unstructured linker (*26-28, 30, 32, 33*), in the absence of an interaction, the structured ER/K linker provides a significant spatial separation between the GPCR and the G protein fused to its ends. Unlike current FRET/BRET sensors that rely on the co-expression of labeled GPCR and G protein subunits (*20-24, 34, 35*), the SPASM sensors require the expression of a single polypeptide that provides 1:1 stoichiometry between the

exogenously expressed GPCR and G protein. Agonist stimulation provides changes in FRET (ΔFRET) comparable to those previously reported using co-expressed FRET/BRET pairs (*20-22*). Hence, the SPASM sensors serve the dual purpose of probing agonist-stimulated changes in GPCR-G protein interaction while examining the downstream response using the same construct.

4.6 Future directions

Malik et al. (*1*) and Semack et al. (*18*) studies give rise to multiple exciting questions and directions: (i) What is the molecular basis of G protein specificity? Specifically, what set of residues, motifs, or 'residue-networks' within the GPCR, that direct G protein selection. How did the specificity of GPCR-G protein interaction evolve within the class A GPCR family? (ii) A second direction that these tools naturally lend themselves to, is exploring how ligands exert their effects on GPCR conformations and GPCR-Gα C-terminal peptide interaction. Many agonists occupy the same ligand-binding pocket within the GPCR; however, they are functionally distinct and are subcategorized into full agonist, partial agonist, inverse agonists, antagonist, and biased agonists. (iii) Lastly, understanding the role of allosteric modulators, which bind to the non-orthosteric site, on stabilization of GPCR conformation?
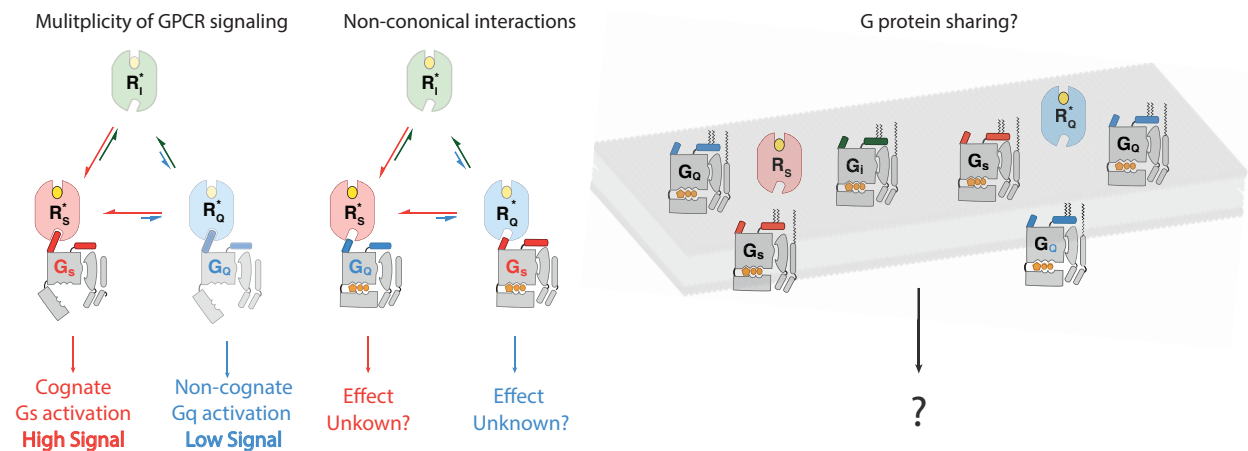
Fig. 4.4: Roles of cognate and non-cognate GPCR-G protein interactions in GPCR signaling. (*Left*) GCPRs (R) are thought to exists in equilibrium of G protein selective conformations. Shown is a strong interaction between Gs selective GPCR conformation and Gs protein resulting in robust downstream signaling. In contrast, abundance of Gq activating conformation yields no or low downstream signaling. (*Middle*) In comparison, effect of non-activating GPCR conformation and G protein are poorly understood. (*Right*) Lastly, in the context of a cellular environment, where multiple GPCR and G proteins are expressed, the effects of non-cognate GPCR-G protein interactions on G protein signaling remains a black box.

Speculating from Semack et al findings (*18*), in lieu of the ^{19}F-NMR (*11*) and the ternary complex model (*36, 37*), these studies suggest a tantalizing idea of G proteins as allosteric modulators of GPCRs. The ternary complex model also supports this framework, where G protein binding stabilizes high affinity interaction between ligand and GPCR (*36, 37*). However, the influence of non-cognate G proteins remains unknown. In general, the focus of most GPCR studies is cognate GPCR and G protein interactions. However, for a given cell with random distribution of GPCR on the plasma membrane, the GPCR may interact with cognate and non-cognate G proteins alike. One interesting avenue to explore with the tools developed here is how non-cognate G proteins influences GPCR conformational heterogeneity and G protein selection (Fig 4.4).

4.7 Caveats and final remarks

FRET and functional studies performed in this work were conducted in live cells, where the GPCR, GPCR interaction with the tethered peptide or G protein, and the tethered G protein are all under regulation by the endogenous GPCR-G protein signaling machinery (*1, 18*). In addition, cellular expression levels, the relative concentration of GPCR and G protein, and the arrangement of these molecules on the plasma membrane may influence FRET ratio, changes in FRET ratio, and the extent of the downstream response. Live cell studies using these sensors should be done in parallel systems to understand if and how the response varies in different cellular contexts. Parallel approaches using these sensors and conventional techniques should be undertaken to facilitate interpretation of collected observations.

The work presented here exploits the unique features of the ER/K linker to advance our understanding of the GPCR-G protein interaction. This thesis has extensively characterized and developed novel peptide and G protein sensors of GPCRs. Peptide sensors were used to explore the molecular basis of G protein selection and activation (*1, 18, 38*) . G protein sensors enabled dissection of a complex interconnected GPCR network in live cells. Sensors made as part of this study are also available through Addgene. Together, this study serves as a blueprint to dissect protein interactions that drive the GPCR signaling cascade. This thesis developed a systematic, quantitative approach to probe the multiplicity of GPCR-G protein pairings and its consequences on second messenger response.

4.8 Acknowledgements

4.9 References

1.   R. U. Malik *et al*., Detection of G protein-selective G protein-coupled receptor (GPCR) conformations in live cells. *J Biol Chem* **288**, 17167-17178 (2013).
2.   H. O. Onaran, T. Costa, Where have all the active receptor states gone? *Nat Chem Biol* **8**, 674-677 (2012).
3.   R. T. Dorsam, J. S. Gutkind, G-protein-coupled receptors and cancer. *Nat Rev Cancer* **7**, 79-94 (2007).
4.   R. O. Dror *et al*., SIGNAL TRANSDUCTION. Structural basis for nucleotide exchange in heterotrimeric G proteins. *Science* **348**, 1361-1365 (2015).
5.   B. K. Kobilka, Structural insights into adrenergic receptor function and pharmacology. *Trends Pharmacol Sci* **32**, 213-218 (2011).
6.   D. L. Farrens, C. Altenbach, K. Yang, W. L. Hubbell, H. G. Khorana, Requirement of rigid-body motion of transmembrane helices for light activation of rhodopsin. *Science* **274**, 768-770 (1996).
7.   S. G. Rasmussen *et al*., Crystal structure of the beta2 adrenergic receptor-Gs protein complex. *Nature* **477**, 549-555 (2011).
8.   D. Wacker *et al*., Conserved binding mode of human beta2 adrenergic receptor inverse agonists and antagonist revealed by X-ray crystallography. *J Am Chem Soc* **132**, 11443-11445 (2010).
9.   A. W. Kahsai *et al*., Multiple ligand-specific conformations of the beta2-adrenergic receptor. *Nat Chem Biol* **7**, 692-700 (2011).
10.   J. J. Liu, R. Horst, V. Katritch, R. C. Stevens, K. Wuthrich, Biased signaling pathways in beta2-adrenergic receptor characterized by 19F-NMR. *Science* **335**, 1106-1110 (2012).
11.   A. Manglik *et al*., Structural Insights into the Dynamic Process of beta2-Adrenergic Receptor Signaling. *Cell* **161**, 1101-1111 (2015).
12.   B. R. Conklin, Z. Farfel, K. D. Lustig, D. Julius, H. R. Bourne, Substitution of three amino acids switches receptor specificity of Gq alpha to that of Gi alpha. *Nature* **363**, 274-276 (1993).
13.   B. R. Conklin *et al*., Carboxyl-terminal mutations of Gq alpha and Gs alpha that alter the fidelity of receptor activation. *Mol Pharmacol* **50**, 885-890 (1996).
14.   H. E. Hamm *et al*., Site of G protein binding to rhodopsin mapped with synthetic peptides from the alpha subunit. *Science* **241**, 832-835 (1988).
15.   E. L. Martin, S. Rens-Domiano, P. J. Schatz, H. E. Hamm, Potent peptide analogues of a G protein receptor-binding region obtained with a combinatorial library. *J Biol Chem* **271**, 361-366 (1996).
16.   P. Scheerer *et al*., Crystal structure of opsin in its G-protein-interacting conformation. *Nature* **455**, 497-502 (2008).
17.   S. Granier, B. Kobilka, A new era of GPCR structural and chemical biology. *Nat Chem Biol* **8**, 670-673 (2012).
18.   A. Semack, M. Sandhu, R. U. Malik, N. Vaidehi, S. Sivaramakrishnan, Structural Elements in the Galphas and Galphaq C Termini That Mediate Selective G Protein-coupled Receptor (GPCR) Signaling. *J Biol Chem* **291**, 17929-17940 (2016).
19.   G. H. Westfield *et al*., Structural flexibility of the G alpha s alpha-helical domain in the beta2-adrenoceptor Gs complex. *Proc Natl Acad Sci U S A* **108**, 16086-16091 (2011).

20. C. Gales *et al.*, Real-time monitoring of receptor and G-protein interactions in living cells. *Nat Methods* **2**, 177-184 (2005).

21. C. Gales *et al.*, Probing the activation-promoted structural rearrangements in preassembled receptor-G protein complexes. *Nat Struct Mol Biol* **13**, 778-786 (2006).

22. P. Hein, M. Frank, C. Hoffmann, M. J. Lohse, M. Bunemann, Dynamics of receptor/G protein coupling in living cells. *EMBO J* **24**, 4106-4114 (2005).

23. M. J. Lohse, S. Nuber, C. Hoffmann, Fluorescence/bioluminescence resonance energy transfer techniques to study G-protein-coupled receptor activation and signaling. *Pharmacol Rev* **64**, 299-336 (2012).

24. K. Qin, C. Dong, G. Wu, N. A. Lambert, Inactive-state preassembly of G(q)-coupled receptors and G(q) heterotrimers. *Nat Chem Biol* **7**, 740-747 (2011).

25. G. Milligan, Insights into ligand pharmacology using receptor-G-protein fusion proteins. *Trends Pharmacol Sci* **21**, 24-28 (2000).

26. R. Seifert, K. Wenzel-Seifert, B. K. Kobilka, GPCR-Galpha fusion proteins: molecular analysis of receptor-G-protein coupling. *Trends Pharmacol Sci* **20**, 383-389 (1999).

27. D. S. Dupuis, S. Tardif, T. Wurch, F. C. Colpaert, P. J. Pauwels, Modulation of 5-HT1A receptor signalling by point-mutation of cysteine351 in the rat Galpha(o) protein. *Neuropharmacology* **38**, 1035-1041 (1999).

28. A. Wise, G. Milligan, Rescue of functional interactions between the alpha2A-adrenoreceptor and acylation-resistant forms of Gi1alpha by expressing the proteins from chimeric open reading frames. *J Biol Chem* **272**, 24673-24678 (1997).

29. T. Wurch, F. C. Colpaert, P. J. Pauwels, Mutation in a protein kinase C phosphorylation site of the 5-HT1A receptor preferentially attenuates Ca2+ responses to partial as opposed to higher-efficacy 5-HT1A agonists. *Neuropharmacology* **44**, 873-881 (2003).

30. T. Wurch, P. J. Pauwels, Analytical pharmacology of G protein-coupled receptors by stoichiometric expression of the receptor and G(alpha) protein subunits. *J Pharmacol Toxicol Methods* **45**, 3-16 (2001).

31. C. J. Swanson, S. Sivaramakrishnan, Harnessing the unique structural properties of isolated alpha-helices. *J Biol Chem* **289**, 25460-25467 (2014).

32. R. Seifert, T. W. Lee, V. T. Lam, B. K. Kobilka, Reconstitution of beta2-adrenoceptor-GTP-binding-protein interaction in Sf9 cells--high coupling efficiency in a beta2-adrenoceptor-G(s alpha) fusion protein. *Eur J Biochem* **255**, 369-382 (1998).

33. K. Wenzel-Seifert, R. Seifert, Molecular analysis of beta(2)-adrenoceptor coupling to G(s)-, G(i)-, and G(q)-proteins. *Mol Pharmacol* **58**, 954-966 (2000).

34. P. Hein, M. Bunemann, Coupling mode of receptors and G proteins. *Naunyn Schmiedebergs Arch Pharmacol* **379**, 435-443 (2009).

35. P. Hein *et al.*, Gs activation is time-limiting in initiating receptor-mediated signaling. *J Biol Chem* **281**, 33345-33351 (2006).

36. A. De Lean, J. M. Stadel, R. J. Lefkowitz, A ternary complex model explains the agonist-specific binding properties of the adenylate cyclase-coupled beta-adrenergic receptor. *J Biol Chem* **255**, 7108-7117 (1980).

37. P. Samama, S. Cotecchia, T. Costa, R. J. Lefkowitz, A mutation-induced activated state of the beta 2-adrenergic receptor. Extending the ternary complex model. *J Biol Chem* **268**, 4625-4636 (1993).

38.   A. Semack, R. U. Malik, S. Sivaramakrishnan, G Protein-selective GPCR Conformations Measured Using FRET Sensors in a Live Cell Suspension Fluorometer Assay. *J Vis Exp*, (2016).

39.   A. Semack, M. Sandhu, R. U. Malik, N. Vaidehi, S. Sivaramakrishnan, Structural elements in the Galphas and Galphaq C-termini that mediate selective GPCR signaling. *J Biol Chem*, (2016).

Appendix 1

G protein-selective GPCR conformations measured using FRET sensors in a live cell suspension fluorometer assay

Ansley Semack, Rabia U. Malik, and Sivaraj Sivaramakrishnan*
(Manuscript modified from *J Vis Exp*).

A1.1 Abstract

F̲örster r̲esonance e̲nergy t̲ransfer (FRET)-based studies have become increasingly common in the investigation of GPCR signaling. Our research group developed an intra-molecular FRET sensor to detect the interaction between Gα subunits and GPCRs in live cells following agonist stimulation. Here, we detail the protocol for detecting changes in FRET between the β_2-adrenergic receptor and the Gαs c-terminus peptide upon treatment with 100 μM isoproterenol hydrochloride as previously characterized[1]. Our FRET sensor is a single polypeptide consisting serially of a full-length GPCR, a FRET acceptor fluorophore (mCitrine), an ER/K SPASM (systematic protein affinity strength modulation) linker, a FRET donor fluorophore (mCerulean), and a Gα c-terminal peptide. This protocol will detail cell preparation, transfection conditions, equipment setup, assay execution, and data analysis. This experimental design detects small changes in FRET indicative of protein-protein interactions, and can also be used to compare the strength of interaction across ligands and GPCR-G protein pairings. To enhance the signal-to-noise in our measurements, this protocol requires heightened precision in all steps, and is presented here to enable reproducible execution.

A1.2. Introduction

G-protein-coupled receptors (GPCRs) are seven-transmembrane receptors. The human genome alone contains approximately 800 genes coding for GPCRs, which are activated by a

variety of ligands including light, odorants, hormones, peptides, drugs and other small molecules. Nearly 30% of all pharmaceuticals currently on the market target GPCRs because they play a large role in many disease states[2]. Despite decades of extensive work done on this receptor family, there remain significant outstanding questions in the field, particularly with regards to the molecular mechanisms that drive GPCR-effector interactions. To date, only one high-resolution crystal structure has been published, providing insight into the interaction between the β_2-adrenergic receptor (β_2-AR) and the Gs protein[3]. Together with extensive research in the last three decades, it reiterates one specific structural component that is critical in this interaction: the Gα subunit c-terminus. This structure is important for both G protein activation by the GPCR[4] and G protein selection[5-6]. Hence, the Gα c-terminus provides a crucial link between ligand stimulation of the GPCR and selective G protein activation.

Research over the last decade suggests that GPCRs populate a broad conformational landscape, with ligand-binding stabilizing subsets of GPCR conformations. While several techniques, including crystallography, NMR and fluorescence spectroscopy, and mass spectrometry are available to examine the GPCR conformational landscape, there is a paucity of approaches to elucidate their functional significance in effector selection[7].Here, we outline a Förster resonance energy transfer (FRET)-based approach to detect G protein-selective GPCR conformations. FRET relies on the proximity and parallel orientation of two fluorophores with overlapping emission (donor) and excitation (acceptor) spectra[8]. As the donor and acceptor fluorophores come closer together as a result of either conformational change in the protein or a protein-protein interaction, the FRET between them increases, and can be measured using a range of methods[8]. FRET-based biosensors have been employed extensively in the GPCR field[9]. They have been used to probe conformation changes in the GPCR by inserting donor and acceptor in the third intracellular loop and GPCR c-terminus; sensors have been designed to probe GPCR and effector interactions by separately labeling the GPCR and effector (G protein subunits/arrestins) with a FRET pair[10]; some sensors also detect conformational changes in the G protein[11]. These biosensors have enabled the field to ask a multitude of outstanding questions including conformational changes in the GPCR and effector, GPCR-effector interaction kinetics, and allosteric ligands[12]. Our group was particularly interested in creating a biosensor that could detect G protein-specific GPCR conformations under agonist-driven conditions. This biosensor

relies on a recently developed technology named SPASM (systematic protein affinity strength modulation)[13]. SPASM involves tethering interacting protein domains using an ER/K linker, which controls their effective concentrations. Flanking the linker with a FRET pair of fluorophores creates a tool which can report the state of the interaction between proteins[12]. Previously[1] the SPASM module was used to tether the Gα c-terminus to a GPCR and monitor their interactions with FRET fluorophores, mCitrine (referred to in this protocol by its commonly known variant, Yellow Fluorescent Protein (YFP), excitation/emission peak at 490/525 nm) and mCerulean (referred to in this protocol by its commonly known variant Cyan Fluorescent Protein (CFP), excitation/emission peak 430/475 nm). From N- to C-terminus, this genetically encoded single polypeptide contains: a full length GPCR, FRET acceptor (mCitrine/YFP), 10 nm ER/K linker, FRET donor (mCerulean/CFP), and the Gα c-terminus peptide. In this study, sensors are abbreviated as GPCR-linker length-Gα peptide. All components are separated by an unstructured (Gly-Ser-Gly)$_4$ linker which enables free rotation of each domain. The detailed characterization of such sensors was previously performed using two prototypical GPCRs: β$_2$-AR and opsin[1].

This sensor is transiently transfected into HEK-293T cells and fluorometer-based live cell experiments measure fluorescence spectra of the FRET pair in arbitrary units of counts per second (CPS) in the presence or absence of ligand. These measurements are used to calculate a FRET ratio between the fluorophores (YFP$_{max}$/CFP$_{max}$). A change in FRET (ΔFRET) is then calculated by subtracting the average FRET ratio of untreated samples from the FRET ratio of ligand treated samples. ΔFRET can be compared across constructs (β$_2$-AR-10 nm-Gαs peptide versus β$_2$-AR-10 nm-no peptide). Here, we detail the protocol to express these sensors in live HEK-293T cells, monitor their expression, and the setup, execution, and analysis of the fluorometer-based live cell FRET measurement for untreated versus drug treated conditions. While this protocol is specific for the β$_2$-AR-10 nm-Gαs peptide sensor treated with 100 μM isoproterenol bitartrate, it can be optimized for different GPCR-Gα pairs and ligands.

A1.3. Protocol:

1.   DNA preparation

1.1. Design sensor constructs using a modular cloning scheme. Please reference the β_2-AR sensor design detailed previously[1].

1.2. Prepare DNA according to commercial miniprep kit protocol and elute in 2 mM Tris-HCl solution, pH 8, at concentration $\geq$750 ng/μL, A_{260}/A_{280} of 1.7-1.9, A_{260}/A_{230} of 2.0-2.29.

2.   Cell culture preparation

2.1. Culture HEK-293T-Flp-n cells in DMEM containing 4.5 g/L D-glucose, supplemented with 10% FBS (heat inactivated) (v/v), 1% L-glutamine supplement, 20 mM HEPES, pH 7.5 at 37 °C in humidified atmosphere at 5% CO_2. Handle cells in biological safety hood for subsequent steps.

2.2. Allow cells to grow to a confluent **monolayer** before passaging into six-well dishes. Time to achieve confluency depends on initial plating density. Use plates that come to confluency within 1-2 days of plating for six-well plating. A confluent 10 cm tissue culture-treated dish has cell density of approximately 4×10^6 cells/mL. See **Figure A1.1** for image of cell culture growth.

2.3. Wash cells with 10 mL PBS, trypsinize with 0.25% trypsin (see Discussion, paragraph 2). Plate 8×10^5 cells/well in 2 mL of media in tissue culture-treated six well dishes and allow to adhere for 16-20 hr.

3.   Transfection conditions

3.1. Stagger transfections for constructs that may require different amounts of time to achieve optimal expression (between 20-36 hr). Synchronize conditions for a unified experiment time. Also have an untransfected control well at equivalent cell density to be used for background noise and scattering subtraction during analysis.

3.2. Bring transfection reagents to room temperature: reduced serum media, DNA, transfection reagent.

3.3. In a biological safety hood combine reagents in a sterile microcentrifuge tube in the following order: mix 2 μg DNA with 100 μL reduced serum media. Spike 6 μL of transfection reagent into media/DNA mix without touching surface of mixture or the side of the tube. Set up one transfection reaction per well. Transfection conditions can be optimized (1-4 μg of DNA, 3-6 μL of transfection reagent) to achieve consistent expression levels. See **Table A1.1** for more optimized ratios.

3.4. Incubate mixture at room temperature in biological safety hood for 15-30 min. Do not use reaction if left to incubate for more than 30 min.

3.5. Add reaction to cells in a drop-wise manner across well and gently shake six-well to ensure thorough mixing. Add one reaction per well.

3.6. After 20 hr of expression, monitor fluorescence using tissue culture fluorescence microscope. Assess population expression with 10X objective and protein localization in a cell at 40X. Observe for protein expression at plasma membrane (PM). If substantial internalization is noted, monitor transfection until significant expression is detected at PM.

4. Reagent and equipment preparation

4.1. Prepare 100 mM drug stocks and store at -80 °C: isoproterenol bitartrate (100 mM in dH$_2$O containing 300 mM ascorbic acid). Make on ice/in cold room, and flash-freeze immediately. Aliquots can be made and used up to one year.

4.2. Prepare Cell Buffer (~ 2 mL/condition) and store in a 37 °C water bath. Make fresh each day. Reference Table 2 for Cell Buffer constituents.

4.3. Prepare Drug Buffer (10 mL) and store at room temperature. Reference Table A1.2 for Drug Buffer constituents.

4.4. Acid wash cuvettes using concentrated HCl. Neutralize with a weak base (1 M KOH), and thoroughly wash cuvettes with dH_2O.

4.5. Prepare work station around fluorometer with several boxes of 10, 200, and 1000 μL pipet tips, a timer set with a 10 minute countdown, an accessible vacuum line with tips for cuvette cleaning, delicate task wipes, and squirt bottle with ultrapure H_2O.

4.6. Heat external water bath for fluorometer and heat block to 37 °C.

4.7. Turn on fluorometer; set fluorescence collection program for CFP collection to excitation 430 nm, bandpass 8 nm; emission range 450 nm – 600 nm, bandpass 4 nm. For YFP collection only as sensor control (see **Discussion**) set excitation to 490 nm, bandpass 8 nm, emission range 500 – 600 nm, bandpass 4 nm. CFP collection settings will be used to acquire a FRET spectrum in this experiment.

4.8. Place twelve (12) 1.5 mL microcentrifuge tubes in heat block as shown in **Figure A1.2** below. These tubes are holders for cell aliquot tubes (500 μL microcentrifuge tubes.) Place a small piece of tissue in holders 1 and 7 to cushion the cuvettes placed here.

Note: Use separate cuvettes for untreated condition and drug condition to prevent cross-contamination.

4.9. Fill holders 2-6 and 8-12 with ~750 μL of water to create a mini 37 °C water bath.

4.10. Place ten (10) 500 μL microcentrifuge tubes for cell aliquots into mini-water baths (holders 2-6, 8-12). Each tube will be an individual repeat of the condition (5 untreated, 5 drug treated.)

4.11.   Monitor cells for expression (see step 3.6).

5.   Experiment & Data Collection

5.1.   Reference Figure 3 for experimental schematic. When cells are ready to be harvested, based on protein expression detected with fluorescence microscope (see Discussion, paragraph 4): in biological safety hood, gently remove ~1 mL of media, resuspend cells in their culture with a P1000 and transfer resuspension into a 1.5 mL microcentrifuge tube.

Note: Avoid using trypsin as it may digest the N-terminus and/or binding pocket of the GPCR sensor.

5.2.   Count cells to ensure proper cell density in resuspension. Optimize resuspension volume for 4 x 10^6 cells/mL.

5.3.   Spin cells in swinging bucket centrifuge at room temperature, 290 x g for 3 min. Remove supernatant after spin.

5.4.   **GENTLY** resuspend cells in 1 mL Cell Buffer (stored at 37 °C) and repeat step 5.3. During second spin, gather 100 mM drug stock aliquot from -80 °C; make 1:100 dilution in Drug Buffer for 1 mM working stock and keep at room temperature.

5.5.   After second spin, remove supernatant and gently resuspend cells in 1 mL of Cell Buffer (4 x 10^6 cells/mL). Measure OD_{600} of the samplein spectrophotometer using 1 mL of cells and 1 mL of Cell Buffer as blank. Cells are briefly dispensed in disposable plastic cuvette and transferred back to a microcentrifuge tube immediately following spec.

5.6.   For a control untransfected cell condition spectrum: gently resuspend untransfected cells in 1 mL Cell Buffer with P1000 pipet, add 90 μL of cells to cuvette and acquire FRET spectrum at excitation 430 nm, bandpass 8 nm, emission 450 – 600 nm, bandpass 4 nm. Collect 3-5 repeat spectra with fresh 90 μL of cells. Keep stock of cells at 37 °C between

specs, resuspend gently with P1000 between each sample aliquot, and rinse cuvette with ultrapure H_2O between samples.

5.7.　For experimental conditions: aliquot 90 μL of transfected cells to each of the 500 μL tubes in holders 2-6, 8-12 in the heat block. Gently resuspend stock of cells with P1000 pipet between each aliquot.

5.8.　After cells are aliquoted, add 10 μL of Drug Buffer to tubes 2-6 for untreated condition samples.

5.9.　Begin experiment by adding 10 μL of 1 mM drug solution into tube 8, **start the timer to countdown from 10 min**, and gently mix tube with P200 pipet. Close tube and return to 37 °C heat block.

5.10. Immediately pick up tube 2, mix gently with P200 (use new tip), add 90 μL of cell suspension to untreated condition cuvette, and place in fluorometer.

5.11. Acquire FRET spectrum at excitation 430 nm, bandpass 8 nm, emission 450 – 600 nm, bandpass 4 nm.

5.12. At 9 min-10 sec, spike tube 9 with 10 μL of 1 mM drug solution, gently mix with a P200 (use new tip), and return tube to heat block.

5.13. Repeat steps 5.10-5.11 with tube 3 and 5.12 with tube 10.

5.14. Repeat steps 5.10-5.13 at 1 minute intervals (08:10, 07:10, etc.) until spectra are collected for all untreated condition samples, and drug has been added to all drug condition samples. Use a fresh tip for each pipet step to prevent cross-contamination.

5.15. At 5 min-10 sec, begin mixing tube 8 (drug condition) gently with P200 pipet, add 90 μL of cell suspension to separate cuvette for drug treated sample and place in fluorometer.

5.16. Acquire FRET spectrum (see step 5.11 for settings.)

5.17. Repeat steps 5.15-5.16 at 1 minute intervals (04:10, 03:10, etc.) for remaining drug condition samples (tubes 9-12).

5.18. After experiment ends, save project files, thoroughly wash cuvettes with ultrapure H_2O, and re-stock tubes for next condition. Note: Take care to prevent cross-contamination in the wash step. Change the tip on the H_2O bottle as well as on the vacuum line in between washes.

6. Data analysis

6.1. Save and export data files in SPC format to be used for analysis. Analysis programs are available for download from the Sivaramakrishnan Lab publication website (upon publication.)*

6.2. Create path files for analysis software which include the analysis programs (v9, v15), untransfected samples files (see step 5.6 for untransfected cell spectrum collection), OUTPUT data file, and comma separated values (CSV) files for data entry.

6.2.1. Enter following information into CSV file (see sample in **Table A1.3**) and designate respective conditions for each sample, including:
File name –individual SPC graph files
Receptor – designate which GPCR construct was tested (*e.g.* B2)
Binder – designate which peptide variant of the construct was tested (*e.g.* S)
Agonist – designate untreated (N) or drug treated (D) conditions

Directory – the path folder in which SPC files are saved, usually organized by date

OD – recorded optical density of sample from spectrophotometer

6.3. Enter file names for untransfected samples (step 5.6) to subtract buffer and scattering noise from samples.

6.4. Enter conditions into analysis program.

6.5. Run programs to analyze samples within individual conditions (v9) and across conditions (v15).

6.6. Exclude sample files which are apparent outliers in the data set, or adjust for subtraction by increasing or decreasing OD value of individual files.

6.7. Export data to OUTPUT file for access to calculated FRET ratios (525 nm/475 nm).

6.8. Calculate ΔFRET by subtracting the average FRET ratio for untreated condition from the individual FRET ratios for treated (drug) conditions.

A1.4. Representative Results:

A generalized schematic of the experiment set up and execution is detailed in **Figure A1.3**. In order to detect a FRET change in the narrow dynamic range of the sensor, it is critical that the nuances of the system be adhered to. Cell quality is imperative to protein expression as well as consistency in sampling. **Figure A1.1** features images of cultured cells growing in a consistent monolayer (10X) that is optimal for six-well plating and transfection **Figure A1.1 (a)** and cells growing in clumped patterns that lead to dendritic shapes **Figure A1.1 (b)** which is not recommended for consistent plating. Transfection conditions can also be optimized in order to achieve reproducible expression. Several conditions have been optimized for the recommended transfection reagent used here. **Table A1.1** details these conditions for reduced serum media. DNA, and transfection reagent ratios.

Once all data has been collected and data entered into the CSV file for analysis (see sample in **Table A1.3**), the generated results will resemble the Raw FRET spectra data shown in **Figure A1.4 (a)** and the normalized, mean FRET spectra shown in **Figure A1.4 (b)**. In **Figure A1.4** the red spectra are the untreated samples and the blue are the drug treated samples. All of the Raw FRET spectra in **Figure A1.4 (a)** have sufficient signal-to-noise range for consistent data analysis (*i.e*. CPS at 450 nm compared to CPS at 475 nm). With this range, the spectra is smoother and the water peak from the sample (Raman peak is at 500 nm) is also minimal. Low expression levels result in a prominent water peak that interferes with data analysis. Data is normalized at 475 nm, setting the CPS of this value to 1.0 **Figure A1.4 (b)**. In this data set for the β_2-AR-10 nm-Gαs peptide sensor, there is a significant change at the 525 nm reading between untreated (red) and treated (blue) samples. The ΔFRET change is calculated from the FRET ratios (525 nm/475 nm) of these data sets and are accessible through the OUTPUT file.

If protein expression is low, there is poor transfection efficiency, or low cell density in the cuvette for fluorescence reading, spectra may appear noisier, as shown in **Figure A1.5**. Compared to **Figure A1.4 (a)** the signal-to-noise range for this data set is not ideal, at approximately 1.0-1.6, with CPS$_{max}$ of 4 x 10$^{5.}$ This low expression level contributes to the jagged spectra seen in the raw data **Figure A1.5 (a)**, however the data is tight and able to be normalized **Figure A1.5 (b)**. Though the water peaks (~500 nm) does not line up completely between data sets **Figure A1.5 (b)** this experiment is still usable for analysis. **Figure A1.6** is representative of an experiment that is inadequate for analysis. While the signal-to-noise of the sample is approximately 2-3 for treated (blue) and untreated (red) samples, cell density in the cuvette across samples is too low (450 nm value of 1x10^5) **Figure A1.6 (a)**. This creates an issue in background subtraction and normalization **Figure A1.6 (b)** and the spectra do not align. Subtraction can be adjusted for samples by increasing or decreasing OD in **Table A1.3**. However, even with low cell density, the water peak (~500 nm) becomes much larger and noisier **Figure A1.6 (c)** and inhibits this data set from further analysis.

A1.5. Discussion:

The tight dynamic range of FRET measurements in this system reinforces the necessity of sensitive quality control in every step of this protocol. The most important steps to ensure a

successful FRET experiment are 1) cell culturing, 2) transfection 3) protein expression and 4) timely, precise coordination during the assay execution.

Cell health and maintenance/plating quality can have a significant impact on the signal-to-noise of the experimental system and poor cell health can make it impossible to detect any consistent change in FRET. Conservatively, cells are healthiest for approximately 20 passages, though this may vary based on cell line, handling, and culture conditions. Once cells have difficulty growing as a confluent monolayer, or begin growing consistently in more dendritic patterns (see **Figure A1.1 (b)**), experimental background noise will be adversely affected. Careful cell maintenance, including routine media changes and regularly removing non-adherent cells and debris from maintenance plates, will enhance the quality of cells for six-well plating and transfections. Cell clumps, which adversely affect transfection efficiency, can be effectively separated into individual cells by trypsinization of maintenance plates: treat 10 cm confluent dishes with 10 mL of 0.25% trypsin for 30 seconds, remove trypsin but leave approximately 200 μL, place dish in 37 °C incubator for 2-3 minutes. Cells will come off dish very easily and are less susceptible to clumping.

It is critical to optimize the transfection step for this experiment. Six-wells must ideally be 60-80% confluent for efficient transfection and optimal expression. If too few cells have adhered (<60%), wait approximately 2-6 hours to transfect, or until at least 70% of cells are adhered. Six-wells that are over-confluent (> 80%) will also reduce transfection efficiency. Transfecting at lower cell confluency increases cell death rate. DNA concentration and purity are also critical (see Step 1.2.) Using low concentration and/or poor quality DNA preparations negatively affect transfection efficiency Transfection conditions can be adjusted per construct; refer to **Table A1.1** for more information.

Accurate and consistent monitoring of protein expression using a tissue-culture fluorescence microscope is another crucial step in this process. Though this step is subject to individual judgement, it is possible to use other techniques, such as microscopy, to monitor expression over time quantitatively, though they are not detailed here. For constructs we have tested successfully in our system, expression takes approximately 18-36 hr to reach optimal expression. In our

experience, constructs that display poor expression during this time window rarely improve after 40 hr. The constructs we have published with have not shown signs of degradation, however this may be an issue for some GPCRs. In our assays, sensor degradation is possible at transfection times over 30 hr. Sensor integrity can be tested using YFP/CFP ratios: 525 nm reading from the YFP-excited (490 nm) spectrum, and 475 nm reading from CFP-excited (430 nm) spectrum. For settings, see step 4.6. Recommended YFP/CFP ratios are in the range of 1.7-2.0, with an ideal ratio of 1.8. This value is dependent on the approximate two-fold greater brightness of YFP relative to CFP[14]. An integral sensor with minimal degradation will therefore contain both fluorophores and have YFP:CFP ratio of approximately 2:1. After sensor quality has been confirmed it is important to confirm protein localization and expression at the plasma membrane. Significant intracellular expression could be a result of either protein degradation, internalization, or ongoing trafficking of the protein. Monitor constructs over time to see if expression is enhanced at the plasma membrane. The next critical challenge in expression is transfection efficiency. Approximately 70%+ transfection efficiency is necessary for adequate signal-to-noise detection in this fluorometer system. If less cells are transfected, the amount of signal-to-noise may still be detectable but will be much less consistent between samples in one FRET experiment. This will hinder accurate data analysis within the narrow dynamic range of the system. Expression levels also present a significant hurdle to achieving ample signal-to-noise during the experiment. For expression levels detectable by the fluorometer, the ratio of signal between 475 nm and 450 nm (cell scattering) of 1.5 is sufficient for detecting a change in FRET, however optimal expression will have a ratio of approximately 2.0+. For reference, the β2-AR data is collected in a signal-to-noise range of 4 x 10^5 CPS (450 nm) to 1 x 10^6 CPS (475 nm), signal-to-noise ratio of 2.5. This ratio will help reduce the amount of variability between samples, which can also affect data analysis. These expression levels are also subject to the sensitivity and optimal alignment of the fluorometer optics; other systems may require different parameters for adequate signal-to-noise optimization.

Cells are extremely sensitive to time and temperature; once the experimental procedure has begun, gentle handling is essential to avoid cell death. Specific logistical measures can be taken to expedite the process and avoid timely mistakes including preparing the work station, making sure all equipment is functioning properly, and planning out the goals of the experiment

beforehand. It is ideal to use cells within 30 min of harvesting, and in our system, this protocol is executed within 20 min. Once the technique is mastered, specifically transfection optimization and the manual dexterity of the exercise itself, this experiment can be used to compare various constructs against each other, generate dose-response curves, and the sensor can be expanded to the full-length G protein.

Though the FRET sensor used here is a unique development in GPCR FRET sensors, this specific experimental setup is detailed as a well-characterized assay for the implementation of the sensor. The fluorometer-based assay allows a large population of cells to be assessed in each experiment and does not rely on purified protein or membrane preps, therefore maintaining an *in vivo* environment. This experimental design has also been optimized to detect very small changes seen in the system upon agonist stimulation of the GPCR.

A1.6. Acknowledgements:

A1.7 Figures and Tables:
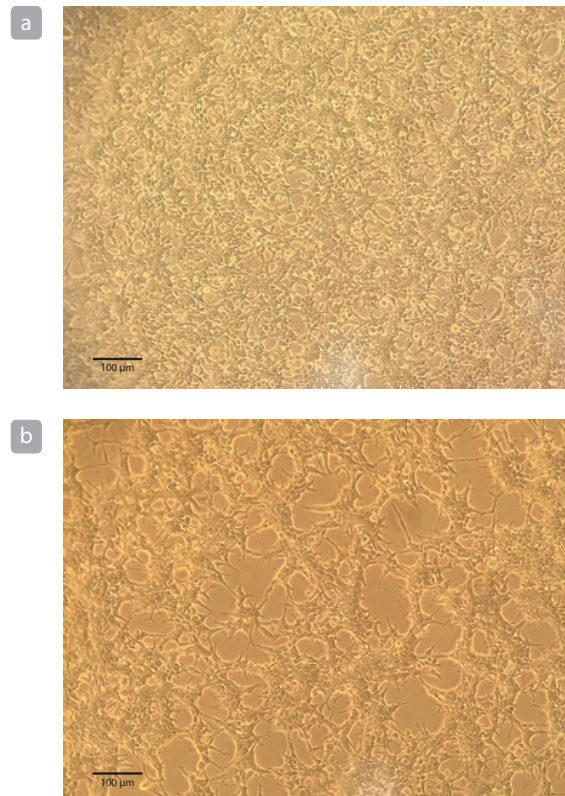
Figure A1.1. Example of cultured cell growth. Cells growing in a monolayer **(a)** are ideal for consistent plating and transfection. Cells that appear to grow in clumps or with dendritic patterns **(b)** may not plate consistently in six-wells, may display poor transfection efficiency, and may create inconsistencies in amplitude of the FRET spectrum. Scale bar = 100 μm.
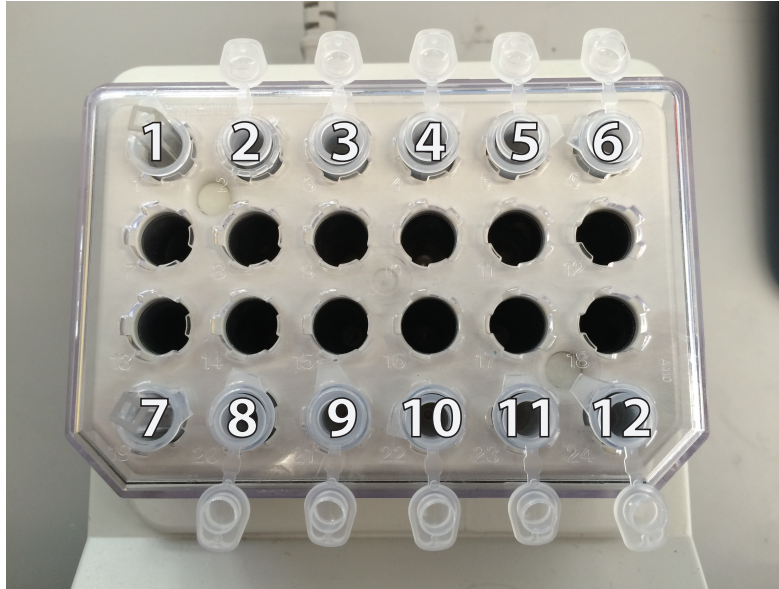
Figure A1.2. Microcentrifuge tube set up and position reference in heat block. Cuvette for untreated samples is in position 1; cell aliquot tubes are in positions 2-6. Cuvette for drug treated samples is in position 7; cell aliquot tubes are in positions 8-12.
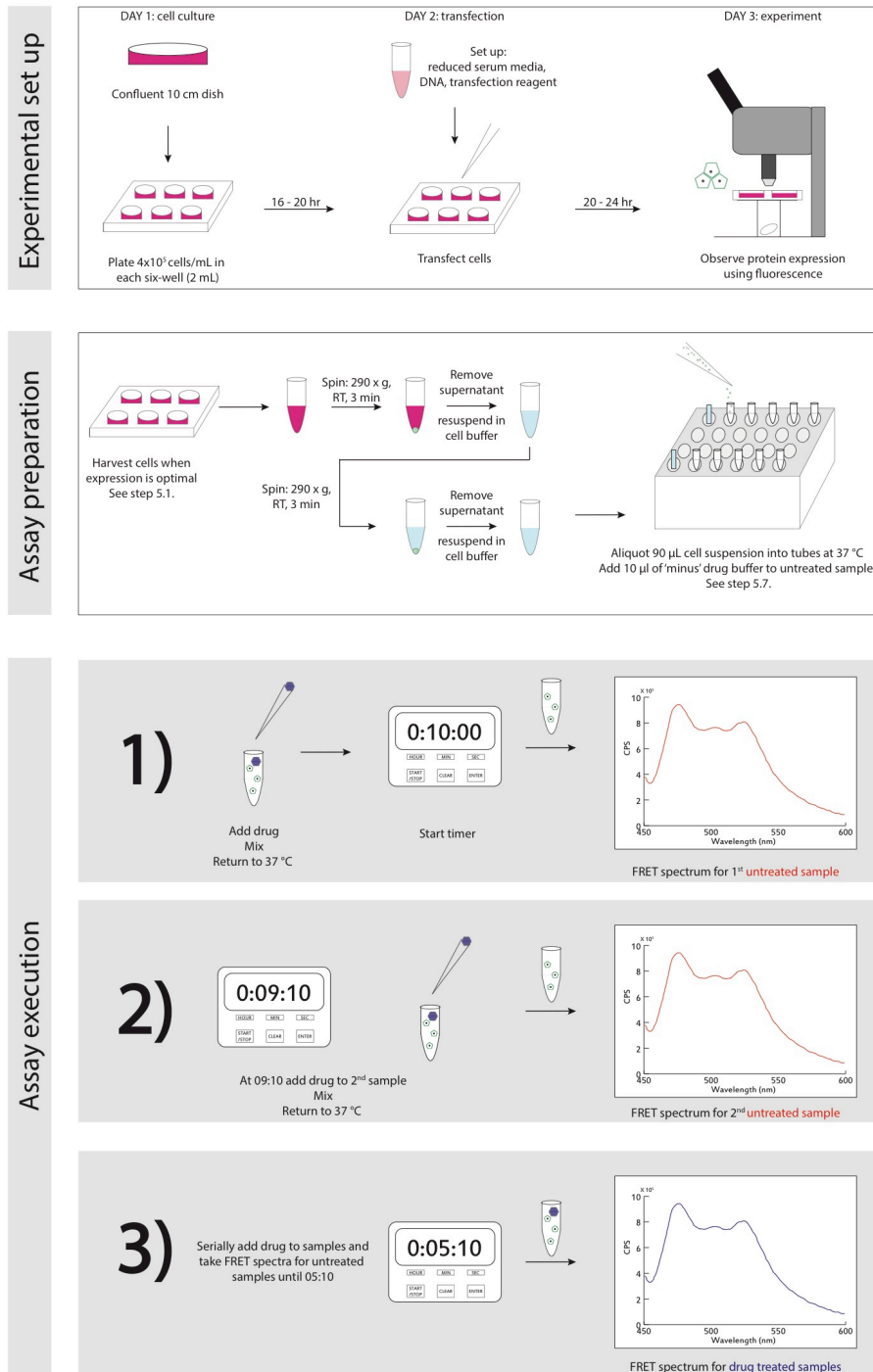
Figure A1.3. ΔFRET experimental schematic. A detailed step-wise guide for experimental set up and execution.
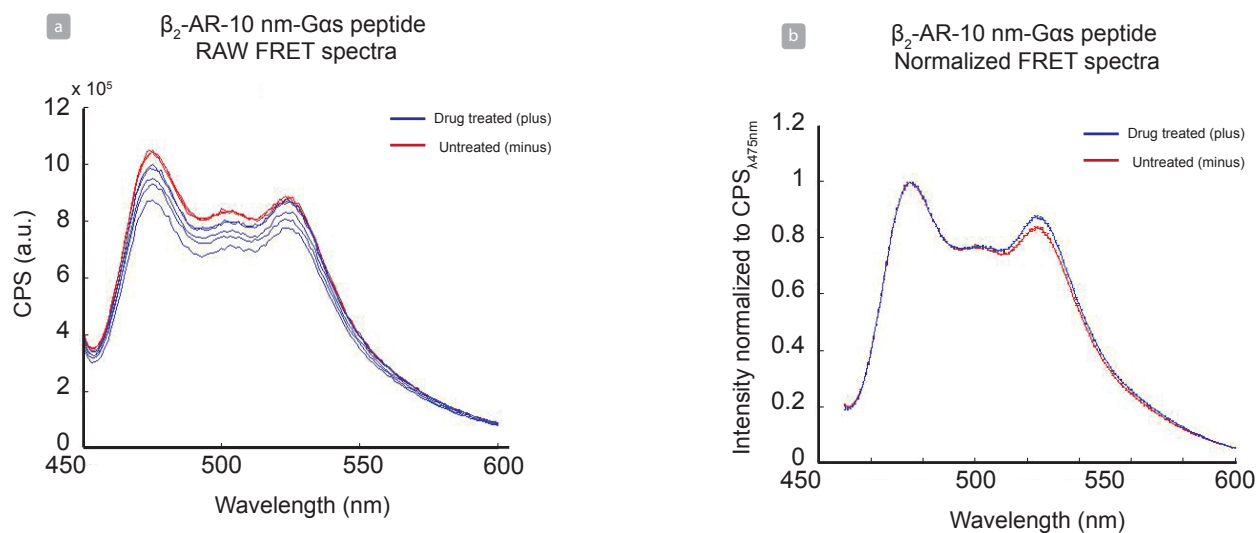
Figure A1.4. Representative data analysis for β_2-AR-10 nm-Gαs peptide +/- drug. Representative image of raw data **(a)** and normalized, averaged data **(b)** collected with the β_2-AR-10 nm-Gαs peptide sensor with untreated (red) samples and treated (blue) samples after 5 minute incubation with 100 uM isoproterenol bitartrate. CFP$_{max}$ emission at 475 nm, YFP$_{max}$ emission at 525 nm.
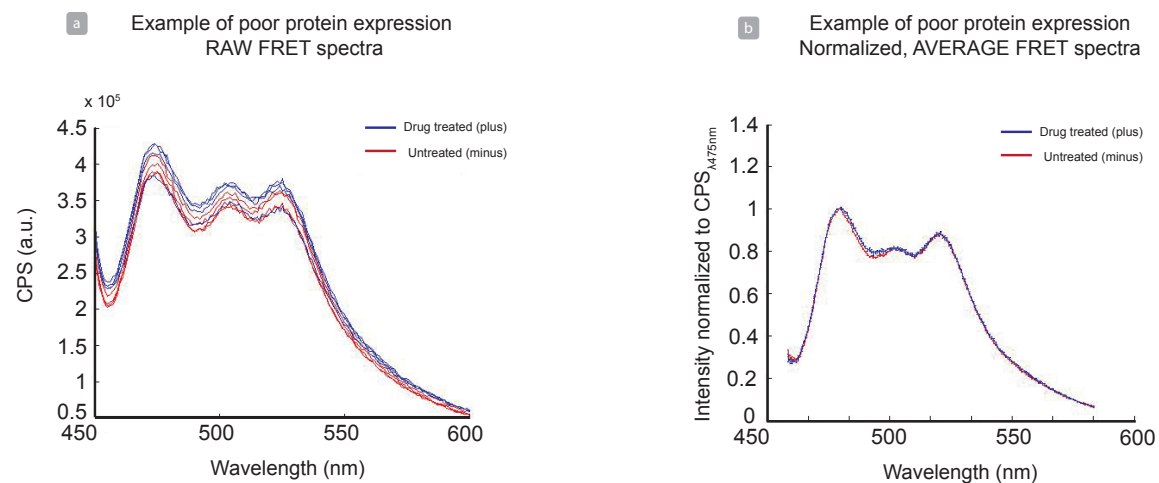
Figure A1.5. Analysis of poor protein expression with raw and normalized data. Noisy raw data spectra **(a)** are a result of low expression levels, low cell density per sample, and/or poor transfection efficiency of construct. This data set is still interpretable as normalized **(b)**, although it is not ideal.
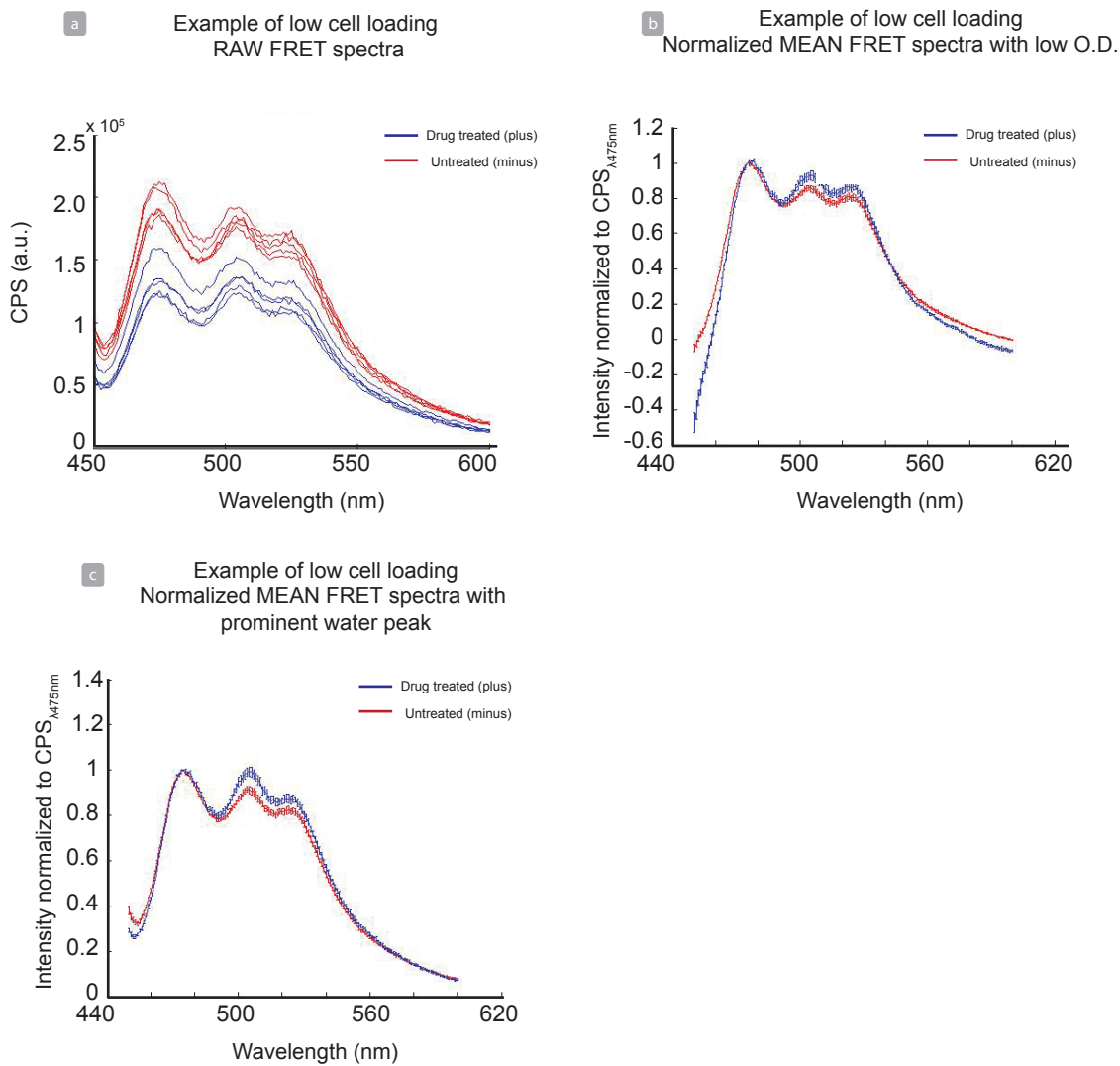
Figure A1.6. Analysis of low cell density in fluorometer cuvette with raw and normalized data sets. The low cell density per sample, seen in raw data **(a)** complicates water/background subtraction **(b,c)** and makes this data set uninterpretable.

Table A1.1 ΔFRET transfection conditions. This table includes the optimized conditions of reagents for transfections into 2 mL wells of HEK-293T cells using the recommended transfection reagent.

Condition	0.5x	0.7x	1x	2x	2x*
DNA	1 µg	1.4 µg	2 µg	4 µg	4 µg
Reduced serum media	100 µL	70 µL	100 µL	100 µL	200 µL
Transfection reagent	3 µL	4.2 µL	6 µL	6 µL	12 µL

*Note: Recommended for exceptionally difficult construct. Caution must be taken, as this condition induces high cell death.

Table A1.2. Live cell ΔFRET buffer constituents. This table details the reagents used to make both Cell Buffer and Drug Buffer for use in the experiment. Make both buffers fresh each day of the experiment; store Cell Buffer at 37 °C, and Drug Buffer at room temperature.

Cell Buffer

Volume	Reagent	Comments
9 mL	ultrapure DNase/RNase free water	
1 mL	HBS (10X), pH 7.4, store at 4 °C:	
	200 mM HEPES	
	50 mM KCl	
	450 mM NaCl	
	20 mM $CaCl_2$- H_2O	
	10 mM $MgCl_2$ - H_2O	
100 μL	20% D-glucose	
15 μL	aprotinin (1 mg/mL in dH_2O)	prevents degradation
15 μL	leupeptin (1 mg/mL in dH_2O)	prevents degradation
100 μL	ascorbic acid (100 mM in dH_2O)*	stabilizes agonist
	*add immediately before beginning assay	

Drug Buffer

Volume	Reagent	Comments
9 mL	ultrapure DNase/RNase free water	
1 mL	HBS (10X), pH 7.4, store at 4 °C:	
	200 mM HEPES	
	50 mM KCl	
	450 mM NaCl	
	20 mM $CaCl_2$- H_2O	
	10 mM $MgCl_2$ - H_2O	
100 μL	ascorbic acid (100 mM in dH_2O)*	stabilizes agonist
	*add immediately before beginning assay	

Table A1.3. Sample CSV file for ΔFRET experiment analysis. This sample data file highlights the entry set after one experiment. Multiple experiments can be entered into the same CSV file and can be discerned under the 'Additive' column if necessary. Each row must be filled out with the following information:

File name – individual SPC graph files
Receptor – designate which GPCR construct was tested (*e.g.* B2)
Binder – designate which peptide variant of the construct was tested (*e.g.* S)
Agonist – designate untreated (N) or drug treated (D) conditions
Directory – the path folder in which SPC files are saved, usually organized by date
OD – recorded optical density of sample in spectrophotometer

Filename	Receptor	Helix	Binder	Agonist	Cell/ Membrane	Additive	Spectra	Directory	OD
Untransfected_Control (01)_Graph.SPC	UN	N	N	N	C	N	FRET	20160101	0.8
Untransfected_Control (02)_Graph.SPC	UN	N	N	N	C	N	FRET	20160101	0.8
Untransfected_Control (03)_Graph.SPC	UN	N	N	N	C	N	FRET	20160101	0.8
B2AR s pep minus (01)_Graph.SPC	B2	10	S	N	C	N	FRET	20160101	0.4
B2AR s pep minus (02)_Graph.SPC	B2	10	S	N	C	N	FRET	20160101	0.4
B2AR s pep minus (03)_Graph.SPC	B2	10	S	N	C	N	FRET	20160101	0.4
B2AR s pep minus (04)_Graph.SPC	B2	10	S	N	C	N	FRET	20160101	0.4
B2AR s pep minus (05)_Graph.SPC	B2	10	S	N	C	N	FRET	20160101	0.4
B2AR s pep drug (01)_Graph.SPC	B2	10	S	D	C	N	FRET	20160101	0.4
B2AR s pep drug (02)_Graph.SPC	B2	10	S	D	C	N	FRET	20160101	0.4
B2AR s pep drug (03)_Graph.SPC	B2	10	S	D	C	N	FRET	20160101	0.4
B2AR s pep drug (04)_Graph.SPC	B2	10	S	D	C	N	FRET	20160101	0.4
B2AR s pep drug (05)_Graph.SPC	B2	10	S	D	C	N	FRET	20160101	0.4

A1.8 References:

1.   Malik, R.U. *et al*. Detection of G Protein-selective G Protein-coupled Receptor (GPCR) Conformations in Live Cells. *J. Biol. Chem*. **288**, 17167-17178, doi: 0.1074/jbc.M113.464065 (2013).

2.   Oldham, W.M., & Hamm, H.E. Heterotrimeric G protein activation by G-protein-coupled receptors. *Nat. Rev. Mol. Cell Bio*. **9**, 60-71, doi: 10.1038/nrm2299 (2008).

3.   Rasmussen, S.G. *et al*. Crystal structure of the β2 adrenergic receptor-Gs protein complex. *Nature*. **477**, 549-555, doi: 10.1038/nature10361 (2011).

4.   Alexander, N.S., Preininger, A.M., Kaya, A.I., Stein, R.A., Hamm, H.E., & Meiler, J. Energetic analysis of the rhodopsin-G-protein complex links the α5 helix to GDP release. *Nat. Struct. Mol. Biol*. **21** (1) 56-63, doi: 10.1038/nsmb.2705 (2014).

5.   Conklin, B.R., Farfel, Z., Lustig, K.D., Julius, D., & Bourne, H.R. Substitution of three amino acids switches receptor specificity of $G_q\alpha$ to that of $G_i\alpha$. *Nature*. **363**, 274-276 (1993).

6.   Conklin, B.R. *et al*. Carboxyl-Terminal Mutations of $G_{q\alpha}$ and $G_{s\alpha}$ That Alter the Fidelity of Receptor Activation. *Mol. Pharmacol*. **50**, 855-890 (1996).

7.   Onaran, H.O. & Costa, T. Where have all the active receptor states gone? *Nat. Chem. Bio*. **8**, 674-677, doi:10.1038/nchembio.1024 (2012).

8.   Jares-Erijman, E.A., & Jovin, T.M. FRET imaging. *Nat. Biotechnol*. **21** (11), 1387-1395, doi: 10.1038/nbt896 (2003).

9.   Lohse, M.J., Nuber, S., Hoffman, C. Fluorescence/bioluminescence resonance energy transfer techniques to study G-protein-coupled receptor activation and signaling. **64**, (2), 299-336, doi:10.1124/pr.110.004309 (2012).

10.   Vilardaga, J.P., Bünemann, M., Krasel, C., Castro, M., & Lohse, M.J. Measurement of the millisecond activation switch of G protein-coupled receptors in living cells. *Nat. Biotechnol*. **21,** 807-812, doi: 10.1038/nbt/838 (2003).

11.   Bünemann, M., Frank, M., & Lohse, M.J. Gi protein activation in intact cells involves subunit rearrangement rather than dissociation. *Proc. Natl. Acad. Sci. USA*. **100** (26), 16077-16082, doi: 10.1073/pnas.2536719100 (2003).

12.   Stumpf, A.D. & Hoffman, C. Optical probes based on G protein-coupled receptors – added work or added value? *Brit. J. Pharmacol*. **173**, 255-266, doi: 10.111/bph.13382 (2016).

13.   Sivaramakrishnan, S. & Spudich, J.A. Systemic control of protein interaction using a modular ER/K α-helix linker. *Proc. Natl. Acad. Sci. USA*. **108**, 20467-20472, doi: 10.1073/pnas.1116066108 (2011).

Shaner, N.C., Steinbach, P.A., & Tsien, R.Y. A guide to choosing fluorescent proteins. *Nat. Methods*. **2** (12), 905-909, doi: 10.1038/NMET

Appendix 2

Molecular mechanisms of G protein activation

A2.1 Abstract

Heterotrimeric G proteins, consisting of Gα, Gβ, and Gγ subunits, are important signaling molecules that play a critical role in wide range of physiological processes. Currently, there are 76 crystal structures of Gα in the inactive and active states, including one in nucleotide empty state in complex with an active G protein coupled receptor (GPCR). Despite the wealth of structural information, the molecular mechanism that result in G protein activation remains an active area of research. The studies discussed in this section explore the molecular mechanisms by which binding of GPCR at distal sites influences G protein's nucleotide state.

A2.2 Introduction

Heterotrimeric G proteins are important signaling molecules as they play a critical role in wide range of physiological processes including cell growth, apoptosis, homeostasis, and immune response. The heterotrimeric G proteins, named for their ability to bind guanine nucleotides (GDP and GTP) are made of α, β, and γ subunits. There are three distinct nucleotide states: (i) inactive GDP bound state, (ii) active GTP bound state, and (iii) transitory nucleotide empty state. Nucleotide state of the G protein is under tight regulation by multiple regulatory proteins. Principal of these regulatory proteins are Guanine nucleotide Exchange Factors (GEF's). G protein coupled receptors or GPCRs function as GEF's. GPCRs convert detection of extracellular stimuli into intracellular response by binding to G proteins and promoting GDP exchange for GTP. In this cycle, the GDP bound G protein binds to the receptor, dissociates GDP and transition into a nucleotide-empty state, and binds to GTP, which subsequently triggers functional dissociation of Gα•GTP and Gβγ subunits. The activated G protein then acts on its effectors to initiate production of second messenger response. The Gα's inherent GTPase activity is very poor. Regulators of G protein Signaling (RGS's) serve as GTPase Activating Proteins (GAP's) by binding to Gα•GTP subunit and enhancing its catalytic activity to inactivate

108

the Gα subunit (*1*). Hydrolysis of the inorganic γ-phosphate converts GTP to GDP and promotes re-binding to Gβγ to re-initiate the G protein cycle (*1*) (Fig. A2.1). Guanine <u>D</u>issociation <u>I</u>nhibitors (GDI's) also regulate this cycle by sequestering the GDP-bound G protein in the cytosol, and thus prevent its association with membranes and subsequent activation by GPCRs. Thus far, there are 40 structures of Gα in the GAP interacting state, 25 in the GTP bound active state, 11 in the inactive GDP state, and one nucleotide empty state in complex with the activated β2-AR (GEF) (*18*). *Despite the wealth of structural information, the molecular mechanism that result in G protein activation remains an active area of research. The studies discussed in this section explore the molecular mechanisms by which binding of GPCR at distal sites influences G protein's nucleotide state.*

A2.3 Gα structure

Considerable insight into the conformational changes in the Gα subunit has been gleamed from the crystal structures of G proteins in various states. The Gα subunit consists of Ras-like GTPase domain (RGD) and an α helical domain (HD) (*2*). RGD is highly conserved across the GTPase superfamily, and is primarily responsible for G protein's catalytic activity (*2*). HD is unique to heterotrimeric G proteins and consists of six α helices and switch I, II, and III regions. Two linkers (L1 and L2) tether HD to RGD. Guanine nucleotides are thought to stabilize the interaction between the HD and RGD domains (*2*). The Gα's switch regions show significant conformational differences between the GDP and GTP bound state (*2*). GTP's inorganic γ-phosphate interacts with switches I and II, and thus stabilize an active Gα conformation that stimulates downstream effectors (*1*). In the absence of the γ-phosphate, in the GDP bound state, the two switches move apart from each other and lose their affinity for downstream effectors (*1*). This is one mechanism by which G proteins store and transmit information based on the conformational state of the Gα subunit.

A2.4 Role of Gα's domain opening in G protein activation

In the transitory nucleotide empty state, double electron-electron resonance spectroscopy (DEER) (*3*), cryo-EM (*4*), and β2-AR-Gs co-crystal structure (*5*) confirm a dramatic domain separation between the Ras-like GTPase domain (RGD) and the α helical domain (HD). Studies suggest that the clamshell like opening of the RGD-HD is one mechanism for facilitating GDP

escape. Molecular dynamic simulation studies of Gi•GDP, Gi•GTP, and Gi•Rhodospin elegantly demonstrate that Gi displays spontaneous RGD-HD opening in the absence of GPCR – albeit at a very low rate (*6*). This phenomenon is indirectly hinted at the lack of crystal structures of this conformation in the absence of a receptor, as the process of crystallography captures the abundant energetically favorable state. Researchers further noted that the domain opening, in the absence of the receptor, is necessary but not sufficient for nucleotide escape (*6*). Under spontaneous separation conditions, GDP still retained strong interactions with RGD and relatively weaker interactions with HD. Binding of the receptor was necessary to enhance domain separation and decrease RGD affinity for GDP to promote nucleotide dissociation (*6*). Nevertheless, the mechanism by which GPCR promote domain opening resulting in robust nucleotide exchange remained unclear.

A2.5 Role of Gα C-terminal α5 helix

A range of biophysical experiments using x-ray crystallography, (*5, 7*), double electron-electron resonance spectroscopy (DEER) (*3*), electron microscopy (*4*), and hydrogen-deuterium-exchange mass spectroscopy (DXMS) (*8*) paved the way for exploring the molecular mechanism of G protein's nucleotide exchange and subsequent G protein activation. These parallel studies concur on the critical role of the Gα's C-terminal α5 helix in G protein activation. In the β2-AR-Gs complex crystal structure, α5 constitutes ~70% of the total β2-AR-Gs interface (*5, 9*).

Comparing the GDP and nucleotide free state, α5 helix often adopts a conformation similar to the one observed in the β2-AR-Gs structure and the rhodopsin-Gi model. In this conformation, α5 helix moves away from the nucleotide-binding site. Repositioning of the α5 helix in these studies, correlate with enhanced mobility in the β6-α5 loop, which directly binds GDP (*6*). Further constraining the α5 helix in the GPCR-interacting conformation, MD simulations predict enhanced domain opening and nucleotide escape (*6*). Researchers proposed a mechanism by which rotation and binding of the α5 helix to the GPCR rearranges non-covalent interactions, resulting in mobility of the β6-α5 loop and loss of affinity of RGD for GDP, leading to domain separation and subsequent nucleotide exchange (*6*).

Insight into how repositioning of the α5 helix influences nucleotide dissociation was gained from comparative structural analysis (*9*) and alanine mutagenesis screening studies (*10*). Alanine screening characterized residues into different clusters. Residues in the G protein-activating

cluster were found in α1 and α5 packed against β1- β3 strands in the nucleotide bound states (*10*). Both sets of studies concurred that in the receptor-bound state the interaction between α1 and α5 is weakened, wherein α5 looses 20% of its Gα interacting contacts with α1 (*9, 10*). Instead, a new set of interactions is formed between α5 and β4-β6 strands. Comparative analysis studies suggested that α1 functions as a hub that links different functional Gα regions. In the nucleotide bound state, α1 makes non-covalent interactions with the N-terminus of α5 through conserved residues to link α5 to the GDP binding site (*9*). One such interaction is coordinated via Gαi's residue F336 positioned at the N-terminus of α5 (*9, 11*). Mutagenesis of F336 perturbs stability of GTP and GDP bound states without altering the ability to form a complex with the receptor (*10, 11*). These studies suggest that the N-terminus of α5 forms a network of interaction with β2 and β3 strands and α1. Repositioning of α5 results in displacement of α5 N-terminus leading to re-organization of this cluster of interaction (*9-11*). Comparative analysis further posits that α1 functions as the molecular switch for GDP release, whereas the α5 helix is the 'distal trigger' that is 'pulled' on by the receptor (*9*).

Additional MD studies conducted by Yao et al. questioned how binding of GDI or GEF's from sites that are distal from the nucleotide-binding pocket, influence the nucleotide state.

To that end, reserachers characterize the structural dynamics of GDI, GDP, and GTP bound states (*12*). Principal component analysis on crystal structures of Gi-family revealed that switch I, II, III regions are highly flexible. Additional ensemble-based correlation network analysis, enabled tracking of changes in the dynamic coupling of residue pairs in Gi bound to GDP, GTP, or GDI states. Analysis revealed an overall 'tightening' or shortening of path-lengths between different distal functional sites within the GTP state compared to the GDP and GDI states. α5 formed a community of interaction with β4 and β6 strands in the GDP bound state, and was additionally linked to β1 and β3 strands in the GTP bound state.

Network path analysis of residues that linked (source) receptor binding site to (sink) nucleotide γ-phosphate binding site and domain interface, revealed additional features that distinguish GDP and GTP bound states. This analysis indicated residues that were on the dominant path linking the source and sink regions. Network path analysis suggested that L32-I339 were key mediators of GTP specific coupling between α5 and β1 strand. Whereas F195 on β3 strand was suggested to couple path between β1 and RGD-HD interface. Interestingly, D333 located on α5-helix is exposed to the solvent, but was identified to be on the path that links receptor binding to

nucleotide exchange. MD simulations of mutants of these residues indicated enhanced domain separation rates where I339A>F332A>L32A>F195L>D333A=WT (Fig. A2.2a). As noted by Dror et al., domain opening is necessary but not sufficient for nucleotide exchange (*6*). The basal activity of these mutants was subsequently examined in live cells. Activity of the G protein was examined for equivalent levels of its activating GPCR. Interestingly, D333A and L32A mutants robustly enhanced basal, receptor free, activity of these mutants in live cells and an enhanced GTPγS incorporation rate (Fig. A2.2 b-f). In line with previous studies, Yao et al study re-affirmed the importance of α5-helix and its interaction with the β6-α5 loop (*13*). It further highlighted an additional role of the β1 strand that directly links the receptor to the phosphate coordinating P-loop.

A2.6 An emerging model of G protein activation

A model encompassing these various biophysical, computational, biochemical and cellular studies (*3-9, 11-13*), suggests that the C-terminus of the α5-helix, rotates, and transitions from a disordered to an ordered state, as it binds the cytosolic core of the receptor. The last C-terminal residues of the α5-helix serve as specific site of interaction with the receptor. Post binding to GPCR, α5 looses previously formed interactions with the Gα subunit. The N-terminus of α5, which does not insert into the receptor, forms a new set of interactions that convey binding of the receptor to the Gα's nucleotide binding pocket. Subsequently, interactions with the β6-α5 loop located at the N-terminus of α5 with β1 and β3 strand are re-arranged. Re-organization of non-covalent interaction between these different hubs weakens the affinity of the RGD for GDP, resulting in domain opening, and GDP dissociation. GTP, which is present at a higher cytosolic concentration than GDP binds and activates the G protein. The residues that regulate nucleotide exchange are found on both the α5 helix (D333 and F332/F336) and on paths that link the α5-β1 strand, which links the distal binding of the α5 to the GPCR to the Gα's phosphate coordinating P-loop. The proposed model needs further verification. Biochemical and cellular studies are needed to test if this mechanism is universal for all G proteins. Further analysis is needed to determine if this mechanism holds true for additional GPCR-G protein combinations.

A caveat to the aforementioned model is that it emphasizes the role of Gα's C-terminal α5 helix in GPCR mediated nucleotide exchange, resulting in robust G protein activation. However, the co-crystal structure of β2-adrenergic receptor in a complex with Gs protein reveals an extensive

interface consisting of β2-AR's intracellular loop 2 (ICL2), transmembrane 5 (TM5) and TM6, with Gαs N-terminal α-helix, and RGD elements including α5 helix, αN-β1 junction, and α4 helix. Initial studies suggest that the Gα's N-terminal α helix is also a key determinant of specificity of GPCR-G protein interaction (*8*). Structural and DXMS studies highlight an additional role of Gα N-terminus α-helix (αN) in G protein activation (*5, 8*), where they note high exchange rates for ICL2 and Gα's α1 helix, and the β1 strand linking ICL2 of the agonist bound receptor to the P-loop that coordinates β-phosphate of GDP in Gαs. Together, these studies suggest that the GPCR engages Gα's N-terminus and alters the position and/or the stability of the β1 strand with associated changes in the P-loop and the α1 helix (*8*). These finding underscore the need to explore the potential role of Gα's N-terminus in GPCR mediated nucleotide exchange.

A2.7 Notes and Acknowledgements

The study exploring mechanism of G protein activation as discussed in Section 4.3 was a collaborative effort between the labs of Barry J. Grant from the Department of Computational Medicine and Bioinformatics, John R. Traynor's lab in Pharmacology at the University of Michigan, and the Sivaramakrishanan lab at the Department of Genetics, Cell Biology, and Development in University of Minnesota. This study was lead by post-doctoral fellow Xin-Qui Yao from the Grant lab and myself. Yao and the principal investigators designed the study. The molecular dynamics stimulations were performed and analyzed by Yao and Grant. Graduate student, Nicholas W. Griggs in the Traynor lab performed the GTPγS incorporation assay. I was a co-author on the study, as I collected critical live cell downstream experiments. All authors reviewed the results and jointly wrote the manuscript. The manuscript entitled 'Dynamic coupling and allosteric networks in the α subunit of heterotrimeric G proteins" was published in the *Journal of Biological Chemistry* on December 24, 2015 (*12*). This study is discussed in light of the previous works published in this area. Selected data sets from Yao *et al*., are presented to facilitate discussion.
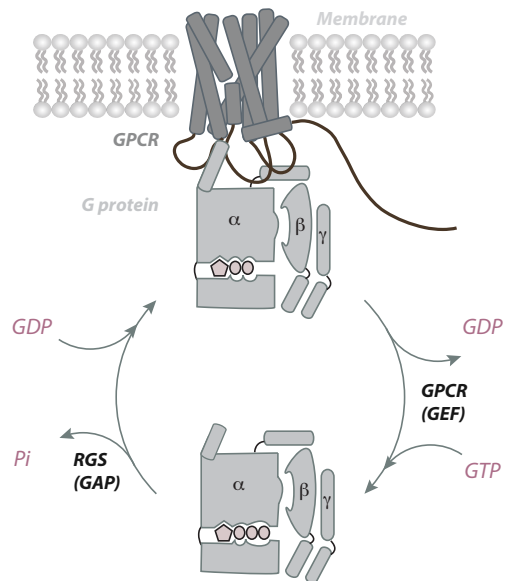
A2.8. Figures

Fig. A2.1: Schematic of the G protein cycle. GPCRs function as guanine nucleotide exchange factors (GEF's) and promote nucleotide exchange from GDP to GTP leading to G protein activation. RGS function as GTPase activating proteins (GAP's) to enhance catalysis of GGTP to GDP, resulting in G protein
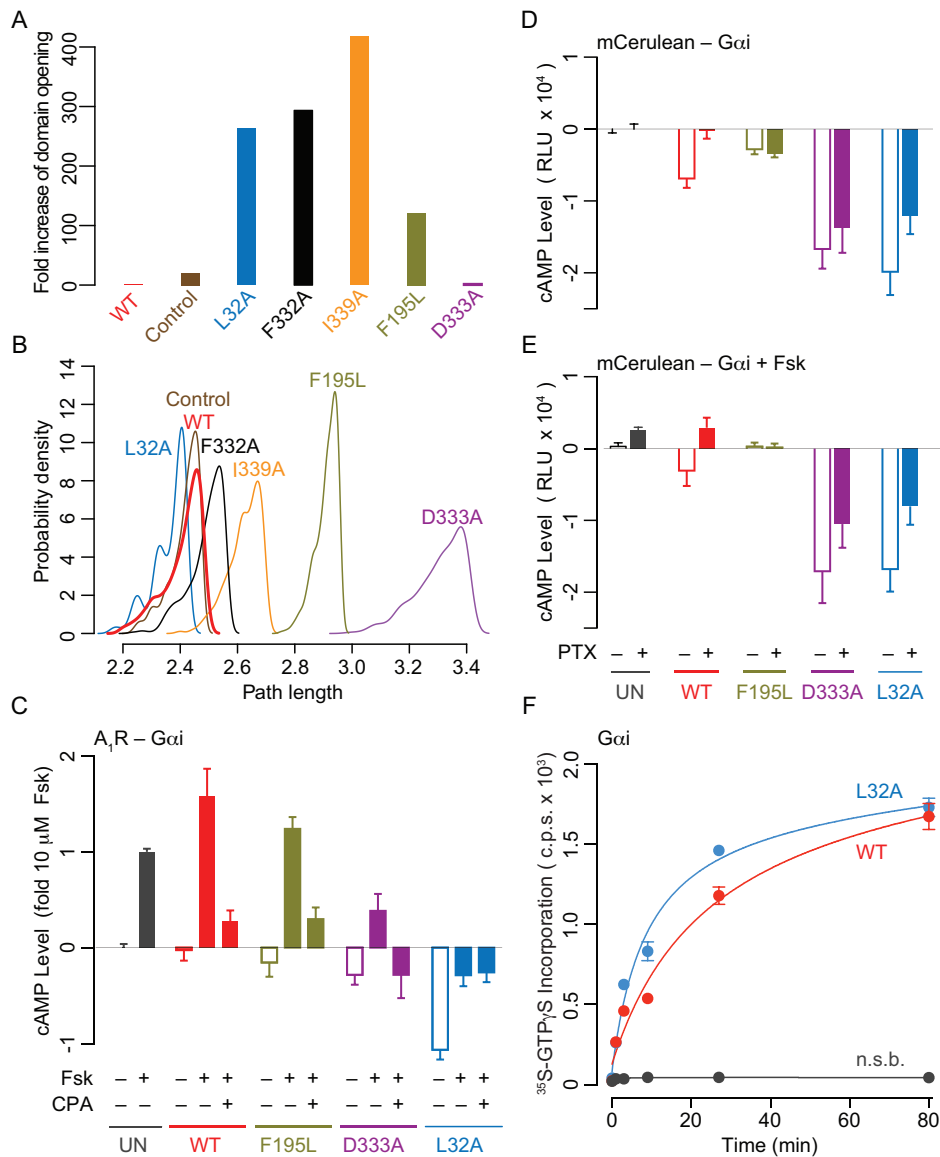
Fig. A2.2: Computational and experimental mutagenesis of on path residues. Computational and experimental mutagenesis of on path residues. a, fraction of domain opening events observed relative to wild-type (WT) simulations for L32A, F195L, F332A, D333A and I339A. The same wild-type simulation protocols and network analysis methods were implemented for all mutant simulations. Domain opening was detected whenever the minimum $C\alpha$-$C\alpha$ distance between LE (on the HD side) and SIII (on RasD) exceeded 10Å in the cumulative 5×80ns simulations. "Control" refers to a set of five separately performed wild-type simulations. Note that all simulations were structurally stable as indicated by standard geometric analysis (data not shown). b, probability density distribution of path lengths from receptor coordinating $\beta 1$ (K31) to RasD-HD interface (D146) in wildtype and mutants. c, cAMP levels for the WT and mutant A1R-$G\alpha i$ fusions for indicated conditions in live HEK293 cells (Untransfected (UN), 10 μM forskolin (Fsk), 12.5 nM N6-cyclopentyladenosine (CPA, A1R agonist)). d & e, cAMP levels for HEK293 cells expressing WT or mutant mCerulean labeled $G\alpha i$, treated without (d) or with (e) forskolin (10 μM Fsk) in the presence or absence of pertussis toxin (PTX). PTX

115

A2.8 References

1.   G. Krauss, *Biochemistry of signal transduction and regulation*. (Wiley-VCH, Weinheim Great Britain, ed. 3rd, 2003), pp. xvi, 541 p.
2.   W. M. Oldham, H. E. Hamm, Heterotrimeric G protein activation by G-protein-coupled receptors. *Nature reviews. Molecular cell biology* **9**, 60-71 (2008).
3.   N. Van Eps *et al*., Interaction of a G protein with an activated receptor opens the interdomain interface in the alpha subunit. *Proc Natl Acad Sci U S A* **108**, 9420-9424 (2011).
4.   G. H. Westfield *et al*., Structural flexibility of the G alpha s alpha-helical domain in the beta2-adrenoceptor Gs complex. *Proc Natl Acad Sci U S A* **108**, 16086-16091 (2011).
5.   S. G. Rasmussen *et al*., Crystal structure of the beta2 adrenergic receptor-Gs protein complex. *Nature* **477**, 549-555 (2011).
6.   R. O. Dror *et al*., SIGNAL TRANSDUCTION. Structural basis for nucleotide exchange in heterotrimeric G proteins. *Science* **348**, 1361-1365 (2015).
7.   P. Scheerer *et al*., Crystal structure of opsin in its G-protein-interacting conformation. *Nature* **455**, 497-502 (2008).
8.   K. Y. Chung *et al*., Conformational changes in the G protein Gs induced by the beta2 adrenergic receptor. *Nature* **477**, 611-615 (2011).
9.   T. Flock *et al*., Universal allosteric mechanism for Galpha activation by GPCRs. *Nature* **524**, 173-179 (2015).
10.   D. Sun *et al*., Probing Galphai1 protein activation at single-amino acid resolution. *Nat Struct Mol Biol* **22**, 686-694 (2015).
11.   A. I. Kaya *et al*., A conserved phenylalanine as a relay between the alpha5 helix and the GDP binding region of heterotrimeric Gi protein alpha subunit. *J Biol Chem* **289**, 24475-24487 (2014).
12.   X. Q. Yao *et al*., Dynamic Coupling and Allosteric Networks in the alpha Subunit of Heterotrimeric G Proteins. *J Biol Chem* **291**, 4742-4753 (2016).
13.   N. S. Alexander *et al*., Energetic analysis of the rhodopsin-G-protein complex links the alpha5 helix to GDP release. *Nat Struct Mol Biol* **21**, 56-63 (2014).